NTNU – Trondheim
Norwegian University of
Science and Technology

Characterization of Bioaerosols using Electron Microscopy with Special Emphasis on Airborne Bacteria

Hanne Grydeland

Nanotechnology
Submission date: June 2014
Supervisor: Antonius Theodorus Johann Van Helvoort, IFY
Co-supervisor: Marius Dybwad, FFI (Forsvarets forskningsinstitutt)
Janet M. Blatny, FFI

Norwegian University of Science and Technology
Department of Physics

Characterization of Bioaerosols using Electron Microscopy with Special Emphasis on Airborne Bacteria

TFY4905 Nanotechnology, Master Thesis

Hanne Grydeland

June 1, 2014

Abstract

Bioterrorist attacks on confined, indoor areas such as underground subway stations by the release of pathogenic microorganisms into air, could pose a threat to public safety. The potential threat may be severe not only due to the adverse health effects themselves, but also because of the lack of efficient and reliable on-site biological aerosol (bioaerosol) monitoring systems. As of the present situation, possible bioterrorist attacks on e.g. underground subway systems may remain undiscovered until infected individuals seek medical assistance, which may not happen before several days after the attack.

Knowledge about the morphology of bioaerosols, as they appear in air, may be important in the development of fast and reliable bioaerosol detectors. This study concentrates on providing such knowledge by investigating and comparing different methods of characterizing bioaerosols by electron microscopy, using aerosolized, vegetative bacteria and bacterial spores as models. The study addresses challenges associated with electron microscopy of bioaerosols, including dehydration artifacts and identification of biological material in a complex, environmental sample. Bioaerosol sampling is also addressed.

The results of this study suggest that sampling, preservation and electron microscopy of bioaerosols is more challenging than the equivalent for non-aerosolized biological material, owing to the complex composite nature of the bioaerosols, and the challenges associated with sampling them. Experiments with energy-dispersive X-ray spectroscopy (EDS/EDX) indicate that bioaerosols can be distinguished from inorganic particles in environmental samples, provided that the bioaerosols are not associated with inorganic material. Conventional scanning electron microscopy (SEM) does not prevent bioaerosol dehydration, and transmission electron microscopy (TEM) does not provide sufficient information about the morphology of bioaerosols. Critical point drying (CPD) is promising in some regards of bioaerosol preparation for SEM, but preserving bioaerosol morphology as it is in air, however, is also dependent on the particles not dehydrating during sampling.

Future studies are necessary to provide an optimal method of bioaerosol characterization using electron microscopy. This work however, provides a comprehensive overview of the challenges faced in such regards, and presents information which may propel research into bioaerosol characterization and detection a small step forward.

Sammendrag

Bioterrorangrep ved luftutslipp av patogene stoffer på avgrensede innendørsområder som t-banestasjoner, kan utgjøre en trussel for samfunnssikkerheten. Den potensielle trusselen kan være alvorlig ikke bare på grunn av de negative helseeffektene i seg selv, men også på grunn av mangelen på et effektivt og pålitelig overvåkningssystem for biologiske aerosoler (bioaerosoler) på stedet. Slik situasjonen er nå, risikerer man å ikke oppdage et eventuelt bioterrorangrep før smittede individer søker medisinsk hjelp, hvilket kan ta opptil flere dager.

Kunnskap om bioaerosolers morfologi, slik de fremstår i luft, kan vise seg å være viktig i utviklingen av raske og pålitelige bioaerosoldetektorer i fremtiden. Denne studien fokuserer på å skaffe til veie slik kunnskap ved å utforske og sammenlikne metoder for å karakterisere bioaerosoler ved hjelp av elektronmikroskopi. Aerosoliserte, vegetative bakterier og bakteriesporer blir brukt som modellsystemer. Studien adresserer utfordringene forbundet med elektronmikroskopi av bioaerosoler, inkludert dehydreringsartefakter og identifikasjon av biologisk materiale i en kompleks, naturlig prøve. Bioaerosolinnsamling blir også adressert.

Resultatene i denne studien antyder at innsamling, bevaring og elektronmikroskopi av bioaerosoler er mer utfordrende enn tilsvarende for ikke-aerosolisert biologisk materiale, på grunn av bioaerosolenes komplekse kompositttegenskaper, og utfordringer med å samle dem inn. Eksperimenter med energidispersiv røntgenspektroskopi (EDS/EDX) antyder at bioaerosoler kan skjelnes fra uorganiske partikler i miljøprøver, gitt at bioaerosolene ikke er forbundet med uorganisk materiale. Konvensjonell sveipelektronmikroskopi (SEM) forhindrer ikke dehydrering av bioaerosoler, og transmisjonselektronmikroskopi (TEM) gir ikke nok informasjon om bioaerosolers morfologi. Kritisk punkttørking (CPD) er lovende i forbindelse med noen aspekter ved bioaerosolpreparering for SEM, men bevaring av bioaerosolmorfologi som den er i lufta, er imidlertid også avhengig av at partiklene ikke tørker under innsamling.

Videre studier er nødvendig for å komme frem til en optimal metode for karakterisering av bioaerosoler ved hjelp av elektronmikroskopi. Dette arbeidet tilbyr imidlertid en helhetlig oversikt over utfordringene som møtes i så måte, og presenterer informasjon som kan føre forskning på bioaerosolkarakterisering og -deteksjon et lite skritt videre på veien.

Preface

This thesis is a result of concluding work in the master's degree programme in Nanotechnology at the Norwegian University of Science and Technology (NTNU). The thesis is written in cooperation with the Norwegian Defence Research Establishment (Forsvarets forskningsinstitutt, FFI) during the spring semester of 2014. The experimental work has been performed at FFI's facilities at Kjeller outside of Oslo, as well as at the EM-lab at the University of Oslo (UiO). Supervisors have been chief scientist Marius Dybwad at FFI, associate professor Antonius T. J. van Helvoort at NTNU and senior scientist Janet Martha Blatny at FFI.

I would like to thank all my supervisors, especially Marius Dybwad, who has been of invaluable help and assistance on a frequent basis during the whole project. I would also like to thank chief scientist Randi Haakenaasen at FFI, for great insight and training in both the theory of electron microscopes and the practical use of SEM. In addition, I would like to thank Gunnar Skogan at FFI for help and great patience with collecting bioaerosols in the FFI aerosol chamber. Without his expertise, most of my results would not be possible.

For expert guidance and help with preparation and microscopy of my bioaerosols, I extend many thanks to head engineer Antje Hofgaard and staff engineer Michaela Salajkova at the EM-lab at UiO. The latter was of outstanding help to me when performing X-ray analysis, providing me with high quality imaging and results. A part of the thesis would not exist without great help from professor Norbert Roos at UiO, who performed the TEM analysis at UiO's EM-lab, and for which I am most grateful.

Contents

Abbreviations

AFM	Atomic force microscopy/microscope
B. anthracis	*Bacillus anthracis*
BG	*Bacillus atrophaeus* (*Bacillus globigii*, *B. subtilis var niger*)
Bioaerosol	Biological aerosol
BSE	Backscattered electrons
C	Carbon
Ca	Calcium
CPD	Critical point drying
Cu	Copper
EDS	Energy-dispersive X-ray spectroscopy
EDX	Energy-dispersive X-ray spectroscopy
EELS	Electron energy loss spectroscopy
EPS	Extracellular polysaccharide
ESEM	Environmental SEM
FE	Field emission
Fe	Iron
FEG	Field emission gun
H	Hydrogen
HPF	High-pressure freezing
kV	Kilo electron volt
LV SEM	Low-vacuum SEM
N	Nitrogen
O	Oxygen
P	Phosphorus
Pd	Palladium
PCR	Polymerase chain reaction
Pt	Platinum
S	Sulfur
S. marcescens	*Serratia marcescens*
SE	Secondary electrons
SEM	Scanning electron microscopy/microscope
Si	Silicon
STEM	Scanning transmission electron microscopy/microscope
TEM	Transmission electron microscopy/microscope
VP	Variable pressure
Zn	Zinc
Zr	Zirconium

1 Introduction

This section is to a large extent based on previous work by this author, conducted as part of the course *TFY4520 - Nanotechnology, Specialization Project*, see [1].

1.1 Bioaerosols

Biological aerosols (bioaerosols) are a heterogeneous group of airborne particles of biological origin. They are a subgroup of biogenic organic aerosols and range from 10 nm to 100 µm in diameter. Bioaerosols can be alive, dead or dormant (e.g. bacteria, fungi and viruses) or consist of products or fragments released from living organisms (e.g. metabolites, pollen, cell debris and biofilm) [2]. In non-fragmented state, the size of bioaerosol components range from about 15 nm to 400 nm for viruses, 0.3 µm to 10 µm for bacteria to 1 µm to 100 µm for e.g. fungal spores, pollen and plant debris [3]. Bioaerosols are generated from a number of different sources, including pollen and spore release from plants and "bubble-burst"-mechanisms in oceans and seas, as well as being a byproduct of industrial, municipal or agricultural activities. Humans may also produce bioaerosols e.g. by coughing [4].

Bioaerosol exposure in an indoor environment is known to cause adverse health effects in humans, among them infectious diseases, allergies, asthma, inflammatory lung diseases, cancer and acute toxic effects [5] [6]. A study by Matthias-Maser et al. [4] suggests that the percentage of bioaerosols in urban and rural areas is a little less than 25% of total particles suspended in air, with no strong seasonal variations. The total amount of bioaerosols in the air and their composition varies with several factors, such as altitude, region, temperature, wind direction, humidity, rainfall [7], season and time of the day [2].

Considering the adverse health effects and fluctuating occurrence of naturally occurring bioaerosols, one might imagine the challenge to detect and correctly assess their risk potential under normal circumstances, not to mention the serious potential hazards of pathogenic substances in harmful concentrations intentionally released and dispersed in air. Confined and often indoor public environments, such as underground subway stations, make an ideal target for bioterrorist

attacks, seeing how most biological substances don't induce any immediate effects in humans after exposure, and therefore are hard to detect early on after dispersion [8]. To better protect and inform the public of potential airborne dangers, it is paramount to map and characterize bioaerosols. Up to now, this field of research has been subject to little investigation, with some exceptions (seen in e.g. [9], [10], [11], [12], [13], [14], [15], [16] and [3]). Although work detailing characterization of bacteria and hydrated structures using electron microscopy has been done (e.g. [17], [18] and [19]), to the author's knowledge, no comprehensive work on characterizing the native size and conformation[1] of bacteria-containing bioaerosols using electron microscopy exist.

[1]Conformation is used in the meaning of structure or shape throughout the text. Morphology is used to denote shape and size. Sometimes the two are used interchangeably.

1.2 Electron microscopy of bioaerosols

Acquiring knowledge about the size distribution of bioaerosols and the size and shape of microorganisms that are associated with bioaerosols, can help advance bioaerosol detector research, and potentially lead to a safer indoor and outdoor air environment. The ability to observe bioaerosols' native conformation is an essential first step in acquiring further useful information about the natural occurrence and state of these airborne particles. There are several factors vouching for using electron microscopy as opposed to conventional optical microscopy to observe the bioaerosols. Considering the small size of the bioaerosol components, the magnification and resolution of an optical microscope will not be sufficient [20] [21], as this is limited by the wavelength of light, yielding a resolution no greater than 200 nm considering a perfect system. Observing bioaerosols in an electron microscope will allow observation of all particles in a sample, including both viable and non-viable bioaerosols, with a greater sense of their structural details, resulting in a considerable advantage in the characterization of such aerosols.

There are however several challenges in imaging bioaerosols using electron microscopy, some of which are mentioned below:

Dehydration in vacuum. Bioaerosols containing hydrated materials such as bacteria are subject to dehydration in the vacuum environment of any standard electron microscope. This dehydration can cause distortion and collapse of native structures, leading to difficulties in identifying and observing the bioaerosols for purposes detailed above [20] [21] [22].

Complex particles. Aerosol components of interest can be covered in inorganic material such as salts, or they may be bundled together, covering each other and hence inhibiting straightforward observation, provided a surface technique is exclusively utilized. The presence of inorganic material can also prevent the bioaerosols to be preserved by conventional, biological preparation methods, as this may dissolve and distort the original bioaerosol conformation. Identifying electron microscopy techniques in which "bulk identification" is possible will hopefully lead to a better characterization of bacteria containing bioaerosols.

Finding the needle in the haystack. The air environment, and hence substrates with samples taken under real conditions, will not contain 100 % bioaerosols. The challenge lies in identifying interesting bioaerosols, i.e. primarily ones containing bacteria, on a substrate containing an abundance of inorganic and uninteresting aerosols in the electron microscope. Finding bioaerosols of interest in environmental samples can be comparable to finding a needle in a haystack.

The motivation for this project is to find a method of circumventing these obstacles in order to provide high-quality images of bioaerosols in their native state. In other words, any electron microscopy technique used to image bioaerosols should retain the bioaerosols' native conformation, should not dry out the sample, should have the potential of identifying interesting particles relatively easy and fast, and should ideally be capable of providing information about the content of the particles and not just surface information.

The collection and preparation of a sample is also vital to ensure good imaging of the bioaerosols. The sampling should be designed in such a way that a representative selection of airborne particles is collected, and to avoid disturbance once they are sampled, bioaerosols should be sampled at the same substrate on which they undergo preparation and imaging. Avoiding preparation methods which introduce distortions, artifacts, extraction of cell contents [23], concealing of structures due to coating [17] and so on is important for high-quality bioaerosol imaging.

1.3 Previous work and project objectives

Preparatory work for this master thesis has previously been conducted as part of the course *TFY4520 - Nanotechnology, Specialization Project*, see [1]. In that study, different methods of bioaerosol observation were evaluated based on a literature study, and a selection of aerosolized bacterial cells and spores were sampled and studied using scanning electron microscopy (SEM). The methods to be explored in this thesis were chosen based on the previous literature study and an evaluation/examination of the experimental results.

The objective of the present project was to:

1. Work further with the outcome of the previously conducted literature study, and select promising methods of bioaerosol preparation and observation. The criteria are that these methods should be able to conserve and convey bioaerosol conformation, and be available at FFI or at a collaborating institution.

2. Carry out available preparation and observation methods on bioaerosols, and assess the quality of the results and whether or not they are satisfactory.

3. If possible, develop a protocol for electron microscope imaging (primarily SEM) that is capable of retaining bioaerosols' native conformation, characterize size and content, and have the potential of identifying interesting particles relatively easy and fast.

2 Theory

This section is partly based on previous work by this author, conducted as part of the course *TFY4520 - Nanotechnology, Specialization Project*, see [1].

2.1 Collecting bioaerosols (for electron microscopy)

The source material for this section is found in [20], [24], [25], [26] and [27] unless otherwise noted.

Even though this study concentrates on observing bioaerosols using electron microscopy, the collection of bioaerosols plays a very important part in ensuring a good electron microscope image. There exists an abundance of different devices for bioaerosol collection, differing from each other in what kind of bioaerosols they collect and what method of further analysis can be used. Some methods for bioaerosol collection are summarized in figure 1.

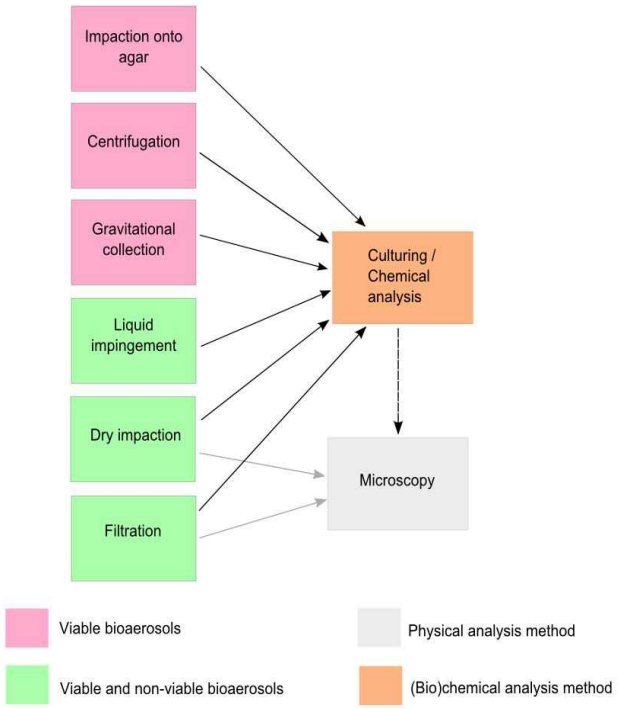

Figure 1: Overview of different bioaerosol sampling and analysis methods. Some of the samplers only recover viable bioaerosols, i.e. bioaerosols containing living microorganisms able to reproduce as they are metabolically active. Figure is based on information from [20], [24], [25], [26] and [27].

By biochemical and chemical analysis of the bioaerosols (see figure 1), it is meant detection and identification of bioaerosols by growth on culture media, rapid biochemical, immunological and molecular biology methods (e.g polymerase chain reaction (PCR), biochemical and immunoassays, chromatography, Raman spectroscopy etc. [28]) [29]. Physical methods, i.e. microscopy, examine the bioaerosols by means of number, size and shape by using different microscopy techniques such as light microscopy, scanning electron microscopy (SEM), transmission electron microscopy (TEM) etc. The important difference between chemical methods and direct microscope observation, is that bioaerosols do not have to be removed from the impaction substrate before being

observed in the microscope.

The filtration method is based on drawing air through filters with uniform pore sizes, thereby collecting particles (both biological and non-biological) larger than a certain size on the filter. Particle deposition onto the filter is mainly due to impaction forces, but interception, diffusion and electrostatic attraction contribute as well [30].

Pollen, spore or particle impaction is a method of collecting airborne particles by impacting them onto an impactor plate, for example glass slides or tape strips. By this method, both viable and non-viable bioaerosols can be collected and subsequently observed by light and electron microscopy.

Liquid impingement collects both viable and non-viable bioaerosols by capturing them in a liquid by means of both diffusion and inertial forces. The particles are left in liquid, which makes the method unsuited for direct microscope observation of the structure of intact bioaerosols. Single microorganism structure, however, is maintained during liquid impingement.

Bioaerosols deposited onto culture medium by impaction, centrifugation or simple gravitation are unsuited for electron microscopy observation without preparation. Only viable bioaerosols are detected, as only these are capable of growing on the media. This method is useful for counting bacterial colonies on media, as well as gaining information of e.g. the physiology and taxonomy of bacterial aerosols [16]. A frequently used impaction sampler is the Andersen sampler, a cascade sampler which consists of up to six stages of culture media in sequence, with successively smaller particles adhering to the culture media.

When considering bioaerosol samplers for the preservation of native structure, it is important to consider factors such as environmental conditions, how easy the sampler is to operate and transport without damage to the aerosols, and its sampling and collection efficiency[2]. The sampler's biological efficiency[3] is also an important factor to consider.

Matthias-Maser and Jaenicke [10] list the following requirements for impaction plates used to sample aerosols for subsequent viewing and analysis in SEM and with energy dispersive X-ray spectroscopy

[2]how good the sampler is at drawing particles in and depositing them.

[3]how well the sampler maintains microbial viability and cell structure of microorganisms during sampling [30].

(EDX/EDS):

1 Should not distort particles during sampling

2 Must be stable to vacuum

3 Surface should be even (so as not to be confused with deposited particles)

4 Elemental background spectrum has to be as low as possible (so as not to overlap particle spectra)

5 Particles should be deposited on top of impaction plates and not sink in adhesive layers (in order to image the whole surface of the particles)

According to Matthias-Maser and Jaenicke, neither glass slides (large elemental background spectra), nor acrylic glass (not stable in vacuum) or adhesives (not in agreement with (5)) are suitable for aerosol collection and observation in SEM/EDX. They suggest to use smooth graphitic foils as impaction plates. Previous studies detailing collection [31] and subsequent SEM of bioaerosols, have commonly used polycarbonate filters.

Bioaerosol collection for TEM observation differ from the above detailed collection for SEM observation. TEM observation requires particulate specimens to rest on a grid (3 mm diameter), which is usually covered with an electron-translucent support film. Copper is commonly used as grid material, as this usually provides sufficient stability to the specimens, but e.g. nickel, gold and gold-coated grids are also available [32]. As for support films, these commonly consist of thin films of plastic, like Formvar, carbon or carbon-coated Formvar. Plastic support films are usually not ideal to use for high-resolution imaging however, as the electrons of the TEM tend to decompose the plastic and drift. Carbon-coatings are therefore provided to plastic support films to stabilize the structures. [33]

For minimal disturbance to the specimens during sampling and preparation, bioaerosols to be observed by TEM should be deposited directly onto a TEM grid, as demonstrated by Pósfai et al. [16] and Li

and Shao [34]. While Pósfai et al. sampled aerosols onto TEM grids covered with carbon-coated Formvar using a streaker sampler[4] which impacted the particles directly onto the grids, Li and Shao collected aerosols by impacting them onto copper TEM grids coated with carbon film using a single-stage cascade impactor.

[4] a one- or two-stage impaction sampler depositing particles in a circular pattern on a rotating filter [35].

2.2 Preparing bioaerosols (for electron microscopy)

The source material for this section is found in [36] and [37], including [38] and [39] unless otherwise noted.

Imaging hydrated specimens in an electron microscope usually requires removal or immobilization of the water inside the specimen, as the microscope's vacuum can prove disturbing to hydrated structures, evaporating the water and damaging both the sample and the electron microscope. The two general methods to prepare hydrated, biological samples for electron microscopy are drying or freezing. In addition, critical point drying (CPD) is frequently used to dehydrate biological material. To ensure toughness and contrast respectively, biological samples are often fixed and stained before imaging. Depending on the chemical used, one of these steps can sometimes substitute the other.

For some methods, no prior studies on the method's application to bioaerosols have been conducted, to the author's knowledge. These methods will be presented here together with studies detailing the method's application to other types of hydrated, biological material under the assumption that these studies can be relevant also to the preparation of bioaerosols, as bioaerosols also contain hydrated structures.

2.2.1 Chemical fixation

The source material for this section is found in [37], [40] and [41] unless otherwise noted.

To kill, stabilize and protect biological material against the potential strain associated with further processing like dehydration, embedding and electron beam exposure, chemical fixation is usually applied to biological specimens as a first step in readying them for electron microscopy. Several different chemicals have been tested and are in use as fixatives, each with individual mechanisms for fixation.

Some commonly used fixatives are the aldehydes formaldehyde and glutaraldehyde, in addition to osmium tetroxide[5]. Aldehyde fixatives stabilize structures by forming (differing) cross-links between proteins in the material they fix, while osmium tetroxide stabilizes lipids. Although these fixatives are used most commonly in liquid state, formaldehyde, glutaraldehyde and osmium tetroxide retain fixation properties in vapor state, as demonstrated by e.g. Füchtbauer et al. [42], Staff et al. [43] and Coetzee et al. [18], respectively.

One challenge with fixation is that diffusion time of the chemical into cells varies with diffusion coefficients and distances, so even though the reaction in itself is quick (a few milliseconds), it can take up to several minutes for the chemical to reach its site of action, if it reaches it at all. Different cellular material can also end up fixing with different rates and chemistries, varying with the fixatives, so the fixation process is to some extent unreliable. Moreover, fixation can distort the objects they cross-link, or structures may not receive sufficient stabilization.

2.2.1.1 Glutaraldehyde fixation

The source material for this section is found in [40] and [41] unless otherwise noted.

[5]Osmium tetroxide is a highly toxic and volatile crystalline solid that must be handled with great care and under a fume hood.

Glutaraldehyde, in liquid form, is the most common primary fixative[6] used prior to electron microscopy [44]. The main method of fixation is the formation of irreversible cross-links[7] by reaction between aldehyde groups on the glutaraldehyde molecules and amino groups in proteins. The cross-linked amino groups form a three-dimensional network throughout the cell cytoplasm, in contrast to formaldehyde fixation, which only produces a two-dimensional amino group network. The glutaraldehyde molecule is represented in figure 2, each end of the molecule constitutes an aldehyde group.

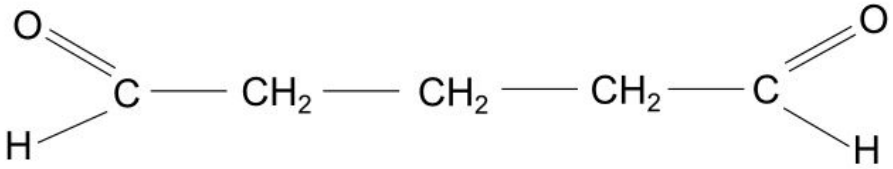

Figure 2: Glutaraldehyde molecule. The molecule contains two aldehyde (-CHO) groups which react to cross-link amino groups on proteins.

During the fixation reaction, reactions between aldehydes and free amino groups lead to acid production and an overall lowering of the pH of the environment. A fall in pH may possibly cause adverse effects such as morphological changes in the specimens. Therefore, glutaraldehyde fixatives are commonly combined with a suitable buffer, which will contribute to maintain initial pH. A study by Hayat [32] lists phosphate, cacodylate, PIPES, MOPS and HEPES as buffers that can be used together with glutaraldehyde for fixation purposes. While glutaraldehyde is at its most effective in cross-linking proteins at pH 7.5-8.0, this excessive polymerization may lead to artifacts in the specimen, so the recommended pH of a glutaraldehyde-buffer complex is within pH 7.2-7.4.

[6]Glutaraldehyde fixation is often succeeded by fixation with osmium tetroxide, as this substance fixes lipids, which are not fixed by glutaraldehyde, and also functions as a heavy metal stain, which enhances contrast [33].

[7]Glutaraldehyde fixation is stronger than formaldehyde fixation, possibly due to the fact that the first produce irreversible cross-links, as opposed to the latter.

2.2.1.2 Glutaraldehyde vapor fixation

Glutaraldehyde can also be used as a fixative in vapor state. Staff et al. [43] used glutaraldehyde vapor to fix pollen grains in order to localize water soluble glycoproteins using immunogold probes. The reason for not choosing an aqueous glutaraldehyde solution for this purpose was to avoid the liquid to displace glycoproteins before localization. Pollen grains fixed by glutaraldehyde vapor (followed by immersion in 2,2-dimethoxypropane and ethanol), showed a wider localization of the water soluble glycoproteins than did the pollen grains fixed by standard, aqueous glutaraldehyde. In the field of artificial scaffold research, glutaraldehyde vapor has been explored for its cross-linking properties, as a means of altering scaffold properties and regulating scaffold degradation, as demonstrated by e.g. Jiang et al. [45] and McManus et al. [46].

As of yet, however, glutaraldehyde vapor fixation has not been used for bioaerosol preparation for electron microscope observation, according to the author's knowledge.

2.2.2 Dehydration

The source material for this section is taken from [32], [36] and [37] unless otherwise is noted.

Several options exist for removing water from specimens in preparation for electron microscopy. Simply drying the specimens in air is the simplest, but this method can prove destructive to native sample configuration, making it an unsuitable method of water removal when the precise imaging of biological structures is desired. Drying specimens by liquid transfer by substituting the water with a water-miscible organic solvent like acetone or ethanol, is another, slightly less destructive, option. This also allows for infiltration of a plastic resin[8] into the specimen, but even this method can be destructive to fragile details in the sample, extracting cell components and causing specimen shrinkage [40]. Liquid transfer is therefore normally preceded by chemical fixation to toughen the structures.

Alternative ways of removing water from biological specimens are by CPD and freezing of the samples.

2.2.3 Critical Point Drying (CPD)

The source material for this section is taken from [41] unless otherwise noted.

CPD is an alternative and common method of drying biological material. In CPD, the removal of liquid from the specimen happens by evaporating the liquid without crossing the liquid-gas boundary. This is desirable because when a liquid crosses the liquid-gas boundary, surface tension in the liquid pulls on solid structures in the specimen, possibly damaging and altering them. The critical point of a liquid is reached by a specific combination of heat and pressure, obtained inside a designated vessel. CPD must be preceded by dehydration (water replacement) by an ethanol series, as water's critical point temperature and pressure is 374 °C and 3.184 psi respectively, which is destructive for biological material. Inside the CPD vessel, the ethanol dehydrant is

[8] The plastic resin is usually hydrofobic, embedding must therefore be preceded by dehydration with organic solvents.

replaced by a transitional fluid, e.g. CO_2 which is warmed up to 31.1 °C and kept at 1.073 psi. The transitional fluid will reach the same density as its vapor phase, and be substituted and released as vapor without damaging the specimen structure. Some tissue can reportedly experience shrinking during CPD, as well as loss of e.g. actin components by solution in the transitional fluid.

Liang et al. (2012) point dried glutaraldehyde and osmium tetroxide-fixed *Penicillium expansum* spores and gold-coated them before observing the spores by SEM [47]. The observed spores did not exhibit apparent signs of vacuum-induced (or other) damage. Ratnayake et al. [48] compared different dehydration methods for biofilm to be observed by SEM, and found that CPD caused less drying artifacts in the sample than chemical drying, but this could be further improved by fixation with glutaraldehyde and pre-fixation with lysine [48]. No study has described CPD of bioaerosols sampled dry and observed by electron microscopy with the aim of maintaining bioaerosol structure. Chung et al. [49] have however aerosolized and sampled bacteria on granular activated carbon and grown it there before critically point drying it and observing it in SEM. Although the aim of that study was not to maintain the exact native structure of dry impacted bioaerosols, the SEM images showed no apparent signs of dehydration artifacts on the bioaerosols deposited on the carbon.

2.2.4 Cryopreparation

The source material for this section is found in [36] and [37], including [38] and [39] unless otherwise noted.

Cryopreparation is a preparation technique for electron microscopy that has been widely explored recently, as it introduces fewer artifacts in specimens than air drying and chemical fixation. It consists of two steps, cryoimmobilization and further preparation of the sample. This further preparation can include freeze-substitution, resin embedding, microtomy and/or staining.

Step 1: Cryoimmobilization

Cryoimmobilization is the immobilization of cells using rapid freezing of the material, i.e. freezing (cellular) water so quickly that ice crystallization does not have the opportunity to occur (vitrification[9]). The advantages of preventing ice crystal formation and bringing cellular components to a rapid standstill, encourage the belief that rapid freezing is a more gentle and structure preserving alternative for immobilization of biological samples than drying in room temperature.

Preventing ice crystal formation by vitrification is important in maintaining native cell structures, as ice crystals form from pure water, displacing solutes inside the cell. This means that inside a cell frozen by conventional methods, ice crystals will form from pure water, thereby increasing the solute concentration in the rest of the cellular water, as cells do not contain 100% pure water. This increase in concentrated solute will impede crystal growth, causing a ramified, branched crystal to form throughout the cell. Separation of solute and pure water inside cells during ice crystallization is unfortunate when the aim is to keep and observe the native conformation of a cell, so vitrification, i.e. rapid freezing, is desired when freezing biological samples for structure conserving purposes.

Rapid freezing can be performed in a number of different ways. For

[9]Vitrification is the formation of a structureless, glass-like solid that is called vitreous ice, forming when water molecules are brought to a standstill so fast that they don't have time to nucleate.

the smallest bacteria, isolated protein complexes, viruses and single cells, rapid freezing is commonly done by **plunge freezing**: plunging them (surrounded by a thin film of water) into a cryogen, a liquid cooled to near its freezing point by e.g. liquid nitrogen. By this method, sample temperatures can drop by up to 10^5 °C/s. [50], freezing the entirety of small samples within milliseconds. As freezing starts on the surface and cooling rates decrease with the depth of the sample[10], larger samples require different rapid freezing techniques. Among the techniques developed and found useful for biological alternatives are **slam freezing**, **jet freezing** and **spray freezing** [51].

Due to the decreasing freezing rates deeper into the sample, ice crystals form instead of vitreous water when approaching the center of the sample. This ice crystal formation can damage surrounding, vitrified areas. One way of avoiding ice crystal formation is to use chemical agents named cryoprotectants, which (1) *lower the temperature at which homogeneous nucleation occurs* (making it tougher for ice crystals to form), (2) *raise the recrystallization temperature* (vitreous ice must reach a higher temperature to turn into ice crystals), and (3) *reduce the free water in the system* (recalling that ice crystals form from free, or pure, water) [52]. Cryoprotectants can be either intra- or extracellular, i.e. they can either penetrate the cell membrane or not. The cryoprotectant should be chosen carefully, as it is paramount to conserve cell structures and make post-preparation as easy as possible. Intracellular cryoprotectants are known to have the potential to interfere with cell physiology more than extracellular cryoprotectants have. In the case of freeze plunging, 1 mm^3 of water can be vitrified using cryoprotectant, according to [36].

Step 2: Preparing the frozen sample

Imaging of (frozen) samples in an electron microscope sometimes requires further preparations. For example, when a sample is to be observed by TEM, it needs to be very thin (down to under 100 nm [53]). Reducing sample thickness can be done by microtomy, the slicing of a specimen into thin slices. By microtomizing the sample and reconstructing images taken in the electron microscope of different slices, one

[10] as water has poor thermal conductivity

can also achieve 3D images of e.g. a cell, with its content clearly separated and not superimposed on top of one another [53], but this method is laborious, however, and with bioaerosols, a good result is strongly dependent on the microtomizing not distorting native bioaerosol conformation in any way.

There are mainly two ways of producing thin samples of rapidly frozen biological material for electron microscopy observation. One route is to subject the samples to microtomy in frozen states. The biological specimens are cut into thin slices while frozen, enabling them to be viewed section-wise in an electron microscope in frozen state, provided that the microscope has a cold stage, i.e. that the microscope is capable of operating while keeping specimen temperature below the temperature at which vitrified water crystallizes (According to [38]: $-135\,^{\circ}\mathrm{C}$). Observation of specimens in frozen state by electron microscopy is called **cryo-electron microscopy**.

The other method for preparing thin cellular samples for observation in an electron microscope using rapid freezing as a preparatory step, is to fix and dehydrate the specimens while they are still in a frozen state. This is called **fixation by freeze-substitution**, and involves using water-miscible organic solvents capable of remaining liquid at low temperatures as fixatives. These will penetrate and cross-link cellular material while it is still cold enough to retain its physiological structure. Fixation by freeze-substitution is followed by embedding the sample in a plastic resin, allowing it to be microtomized and observed in an electron microscope at room temperature conditions.

The different cryopreparation methods are summarized in figure 3.

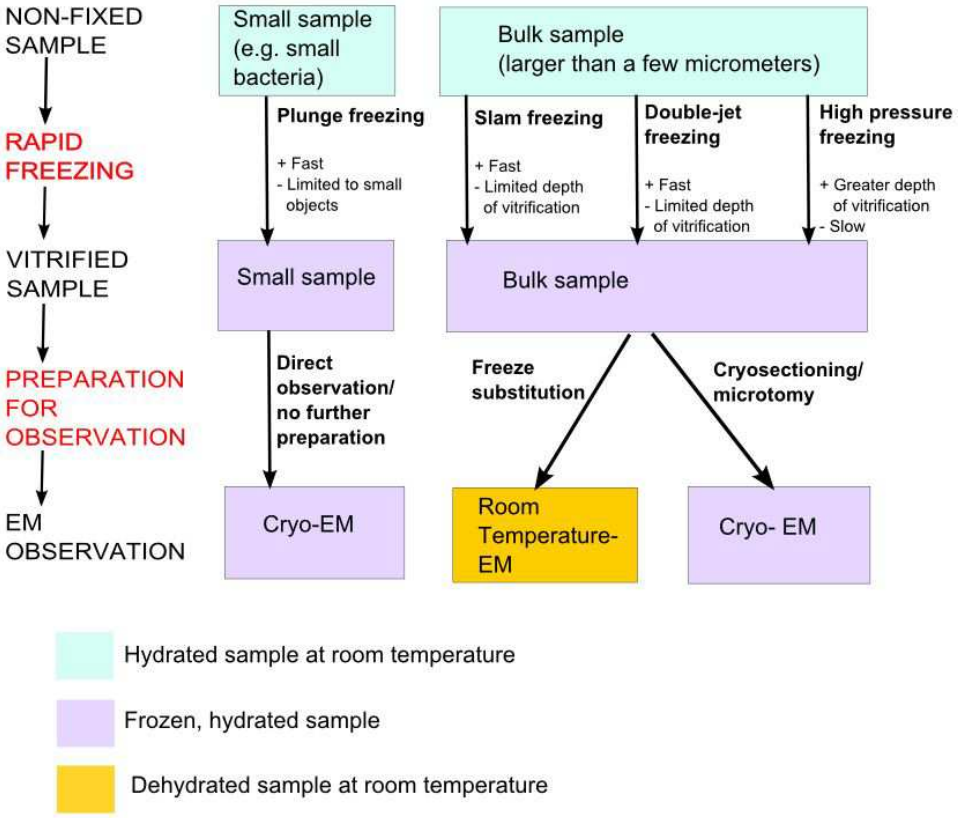

Figure 3: Overview of different cryopreparation methods and further preparation routes. Advantages and disadvantages of each technique are included. Modified version of figure from [36].

2.2.5 Sputter coating

The source material for this section is found in [41] and [54] unless otherwise noted.

Coating bioaerosols with a conducting material (e.g. Au, C, Cr, Pt or Pd) before SEM is usually necessary to avoid charging effects due to electrons from the electron beam being "trapped" in the specimen[11]. These charging effects cause low resolution and poor image quality, and are therefore undesired.

Coating is usually conducted in a sputter coater, where the operator can control coating material and thickness. Choice of coating material is important in deciding the properties of the coated specimen. Ideally, the material should have high electric conductance and electron density, allow for a high secondary electron release from the specimen beneath and not form oxides nor granular structures when thin. Gold has been used to coat bioaerosols in the past [20], and is a popular coating material, but it has a coarse structure when viewed at high magnifications, making gold a less ideal coating material prior to electron microscopy, even though it meets four out of five material criteria. Different metals and alloys have been researched for their coating properties, but no perfect coating material has been found, owing to even fine-grained materials' ability to react and form visible structures with different substrates. It has been found that as long as the coating layer is kept under 2 nm, a Pt/Pd alloy works well when coating biological samples [54]. However, at very high magnifications, coating, independent of coating material, may limit resolution by covering small structures and introducing a characteristic surface structure.

The coating material for samples to be examined by EDX, should ideally be of low atomic number as to not interfere with element spectra. A common coating material is thus carbon, as used by e.g. Matthias-Maser et al. (2000)[55] when examining bioaerosols from water by SEM and EDX.

The thickness of the coating layer is decided by the need for electrical conductivity and reduction of charging effect (favoring thicker layer)

[11]The trapped charges may deflect the beam when this is incident on a charge-accumulated area in the sample.

and the need for good structure reproducibility and no externally introduced structure (favoring thinner layer). Usually, the thickness of a coating layer on a sample prepared for field emission (FE) SEM is between 0,5 nm and 2 nm.

The sputter coater operates in vacuum, and is thereby a possible point of dehydration artifact introduction when readying bioaerosols, or other biological material, for electron microscopy. Coetzee et al. [18] considered this when preparing fungal structures for observation by ESEM, and sputter coated the specimen in a sputter coater with higher pressure than standard apparatus. They observed that this improved the structural integrity of the samples compared to sputter-coating in normal vacuum mode.

2.3 Electron microscopy of bioaerosols

When using electron microscopy to observe and image bioaerosols or other biological structures, there is a multitude of different electron microscopes and techniques to choose from. Some of the following techniques have been performed on bioaerosols, but in the case where no previous study has detailed a technique's applicability to bioaerosols, studies of subjects similar to bioaerosols are presented. Similar subjects can be bacteria and other hydrated structures.

2.3.1 Transmission Electron Microscopy (TEM)

The source material for this section can be found in [41], [56] and [57] unless otherwise noted.

TEM is a microscopy technique that uses an electron beam to image thin specimens (<100 nm) in vacuum with an obtainable resolution down to below 1 Å [58]. The electron beam travels through the whole sample simultaneously (not scanning it point by point) and different signals are collected and detected on both sides of the sample. Signals generated from a thin specimen upon impact with a high energy electron beam are presented in figure 4.

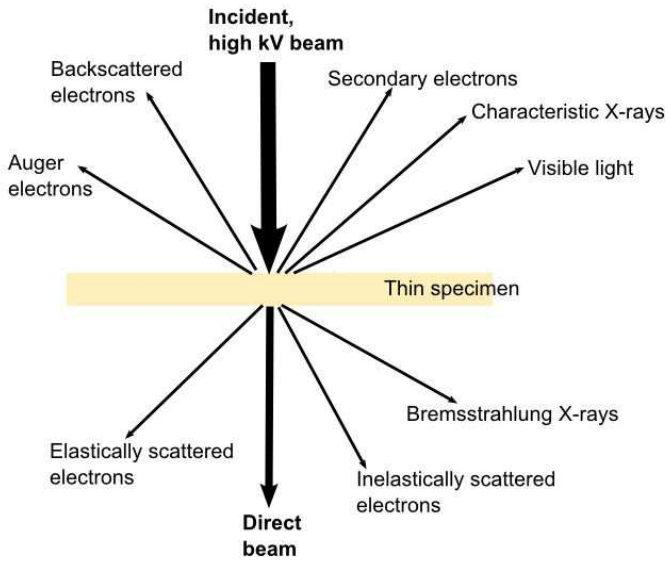

Figure 4: Schematic overview of signals generated in a thin sample when it is hit by a high electron energy beam. Most of these signals can be detected in TEM. Modified version of figure from [56].

The advantage of TEM is that it can yield high-resolution images of a specimen, as well as structural information as the electron beam diffracts on impact with crystalline material. Because bioaerosols are normally amorphous and not crystalline, the objective of using TEM to image such samples would be to obtain mass-thickness contrast, and not crystal diffraction patterns. In bioaerosol context, the advantage of TEM is its high resolution and possibility of transmitting electrons through samples, thereby revealing inner content, which can be useful when interesting contents of the bioaerosols, microorganisms, are covered by inorganic material and cell debris.

In order for the electron beam to be able to pass through the specimen, bioaerosols should not be thicker than approximately 100 nm; thicker samples will block electron beams up to 125 kV from passing through. Higher beam acceleration voltages will allow the sample to be slightly thicker, but are more destructive to biological material. Samples 30 nm to 60 nm thick give the best resolution, according to Bozzola

[41].

TEM resolution is in the size order of electron beam wavelength, and is limited by beam diffraction[12]. This limitation is accounted for in Abbe's equation, giving the resolution limit in a perfectly optical system:

$$d = \frac{0,612\lambda}{n_0 sin\alpha} \tag{1}$$

The resolution, d, is the shortest distance two points can have between each other in order to still be distinguishable from one another, λ is the electron wavelength, n_0 is the index of refraction of the medium the electron beam travels through, and α is half the angle of the light cone entering the objective (half the aperture angle in radians). This is just the theoretical resolution, if aberrations or distortions are present, the practical resolution limit will be larger.

The wavelength of electrons varies with the beam energy, as shown below:

$$\lambda = \frac{h}{p} = \frac{hc}{\sqrt{E_{tot}^2 - m_0^2 c^4}} \tag{2}$$

or alternatively:

$$\lambda = \frac{1.23}{\sqrt{V}} \tag{3}$$

Here, h is the Planck constant and p is the electrons' momentum. E_{tot} is the total energy of the beam, while m_0 denotes the resting mass, and c the speed of light. In equation 3, λ is given in nm when V, the acceleration voltage, is given in kV. Calculating the wavelength for different beam energies gives the results presented in table 1:

[12]No two objects can be distinguished from each other if their first diffraction peaks are closer to one another than the distance between one diffraction pattern's maximum and first minimum.

Table 1: Wavelength of electrons at different energies.

Energy [kV]	λ [Å]
1	0.39
10	0.12
25	0.077
200	0.025

The theoretical resolution attainable by using a 200 kV acceleration voltage is approximately 0.0013 nm, found by inserting the electron wavelength into equation 1 and using 1.5 as n_0 and 0.9 as $sin\alpha$. Real resolution is restricted by conditions given by the lenses, such as spherical and chromatic aberration and astigmatism, giving obtainable resolutions less than 0.1 nm as mentioned earlier.

Some researchers have detailed observation of bioaerosols by TEM. A study by Pósfai et al. [16] describes sampling and subsequent study of aerosol bacteria with TEM, using an acceleration voltage of 200 kV. Bacterial structures were clearly visible. A study by Glikson et al. [11] details the sampling of aerosols (including pollen and fungal bioaerosols) in Brisbane, Australia, and preparation and observation of these aerosols by TEM. Results from the analysis could be used to distinguish between different types of aerosols, as well as their size. While Pósfai et al. did not prepare their samples specifically, Glikson et al. dried, embedded and sectioned the aerosols before TEM observation. None of the studies describe distortions due to TEM vacuum, although vacuum-induced distortions are known to happen to biological material. Using an atomic force microscope (AFM), Gwaze et al. [22] reported that water-containing ammonium sulphate aerosols with an aerodynamical diameter between 0.2 µm and 0.7 µm shrunk up to 75% when exposed to TEM vacuum.

Another challenge with TEM imaging of biological material, is the heating of the material during electron beam impaction. This is a problem for biological samples in particular, because of their low conductivity.

2.3.2 Scanning Electron Microscopy (SEM)

The source material for this section can be found in [41] and [57] unless otherwise noted.

SEM is a microscopy technique used to image specimens in vacuum with a possible resolution down to 1 nm (in a high-resolution SEM), using a focused electron beam probe that scans the surface of the sample in a raster. Information from SEM originates from interactions between electron beam and sample in a given volume under the sample surface, which generate signals in the form of mainly electron or X-ray radiation. Some of the signals generated in a thick sample on impact with an electron beam are presented in figure 5. Non-conducting samples can trap the electrons impacted on the surface, leading to charge build-up and degrading of the image quality.

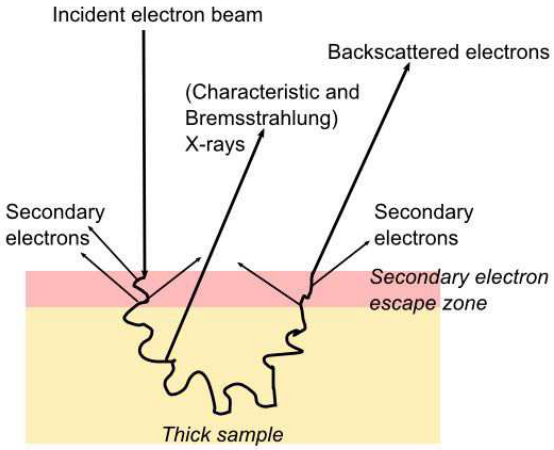

Figure 5: Schematic overview of some of the signals generated in a thick sample when it is struck by an electron beam. Figure inspired by [57].

SEM based on secondary electrons (SE) provides information about sample topography and composition, providing large depth of field which yields a three dimensional-like image of the sample surface. As information about the sample comes from a limited area given by the

beam spot size, the magnification in SEM is dependent on the spot size of the beam used to raster the surface; smaller beam size permits higher resolution.

The advantage of SEM over other electron microscopes, is the generation of intuitive, high-resolution, three dimensional-like images of larger, unsectioned samples. In bioaerosol context, this is useful because the specimens do not have to be microtomized, and can thereby maintain their structure better, while the resolution is much higher than that of a light microscope[13], and is high enough to discern bioaerosol components.

Several studies on imaging bioaerosols by conventional SEM have been done, using various techniques for preparing samples. Matthias-Maser and Jaenicke [10] have reported on biological aerosols sometimes being unstable to the electron beam of the SEM during an experiment, and Vestlund [20] noted distortion in bioaerosols prepared and observed in vacuum. Many articles do not mention shrinkage or morphology changes of unprepared or only coated bioaerosols in SEM vacuum [3] [11] [14], however, even though this is a well-known problem for biological material [21] [17] [59]. Exposing water-containing aerosols, among many of them biological particles (e.g. about 50 % brochosomes), to SEM vacuum and comparing sizes before and after vacuum exposure using AFM, Gwaze et al. [22] found a shift in particle size average from 0.63 μm before exposure, to 0.25 μm and 0.54 μm after exposure to SEM vacuum. Gwaze et al. attributed the size decrease to vacuum-related losses of water and volatile compounds and possible thermal degradation of the particles due to the electron beam.

[13]Light (optical) microscope resolution is theoretically approximately 200 nm, but is lower under real circumstances due to lens imperfections.

2.3.3 Scanning Transmission Electron Microscopy (STEM)

The source material for this section can be found in [60] and [41] unless otherwise noted.

STEM combines the features of both SEM and TEM, it is something in between SEM and TEM. STEM is able to both raster the surface of a sample using a fine electron probe and transmit the electrons through the sample to obtain diffraction patterns and information about the inside of the sample. A requirement for the transmission function to work, however, is that the sample needs to be thin, it should be as thin as samples for TEM. STEMs can be TEMs with a raster function built in or SEMs with added transmission detectors. STEMs can contain a selection of SE, backscattered electrons (BSE), X-ray, annular dark field and bright field detectors as well as an electron energy loss spectrometer (EELS) positioned underneath the viewing screen. Multiple detectors working simultaneously allow the STEM to collect the maximum possible information from each scan, thus utilizing and exploiting every electron in the electron beam. STEM can yield both topographical, structural, elemental and mass information of a sample, owing to the array of detectors. What kind of image that is received in STEM is dependent on the detector used. Bright field STEM delivers mass-thickness contrast (similar to bright field TEM), while annular dark field STEM is sensitive to atomic number as well.

STEM allows for resolutions close to that of TEM, using a field emission electron source it can achieve resolutions down to 2-3 Å [61] or recently even sub-ångström resolution using an aberration-corrected 300 keV STEM. For the imaging of biological specimens, an advantage of STEM as opposed to TEM is the ability to image samples in dark field mode without requiring staining. This is due to STEM's high signal to noise-ratio owing to the annular dark field detectors in STEM being able to collect all scattered electrons even at large angles [62] [61].

Increasing the acceleration voltage in STEM will increase the allowable specimen thickness and increase spatial resolution of the bulk as the electron wavelength is shortened. However, even though the specimen can be thicker in STEM than in TEM and still provide a transmission image, a 200 keV STEM will not be able to transmit electrons through samples thicker than a few micrometers [63].

Another advantage of STEM is the possibility of putting together a 3D representation of a specimen (including its inside) from a series of scan images taken successively deeper into the sample. This technique requires an aberration-corrected STEM with a small depth of field. This technique, however, works only for very thin, non-biological specimens, so it is not suitable to use with bioaerosols. The tomography technique, imaging a series of thin slices, could be applicable to bioaerosols for generating a 3D image.

No detailed study on imaging bioaerosols using STEM has been reported, according to the author's knowledge. According to Colliex and Mory [62], the annular dark field STEM technique is capable of imaging any type of cryofixed specimens, even though they designate the technique to specifically apply to small macromolecules (such as DNA) and supramolecular structures (such as virus heads). According to Wall and Hainfeld [61], the best way to prepare specimens (here: Tobacco Mosaic Virus for nucleic acid observation) is by freeze-drying, as this prevents distortions during drying and do not obscure portions of the sample as it does not introduce a second medium. This is a dated study however, a study by Bárcena et al. [64] suggests that cryoimmobilized frozen-hydrated biological specimens are very sensitive to radiation damage, and the allowable electron dose is therefore a limiting factor for imaging [65].

2.3.4 Energy-Dispersive X-ray Spectroscopy (EDX)

The source material for this section can be found in [41], [57] and [56] unless otherwise noted.

EDX is a spectroscopy technique which in combination with SEM, TEM or STEM can yield qualitative and quantitative information about the elemental composition of a sample. The technique is based on a detector detecting X-ray signals emitted from the sample on interaction between electrons in an electron beam and atoms in the observed sample[14]. As the X-ray radiation emitted is unique for each element (and for each electron transfer between different electron energy levels), different elements heavier than atomic number 8 (Mavrocordatos et al. [66]), 6 (Bozzola and Russell [41]) or most recently: 5 (Egerton [67])[15], can be distinguished and traced to a specific location on the specimen. This tracing can generate different types of maps and spectra, showing the presence of different elements in the sample qualitatively with resolutions down to approximately 10 nm for biological material.

Automatic detection and elemental analysis of specimen particles is possible using specialized software in combination with X-ray detection.

Using EDX for quantitative analysis is generally more challenging than qualitative analysis, requiring stringent specimen preparations and yielding an error of approximately 20 % [66]. Optimal EDX specimens, regardless of whether used in SEM, TEM or STEM, should be thin and smooth and electrically and thermally conductive to obtain high-quality EDX results, in addition to being surrounded by elements of low atomic number to avoid interfering X-ray signals. When EDX is conducted on bulk specimens, lower resolution of qualitative results and restricted quantitative results are expected, due to large lateral and radial interaction volume of the primary electron beam into the sample, as well as uneven sample surface.

[14] When electrons interact with atoms in the sample, they can eject electrons from shells of these atoms, leading to higher-energy electrons taking their place, and subsequently emitting characteristic X-ray radiation. The continuous X-ray radiation spectrum appears as a background spectrum due to the slowing of, and subsequent emission of X-rays from, electrons on impaction with atoms.

[15] demonstrating the technological developments due to detectors with thinner windows and no windows.

EDX is most commonly used in combination with SEM, and detection is carried out at higher acceleration voltages than in conventional SEM. The high acceleration voltages can potentially induce changes in volatile biological specimens during analysis.

Matthias-Maser and Jaenicke [10] have carried out studies of SEM EDX on 0.2 µm - 10 µm aerosols sampled on graphitic foil collection plates. They categorized bioaerosols based on the three following criteria: 1) Rod-, elongated, curved or special morphology; 2) EDX-spectrum showed high background and/or small peaks of (Si, Cl), P, S, K and Ca [55]; 3) Shape changes during EDX or no shape changes. Matthias-Maser and Jaenicke used the results to map the relative amount of bioaerosols to aerosols, but did not conduct a quantitative EDX analysis, the results were derived only after qualitatively characterizing all aerosols present in the sample. All bioaerosols could not be detected however, as some vanished in the vacuum and under the electron beam without leaving any residue.

2.3.5 Cryo-electron microscopy

The source material for this section is taken from [23] unless otherwise noted.

To keep samples that are frozen by cryo-techniques cold during electron microscopy observation, it is necessary that microscopes maintain the samples' cryogenic temperatures. Cryo-electron microscopy includes cryo-SEM, cryo-TEM and cryo-STEM and consists of respective microscope equipment equipped with a cold-stage sample holder maintaining temperatures below $-135\,^{\circ}\mathrm{C}$, which is the temperature at which vitrified water recrystallizes [38]. The advantage of cryo-electron microscopy is that samples can be viewed at equally high resolution as in conventional electron microscopy, due to the observation taking place in vacuum, while the samples still can retain their structure due to the immobilization of intracellular water at cryogenic temperatures.

Dohnalkova et al. [23] have imaged bacterial cells both by cryo-SEM and cryo-TEM. To avoid charging effects, the rapid-frozen bacteria were coated with platinum prior to observation in the cryo-SEM apparatus. The rapid-frozen cells to be observed with cryo-TEM were not microtomized. The temperatures of the cryo-SEM and -TEM cold-stages were respectively $-180\,^{\circ}\mathrm{C}$ and $-178\,^{\circ}\mathrm{C}$ before and during imaging. The extracellular polysaccharide (EPS) structure of the bacterial cells in the cryo-TEM images was reported on having low contrast against the surrounding vitrified water due to little difference in the electron density of the two phases. The EPS in the cryo-SEM images was clearly visible, but as the temperature of the sample was raised, the structure started collapsing at around $-150\,^{\circ}\mathrm{C}$.

No study on the observation of bioaerosols sampled on filter, rapidly frozen and observed with cryo-electron microscopy has been published, according to the author's knowledge.

2.4 Nature of bacterial species included in this study

Bacillus globigii (BG)[16] spores are endospores formed from Gram positive, aerobic microorganisms, and they are very resilient and capable of enduring extreme conditions such as e.g. temperature variations and desiccation [68]. The size of a *BG* spore is approximately 1.0-1.6 μm in length and 0.6-0.9 μm in width [69]. *BG* spores are commonly used as a *Bacillus anthracis* (*B. anthracis*) (causative agent for anthrax) simulant, as they resemble *B. anthracis* spores in particle size and dispersion characteristics, and are deemed harmless for healthy human adults [70]. Due to their toughness, spores should not experience significant conformational change in the SEM vacuum, but some species of spores are surrounded by exosporium, which is volatile in vacuum. *BG* spores are not covered in exosporium, but *B. anthracis* spores are covered in this [71], hence the two spore species will most likely look different in the electron microscope.

Serratia marcescens (*S. marcescens*) is a Gram negative, rod-shaped bacterium approximately 0.9-2.0 μm in length and 0.5-0.8 μm in width [72]. It can cause disease in plants and act as an opportunistic human pathogen [73] causing infections in body sites [68]. *S. marcescens* is commonly used as a simulant for other vegetative Gram negative bacteria. Gram negative bacteria are less resistant to physical disruption than Gram positive bacteria [74], and *S. marcescens* bacteria are more vulnerable to dehydration under vacuum conditions than *BG* spores.

[16] Also known as *Bacillus atrophaeus* and *B. subtilis var. niger*

3 Experimental

To ensure reproducibility and comparability of the experimental results, a set of protocols were collected in conjunction with the experimental work demonstrated in this thesis. Appendix A contains protocols for buffer fixatives, sputter coating and CPD. The collection of bioaerosols for TEM and SEM observation is presented in the following sections.

3.1 Bioaerosol collection

As SEM and TEM imaging requires bioaerosols to be deposited on different substrates, two individual procedures for the collection of bioaerosols were followed for SEM and TEM respectively.

3.1.1 Collection of bioaerosols for SEM observation

Desired bacterial cells or spores to be observed by SEM[17] were aerosolized inside a sealed aerosol chamber using a Hudson nebulizer (producing droplets up to 10 μm in diameter) or a Sonotek ultrasonic atomizer nozzle (producing larger droplets of approximately 38 μm in median diameter). Only one bacterial species was disseminated at the time. Millipore sampling cassettes, each equipped with a 25 mm Millipore Isopore^{TM} hydrophilic polycarbonate membrane filter with pore size 0.4 μm, were placed in the aerosol chamber.

The bioaerosols containing bacterial cells or spores were kept circulating inside the chamber by a system of fans. Air from the aerosol chamber was drawn through the cassettes at approximately 12 liters of air/min for 10 minutes, thereby depositing bioaerosols onto the filter inside the cassettes.

After sampling, the aerosol chamber was ventilated and the filter cassettes removed.

[17]The bacterial cells and spores used in this study were pre-freeze-dried, -milled and washed three times with water. The bacterial cells and spores were dispersed in water in high concentration.

3.1.2 Collection of bioaerosols for TEM observation

For sampling of bacterial cells or spores on TEM grids for subsequent TEM observation, a six-stage Andersen sampler was used to sample species directly onto the grids. The TEM grids used were copper grids (3 mm in diameter) covered with carbon-coated Formvar functioning as support film[18]. The grids were produced by Ted Pella, Inc. TEM grids destined for sampling were placed on an acrylic glass plate in a glass Petri dish in the last stage of the Andersen sampler (see figure 6), ensuring the sampling of particles larger than approximately 0.65 µm in diameter. All other stages of the Andersen sampler were kept free of objects.

Figure 6: The Andersen sampler used to sample bioaerosols directly onto TEM grids. (a) The completely assembled Andersen sampler. The TEM grids were placed in the last stage, i.e. the bottom of the sampler. (b) The inside of the last stage. The disk in the back of the image in (b) contains a large number of 0.24 mm holes, and goes over the glass petri dish and acrylic glass plate, which contains the TEM grids. The green markings represent spots that lie directly underneath a hole.

[18]Carbon Type B (15-25nm) with Formvar on 200 mesh [75] [76].

To ensure direct sampling of bioaerosol particles onto the TEM grid, the grid needed to be placed directly under one of the 0.24 mm in diameter holes of the last stage of the sampler, which was challenging considering that the small hole size prevented both penetration (of a rigid tool for marking purposes) and visual inspection through the holes. This was solved by first sampling a high concentration of *S. marcescens* bioaerosols on the empty acrylic plate fixed to the sampler base by double-sided tape, and marking off the visible spots where particles had deposited on the plate with a waterproof marker. The exterior of the Andersen sampler was also marked, so that the different compartments could be aligned correctly every time. The bacteria could then be cleaned off the acrylic plate, and TEM grids placed on a penned dot with some double-sided tape in the corner, to be sure that bioaerosol particles deposited directly onto the grids. The setup with markings is illustrated in figure 6. The setup is devised and crafted by the author.

The sampler with grids was placed inside the aforementioned aerosol chamber, and the same mechanisms as before contributed to droplet dispersal and air flow through the chamber, leading to air flow through the Andersen sampler and deposition of particles onto the TEM grids carefully positioned inside the sampler. Air was sucked out of the Andersen sampler at approximately 28 liters of air/min.

After sampling, the aerosol chamber was ventilated and the TEM grids removed from the Andersen sampler.

3.2 CPD of bioaerosols containing *BG* spores or *S. marcescens* vegetative cells fixed by 10% glutaraldehyde vapor

For the whole process of CPD of respectively *BG* spore- and *S. marcescens*-containing bioaerosols, particles were sampled on eight filters in total (four for each species, including two each for single and aggregate particles, respectively). Only four pieces of filter underwent CPD, as the rest of the filters were used as references to compare the effects of CPD to glutaraldehyde vapor fixation as well as to no specific preparation procedure.

BG spores and *S. marcescens* bacteria were chosen because of availability at FFI and because the two species represent resilient and sensitive particles, respectively. The *BG* spore bioaerosols will therefore provide a reference to bioaerosol imaging with little particle collapse, while the *S. marcescens* bioaerosols simulate the challenging behavior of most environmental bioaerosols.

The entire sample set and individual process routes are presented in figure 7.

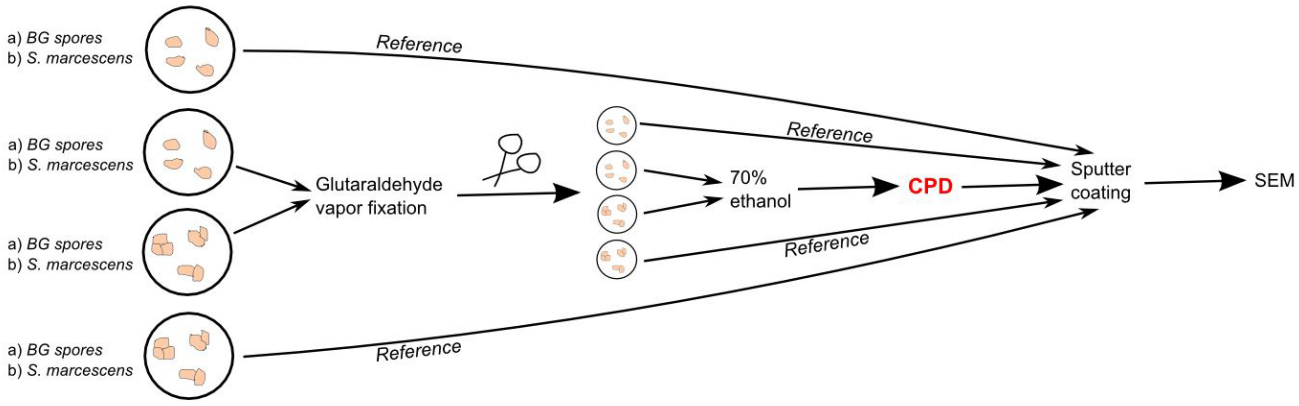

Figure 7: Schematic overview of SEM filter samples and process routes for CPD experiment with 10% glutaraldehyde vapor fixation, including reference samples. The circular figures represent the filters after sampling of bacterial cells or spores. Note that the top filters represent filters containing small bioaerosols, and the bottom filters represent filters containing large bioaerosols. After fixation, filters were cut into smaller pieces by scissors to fit into the CPD holder. All samples were sputter coated with Pt/Pd.

3.2.1 Collection

Collection of *BG* spore and *S. marcescens* bioaerosols followed the procedure described in section 3.1.1. The collection procedure was repeated four times with two filters each time, collecting both small and large droplets of both *BG* spore and *S. marcescens* solution aerosolized in the aerosol chamber. Both the Hudson nebulizer and the Sonotek ultrasonic nozzle were used to produce small and large droplets, respectively.

3.2.2 Fixation

To both neutralize the pathogenic *S. marcescens* bacteria and stabilize the particle structures, fixation was applied to the specimens directly after collection. The choice of glutaraldehyde as fixation chemical was based on availability at FFI as well as low toxicity.

For the fixation, an original setup was devised which allowed glutaraldehyde solution to vaporize and deposit onto selected specimens, without heating them, and also prevent the vapor escaping into the laboratory environment. The specimens, on filter or TEM grid, were placed on top of a solid plastic cylinder, which together with an identical cylinder comprised a column 9 cm in height and 6 cm in diameter. This column was put on a heating plate together with a magnet stirrer and an aluminum foil cup containing 14 ml aqueous glutaraldehyde solution of 10% concentration. The plastic material of the column conducted heat very slowly, and prevented specimens from heating to the same temperature as the heating plate.

A glass beaker was placed over the hot plate, and sealed by aluminum foil and tape. The entire setup was contained inside a fume hood and allowed to sit overnight for approximately 19 hours. The hot plate was kept at 50 °C for the first hour, then turned off. The magnet stirrer stirred for the duration of the fixation procedure. The setup is pictured in figure 8.

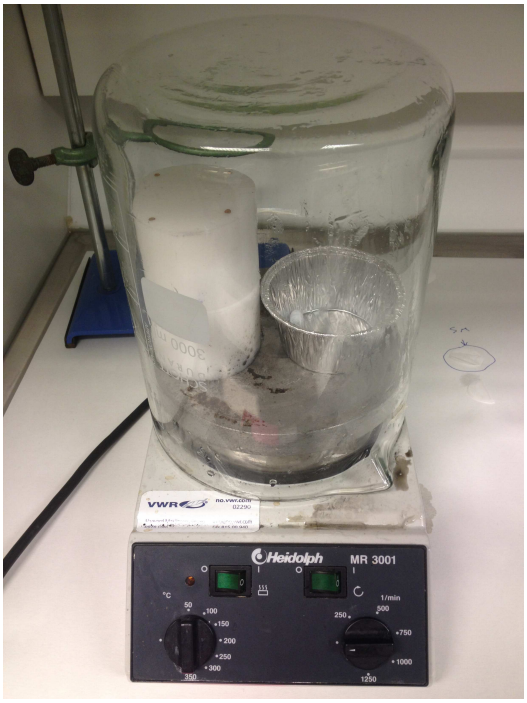

Figure 8: The 10% glutaraldehyde vapor fixation setup. The heating plate was held at 50 °C the first hour, then turned off. The magnet stirrer was kept on for the entirety of the fixation, approximately 19 hours. The opening (spout) in the glass beaker was sealed with aluminum foil and tape during the experiment.

After 19 hours of vapor fixation, the specimens were removed from the setup and cut in smaller pieces by scissors. A piece of each filter[19] was placed inside individual cell culture plates and a solution of 70% ethanol was added to the plates, so that the filter pieces were submerged in liquid. For a better overview of the process, consult figure 7.

The cell culture plates were covered with a lid and wrapped with Parafilm (to contain moisture), before being transported (horizontally) to the CPD location.

[19] cut into asymmetric shapes identifying correct side up

3.2.3 CPD processing

The CPD took place at the EM-lab at the University of Oslo (UiO). Filter pieces were quickly transferred from cell culture plates containing 70% ethanol to a CPD sample holder and dehydrated in an ethanol series. The samples then underwent CPD in a Bal-Tec CPD instrument. The procedure is described more closely in section A.2 in appendix A.

3.2.4 Sputter coating

All the *BG* spore and *S. marcescens* samples, including both unfixed, fixed and critically point dried, were coated with a 2 nm Pt/Pd layer according to the protocol in section A.3 in appendix A.

3.2.5 SEM observation

All the bioaerosol-containing filters, regardless of preparation method, were imaged in a Hitachi SU6600 analytical variable pressure (VP) field emission gun (FEG) SEM and analyzed in secondary electron (SE) mode. The bioaerosols were analyzed in SEM at magnifications of 6000x and 30000x, as well as at some other situation adapted magnifications, in order to get both an overview of the particles on the filters and more detailed images of the bioaerosols. All SEM micrographs were taken at acceleration voltage 1 kV, probe current small, condenser lens 20, extraction voltage 1.80 kV and working distance $\sim$6 mm.

Due to the large number of particles on each filter, it was not possible to examine all the particles present on each filter within the scope of this thesis. To ensure representativity of the particles presented in the SEM micrographs, multiple images were taken at five different locations on each filter (in the center, and in four directions ("north, east, south, west")). The micrographs presenting the most clearly represented and common particle conformations were then chosen out of these to be presented in this thesis.

3.3 CPD of bioaerosols containing *S. marcescens* vegetative cells fixed by 70% glutaraldehyde vapor

To provide an alternative to the water rich 10% glutaraldehyde fixation detailed in the above section 3.2, 70% aqueous glutaraldehyde vapor was used to fix small and large *S. marcescens* bioaerosols. An overview of the experimental setup is presented in figure 9.

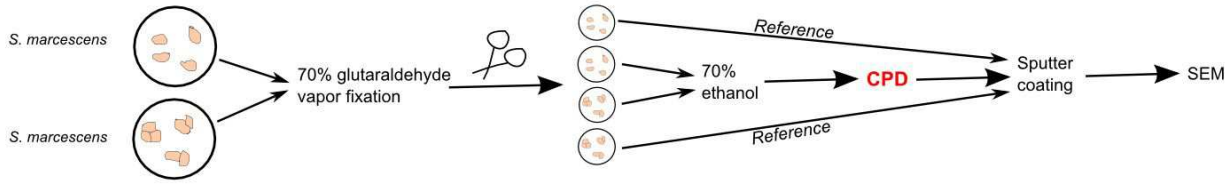

Figure 9: Schematic overview of SEM filter samples and process routes for CPD experiment with 70% glutaraldehyde vapor fixation, including reference samples. The circular figures represent the filters after sampling of bacterial cells. Note that the top filters represent filters containing small bioaerosols, and the bottom filters represent filters containing large bioaerosols. After fixation, filters were cut into smaller pieces by scissors to fit into the CPD holder. All samples were sputter coated with Pt/Pd.

3.3.1 Collection

Collection of small and large *S. marcescens* bioaerosols to be fixed by 70% glutaraldehyde vapor was carried out identical to the collection of bioaerosols to be fixed by 10% glutaraldehyde vapor. The procedure is described in section 3.1.1. Both small and large bioaerosols containing *S. marcescens* bacteria were aerosolized and sampled in the aerosol chamber.

3.3.2 Fixation

Fixation with 70% aqueous glutaraldehyde fixation was carried out inside a fume hood directly after bioaerosol collection. The filters con-

taining specimens to be fixed were placed under an upturned glass dish, together with two small plastic disks containing a few milliliters of 70% aqueous glutaraldehyde solution each. The setup is presented in figure 10.

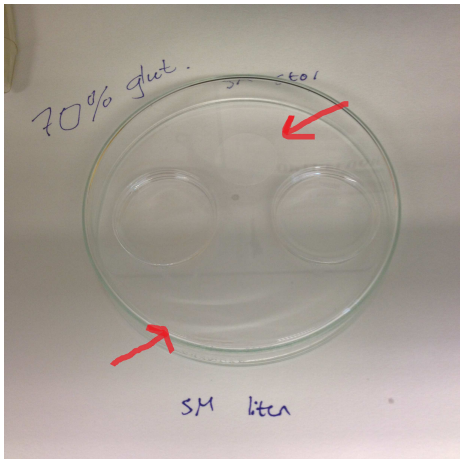

Figure 10: The 70% glutaraldehyde vapor fixation setup. The filters are indicated by red arrows.

The setup was allowed to sit overnight, and the filters were then cut into asymmetric shapes using scissors, submerged in 70% ethanol and transported to the CPD location. The remaining filter parts were kept as references, in accordance with the setup in figure 9.

3.3.3 Further preparation and observation

After fixation, the samples underwent the identical steps for CPD, sputter coating and SEM observation as detailed in sections A.2 and A.3 in appendix A, and in section 3.2.

3.4 CPD of *BG* spores and *S. marcescens* bacteria fixed by 2.5% liquid glutaraldehyde solution

In order to investigate the shape of the bacterial cells or spores before aerosolization, solutions of *BG* spores and *S. marcescens* vegetative bacteria were fixed by glutaraldehyde in liquid state and subjected to CPD. Some of the solution did not undergo fixation or CPD for reference purposes. The experimental setup and process routes are presented in figure 11.

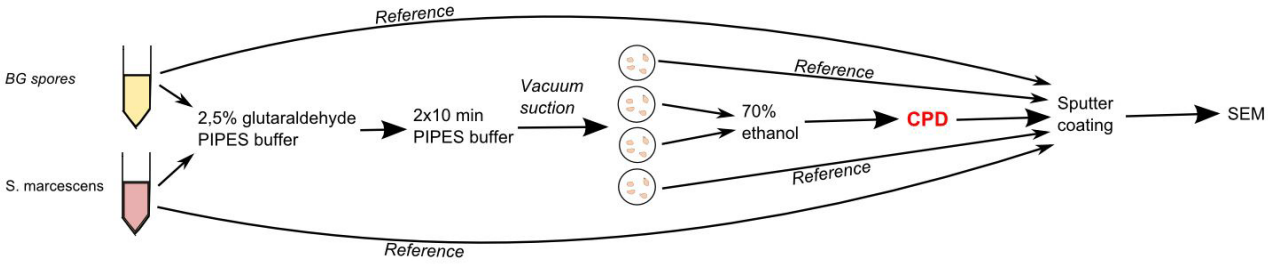

Figure 11: Schematic overview of process routes for the CPD experiment with 2.5% liquid glutaraldehyde fixation, including reference samples. The bacterial cells and spores were washed with PIPES buffer before the start of the process. All samples were sputter coated with Pt/Pd.

3.4.1 Fixation with 2.5% liquid glutaraldehyde solution

Before fixation, plastic tubes containing approximately 5 ml high concentration solutions of *BG* spores and *S. marcescens* bacteria, respectively, were spun down to produce pellets[20] of the bacterial cells and spores. The supernatant was removed and replaced by freshly prepared PIPES buffer[21], and the tubes were shaken and spun down to produce pellets again. This was repeated two times, until the supernatant was clear in color.

Approximately half the supernatant was removed and the tubes were shaken to evenly distribute the bacterial cells and spores in the

[20] By a centrifuge rotating at 6000 rpm for five minutes.

[21] According to recipe in section A.1 in appendix A, minus glutaraldehyde.

solution. A small amount (∼0.5 ml) of this solution was then transferred to polycarbonate filters by an original setup involving water suction[22]. The setup used in this study is pictured in figure 12. These filters served as reference to fixed and critically point dried samples, see figure 11.

Fixation with liquid glutaraldehyde was performed in a PIPES buffer. To make 100 ml of 2.5% glutaraldehyde in PIPES buffer solution with pH 7.2-7.4, the protocol in section A.1 in appendix A was followed.

The glutaraldehyde buffer solution was added to the plastic tubes containing pellets of the washed *BG* spores and *S. marcescens*, respectively. This was stirred briefly and allowed to sit overnight at 4 °C.

The next day, the bacterial cell and spore solutions were spun down to form pellets again, and the supernatant removed. A freshly prepared PIPES buffer not containing glutaraldehyde was added to the tubes, which were shaken and centrifuged for five minutes. The supernatant was again removed, and the last step was repeated once.

After the removal of approximately half the supernatant, the tubes containing the bacteria and spores were shaken to produce a solution of bacterial species in even distribution. Identical to the reference samples, approximately 0.5 ml of fixed solution containing *BG* spores and *S. marcescens* bacteria respectively, were transferred to polycarbonate filters by water suction, as pictured in figure 12.

[22]The function of the water suction was to provide the force needed for the particles to adhere to the filter surface. A similar setup using a vacuum flask is described by Kaláb, Yang and Chabot [77].

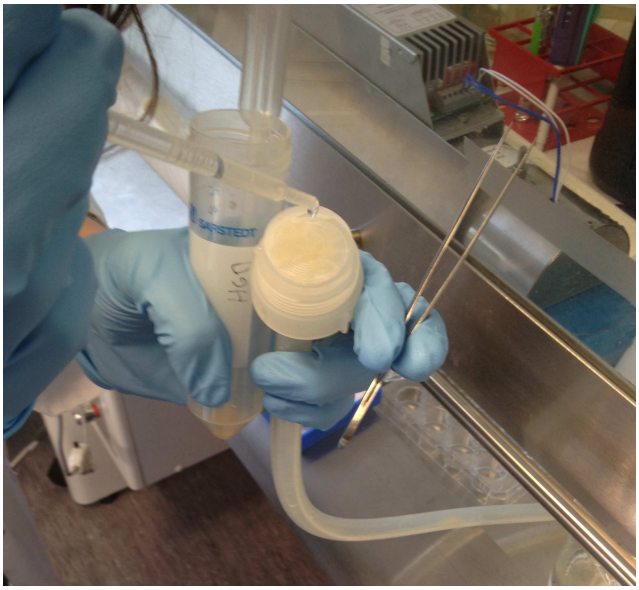

Figure 12: The transfer of fixed bacterial cells and or spores (here: spores) from solution to filter by water suction. A pre-cut 0.4 µm polycarbonate filter was placed on a plastic grid attached to a water suction system. To ensure vacuum suction and to simultaneously produce reference samples, several filter pieces were arranged to cover the entire plastic grid.

When the liquid was no longer visible on the filters, a small amount of ethanol was added to ensure extra adherence of the particles to the filter surfaces. When still wet, although liquid was no longer visible, filters were transferred to individual cell culture plates and submerged in 70% ethanol. These were then transported to the CPD location.

3.4.2 Further preparation and observation

The CPD, sputter coating and SEM procedures for the bioaerosols fixed by 2.5% liquid glutaraldehyde, followed the protocols detailed in sections A.2 and A.3 in appendix A, and in section 3.2, respectively.

3.5 CPD of bioaerosols containing *BG* spores or *S. marcescens* vegetative cells sampled on TEM grids and fixed by 70% glutaraldehyde vapor

This experiment assumes that carbon-coated Formvar TEM grids are hydrophobic [78] [79] [80], and explores the difference in adherence properties between these and hydrophilic polycarbonate filters. In order to investigate whether the bioaerosols would adhere better to TEM grids than polycarbonate filters during CPD, small and large *BG* spore and *S. marcescens* bioaerosols were sampled on TEM grids and subjected to CPD. For reference purposes, some filters did not undergo fixation or CPD. The process routes for this experiment are presented schematically in figure 13.

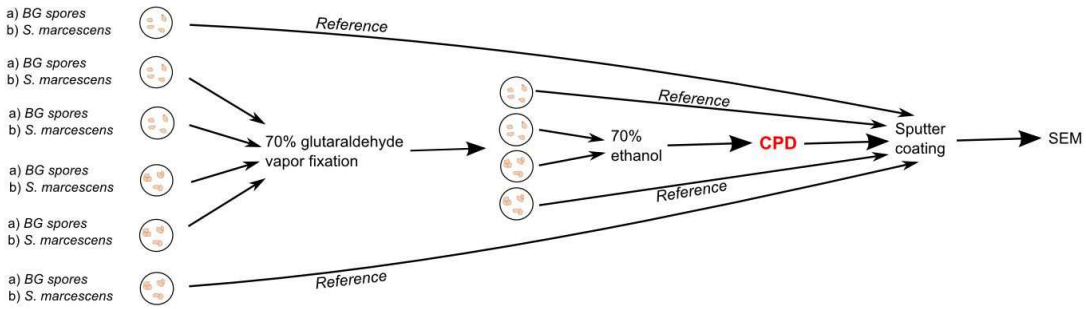

Figure 13: Schematic overview of process routes for the CPD experiment with bioaerosols sampled on TEM grids, including reference samples. 70% aqueous glutaraldehyde vapor fixation was used. Note that the top filters represent filters containing small bioaerosols, and the bottom filters represent filters containing large bioaerosols. All samples are sputter coated with Pt/Pd.

3.5.1 Collection

Small and large droplets of aerolized *BG* spores and *S. marcescens* bacteria were sampled on TEM grids according to the protocol described in section 3.1.2. The concentration of droplets per ml air during sampling

is indicative of bioaerosol concentration[23], and is given in table 2.

Table 2: Size and concentration of droplets per ml air during sampling of bioaerosols onto TEM grids for SEM imaging. Numbers were recorded in the aerosol chamber during aerosolization of bacterial cells or spores from solutions. The droplet concentration is indicative of bioaerosol concentration.

	Concentration [# of particles / ml air]	Particle size ≥ [μm]
Small *BG* spores	51.4	0.626
Small *S. marcescens*	157.3	0.626
Large *BG* spores	4.7	1.5
Large *S. marcescens*	4.3	1.5

3.5.2 Fixation, preparation and observation

Further preparation of the specimens was carried out in accordance with the plan in figure 13. Fixation with 70% glutaraldehyde vapor, subsequent CPD, sputter coating and SEM observation of the bioaerosols on the TEM grids were done according to procedures described in section 3.3, sections A.2 and A.3 in appendix A, and in section 3.2, respectively.

[23]Not all droplets counted during the sampling of small bioaerosols contain spores or bacteria, hence these numbers are only indicative of the actual spore/bacteria concentration.

3.6 TEM of bioaerosols containing *BG* spores or *S. marcescens* vegetative cells

Small and large droplets of both *BG* spore and *S. marcescens* bioaerosols were collected on TEM grids and analyzed by TEM at the EM-lab at UiO. This experiment was conducted in order to investigate what type of information TEM can yield when applied to bioaerosols, compared to SEM.

3.6.1 Collection and fixation

The collection of the specimens followed the protocol outlined in section 3.1.2, depositing bioaerosols directly onto TEM grids. Directly after sampling, fixation in 10% glutaraldehyde vapor was carried out as described in section 3.2. After fixation, the TEM grids were placed in individual, new containers where they were stored for 24 hours before transport to the TEM, where TEM was carried out immediately.

3.6.2 TEM observation

The TEM procedure was performed using a Phillips CM200 TEM operating in bright field mode at 120 kV with a CCD (charge-coupled device) operating at 11 Mb. The representativity of the particles shown in the bright field TEM micrographs is ensured by small size and low particle density on the TEM grids used in the imaging, yielding a small selection from which to choose micrographs.

3.7 EDX of environmental bioaerosol sample

In order to address the "needle in the haystack" issue, i.e. investigating initial methods for the automatic detection of bioaerosols against a natural background, environmental air samples were investigated by EDX. The samples investigated were sampled by drawing air onto Millipore polycarbonate filters[24] through a Millipore sampling cassette. The sampling took place indoors during daytime (11:40 am - 12:40 pm) and nighttime (04:00 am - 05:00 am) at the Nationaltheatret underground subway station in Oslo, Norway, in the middle of February 2011. The sampling conditions (not method) are described in a study by Dybwad et al. [81]. The underground subway station was nonoperative and closed to the public during nighttime sampling, and the activity on the location reduced to occasional maintenance work, and sometimes the passing of diesel-powered maintenance trains in the adjacent tunnel network [81]. The filters containing the aerosols have been contained in their sampling cassettes and stored refrigerated in a desiccator since collection.

Prior to subjecting the samples to SEM and EDX, the filters were mounted on SEM stubs and sputter coated with Pt/Pd according to standard protocol as described in section A.3 in appendix A. This coating was done to ensure comparability between SEM micrographs of the particles, although coating with heavy elements could possibly cover signal peaks from elements of low atomic number during EDX.

3.7.1 EDX procedure

EDX was carried out at the EM-lab at UiO using a Hitachi S-4800 FE-SEM using the Quantax microanalysis system with Esprit software by Bruker Nano. EDX was carried out at 10 kV acceleration voltage at 15 mm working distance. Automatic spectrum and map analysis was utilized.

Element mapping was performed for 5 minutes for specimens sampled during daytime, and 3 minutes for specimens sampled during nighttime, due to higher count rate for the latter samples (200-400 counts per second for daytime samples versus 1500-2700 counts per

[24]Identical to the polycarbonate filters used throughout this study.

second for nighttime samples). All point spectra were acquired for 3 minutes each.

Prior to EDX analysis, particle-containing areas were chosen at random and imaged at 1 kV acceleration voltage and 4 mm working distance in ordinary SE SEM mode, both at low and high magnification, ensuring high resolution micrographs. The same areas did then undergo both element mapping and spectrum analysis using EDX. The filter material itself was also subjected to spectrum analysis.

4 Results

4.1 Electron microscopy of specimens undergone no fixation, fixation and CPD

In this section, SEM micrographs of polycarbonate filters containing unfixed, fixed and critically point dried bioaerosols (containing *BG* spores and *S. marcescens* vegetative cells) are presented. The results are presented in sections depending on fixation method used on the specimens. One section is dedicated to micrographs of unfixed, fixed and critically point dried bacterial cells and spores originating directly from liquid solution. The last section is dedicated to SEM micrographs of TEM grids containing unfixed, fixed and critically point dried *BG* spore and *S. marcescens* bioaerosols.

4.1.1 10% glutaraldehyde vapor fixation

4.1.1.1 Small *BG* spore bioaerosols

Figure 14 presents selected SEM micrographs of the filters containing unfixed, fixed and critically point dried *BG* spores, respectively. The spores are mostly dispersed singularly on the filters, although some are gathered in aggregates of two or more particles. The filter undergone CPD seem to contain slightly less particles than the two filters not undergone CPD.

All filters in figure 14 contain some collapsed spores, as shown in figures 14(a), (c) and (e), but the majority of particles on the filters exhibit a structurally more intact morphology. Figures 14(b), (d) and (f) provide a closer look at the morphology of the unfixed, fixed and critically point dried *BG* spores, revealing little morphological difference between the differently prepared particles. The spores undergone either solely fixation or fixation followed by CPD, as represented by figures 14(c)-(f), might be said to appear a little "puffier", or smoother, than the unfixed specimens represented by figure 14(b).

On comparison with critically point dried specimens of comparable [82] [83] *B. subtilis* spores as given by Zhou et al. [84], the critically point dried *BG* spores in figure 14 appear very similar, both in shape and size. Given the strong resemblance between the spores of all three preparation methods, the unfixed and fixed particles in figure 14 also resemble the critically point dried spores of Zhou et al.

Most of the observed spores of different preparation methods fall within the expected *BG* spore size range[25]. Figure 14(e) reveals the presence of a structure not observed at the unfixed and fixed, but not critically point dried, filters in figure 14(a)-(d). These structures are highlighted by red arrows. Present on all filters are smaller fragments approximately 0.2-0.4 µm in diameter, one such fragment is highlighted by a green arrow in figure 14(d).

[25] 1-1.6µm x 0.6-0.9µm [69]

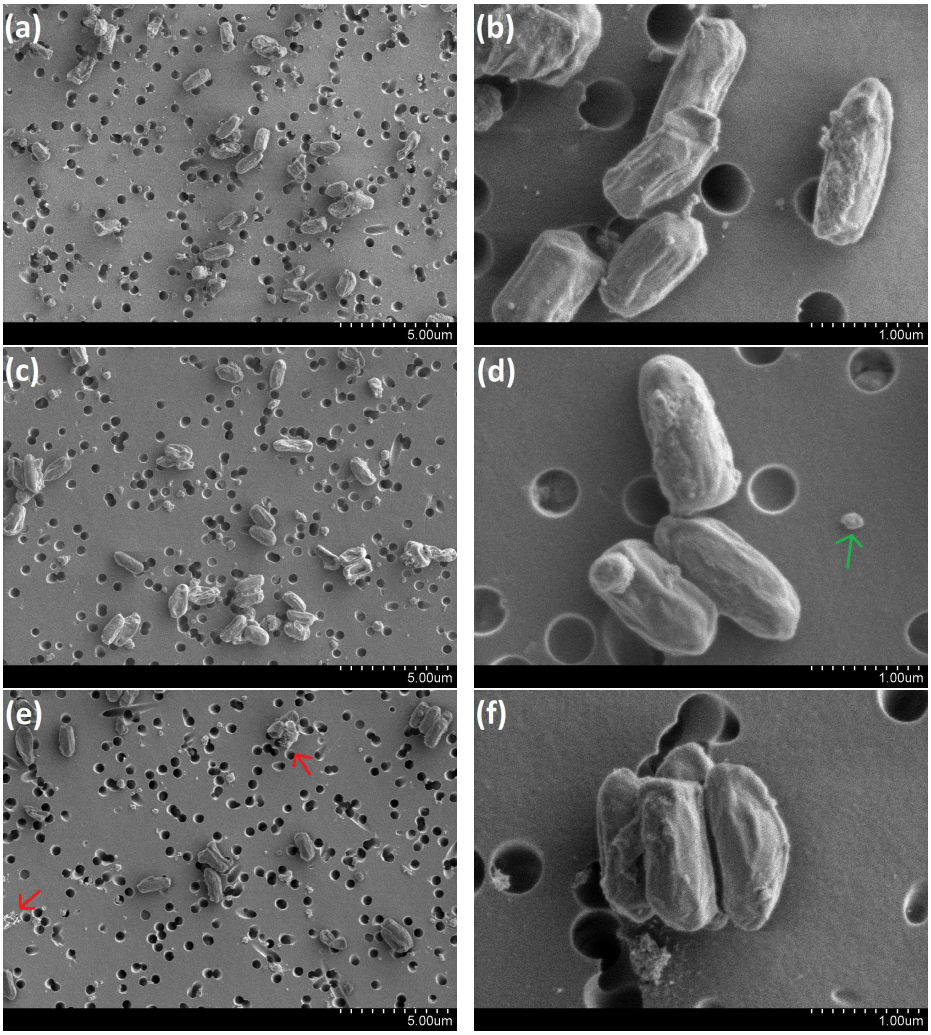

Figure 14: SEM micrographs of small *BG* spore bioaerosols sampled on a filter at small and large magnification. The bioaerosols have undergone the following preparation methods: (a) and (b) no fixation, (c) and (d) fixation, no CPD, (e) and (f) fixation and CPD. The green arrow in (d) highlights a small structure approximately 0.2-0.4 µm in diameter. Such structures are present on all filters. The red arrows in (e) highlight similar structures only present on filters undergone CPD, see larger image in figure B.1 in appendix B.

4.1.1.2 Large *BG* spore bioaerosols

Figure 15 provides an overview of, and closer look at, the large *BG* spore bioaerosols deposited on polycarbonate filters. The bioaerosols in figures 15(a)-(d) have not undergone CPD, and are unfixed and fixed respectively, while the bioaerosols in figures 15(e) and (f) have been fixed and critically point dried. While the filters not undergone CPD contain many relatively large bioaerosols, and these clearly consist of several *BG* spores, the filter undergone CPD is only barely populated by bioaerosols, and none of equivalent (large) size order. The only particles observed on the latter filter are dispersed in singles or aggregates much smaller than those seen on the filters not undergone CPD.

A closer look at the unfixed, fixed and critically point dried particles, as seen in figures 15(b), (d) and (e), reveals little to no difference in the conformation of the individual *BG* spores of different preparation background. The conformation of the individual *BG* spores composing these large bioaerosols, differ from neither the conformation of the *BG* spores in figure 14, nor from that of the critically point dried spores from reference [84].

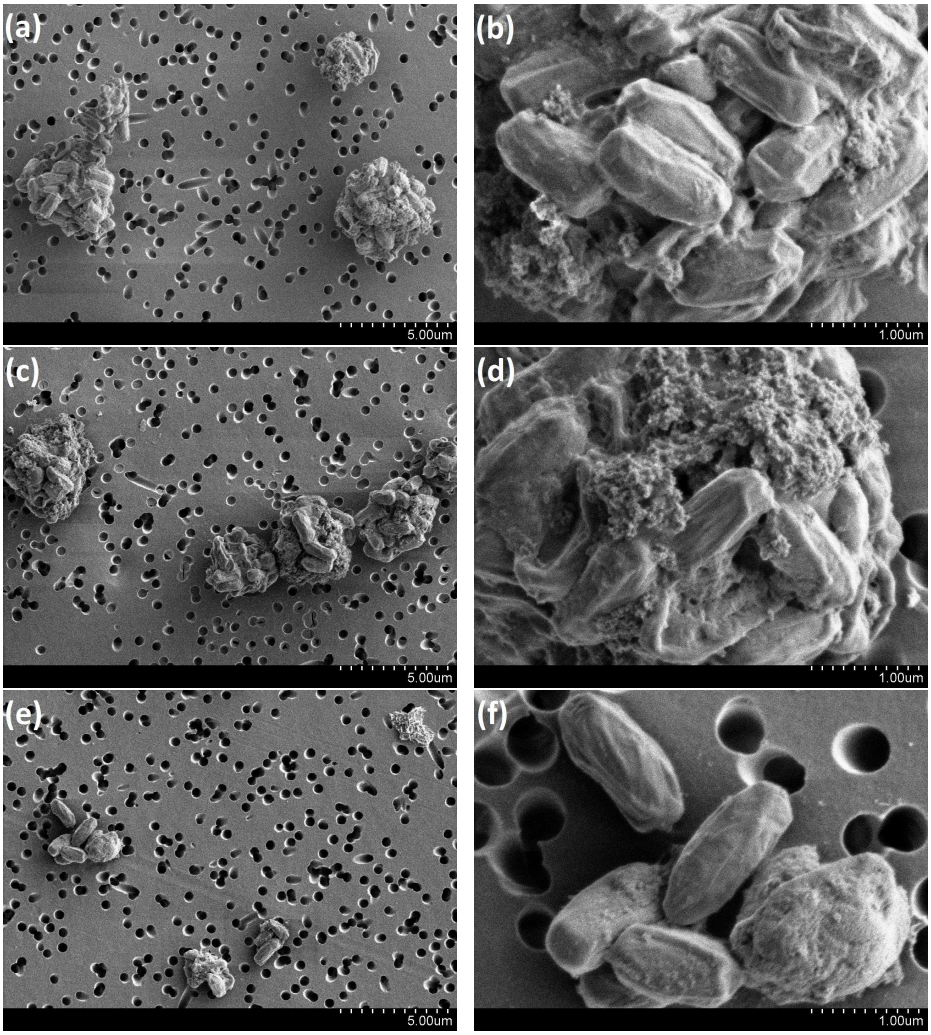

Figure 15: SEM micrographs of large *BG* spore bioaerosols sampled on a filter at small and large magnification. The bioaerosols have undergone the following preparation methods: (a) and (b) no fixation, (c) and (d) fixation, no CPD, (e) and (f) fixation and CPD.

Figures 16(a) and (b) provide a full overview of a single unfixed and fixed large *BG* spore bioaerosol, respectively. The filter undergone CPD is not represented in figure 16 because no large bioaerosols were observed on this filter. Figure 16 clearly shows that the bioaerosols

consist of many individual *BG* spores, in addition to a second, rough material. It is not possible to obtain information about the insides of the bioaerosol particles from these micrographs.

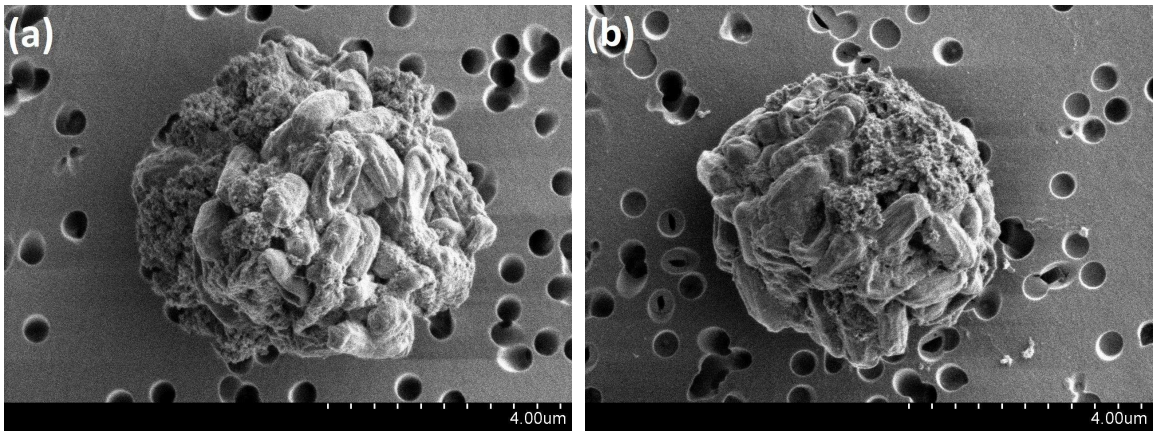

Figure 16: SEM micrographs of large *BG* spore bioaerosols sampled on a filter. The bioaerosols have undergone the following preparation methods: (a) no fixation, (b) fixation, no CPD. The filter undergone CPD lacked bioaerosols of this (large) size, and is not represented in the figure.

4.1.1.3 Small *S. marcescens* bioaerosols

Regarding small *S. marcescens* bioaerosols, there is a large difference between the appearance of the unfixed particles, and the fixed and critically point dried particles, as illustrated by figure 17. While the unfixed *S. marcescens* bacteria are clearly visible as single particles on the filter, the fixed and critically point dried particles have a different appearance. The surface of the fixed and critically point dried particles looks rougher than that of the unfixed bacteria, and the particles appear covered in what looks like foreign material. Smaller fragments approximately 0.1-0.3 µm across, are present on the filter in figure 17(b).

None of the bacteria in figure 17 resemble critically point dried *S. marcescens* bacteria as presented by e.g. Lamed et al. [85], Strobel et al. [86] and Mondaca et al. [87], but they differ in different ways. The fixed and critically point dried bacteria look fuller, or more hydrated, and their shape is closer to the reference bacteria, than that of the unfixed bacteria. The latter's surface structure, however, is the closest to the reference samples' surface structure.

The length of most of the bacteria on all filters, is below, or on the low side of, the expected *S. marcescens* size range[26].

A unique structure, similar to those highlighted by arrows in figure 14(e) was also present on the critically point dried filter containing small *S. marcescens* bioaerosols. This structure is imaged in figure B.1 in appendix B. The particle density on all three filters is approximately the same.

[26] 0.9-2.0 µm x 0.5-0.8 µm [72]

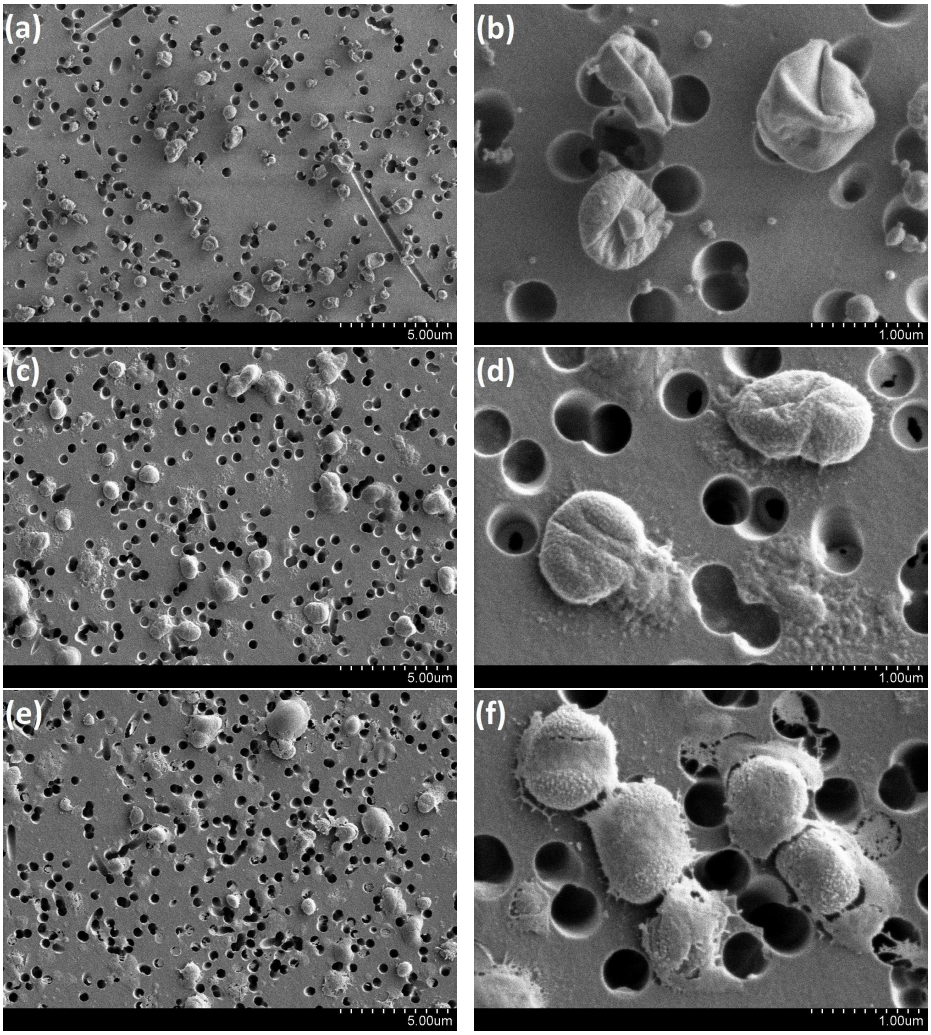

Figure 17: SEM micrographs of small *S. marcescens* bioaerosols sampled on a filter at small and large magnification. The bioaerosols have undergone the following preparation methods: (a) and (b) no fixation, (c) and (d) fixation, no CPD, (e) and (f) fixation and CPD.

4.1.1.4 Large *S. marcescens* bioaerosols

Figure 18 presents an overview of, and closer look at, unfixed, fixed and critically point dried large *S. marcescens* bioaerosols deposited on filters. The unfixed bioaerosols in figures 18(a) and (b) clearly differ from the fixed and critically point dried particles in figures 18(c)-(f) by their shape, which appears next to spherical. The particles undergone fixation and CPD are flatter and stretch over a wider area; they seem dissolved. While the critically point dried particles appear to have some three dimensional shape, the particles on the filter that is fixed only, look the flattest.

The morphologies of the individual *S. marcescens* bacteria constituting the fixed and critically point dried bioaerosols in figure 18, resemble to some extent the critically point dried bacteria from references [85], [86] and [87]. The bacterial cells in figures 18(c)-(f) appear flatter and with more edges than the reference particles, however, and have a rougher surface, similar to that of the particles in figure 17(c)-(f). The size of most of these bacteria is also below, or on the low side of, the expected *S. marcescens* size range. The individual *S. marcescens* bacteria composing the unfixed bioaerosol in figure 18(b) are barely discernible as individual particles.

Because of the large difference between the particles of the three preparation methods regarding appearance and size, it is difficult to compare the filters regarding particle density. However, the filter in figure 18(a) containing unfixed bioaerosols, appears to hold the highest number of particles.

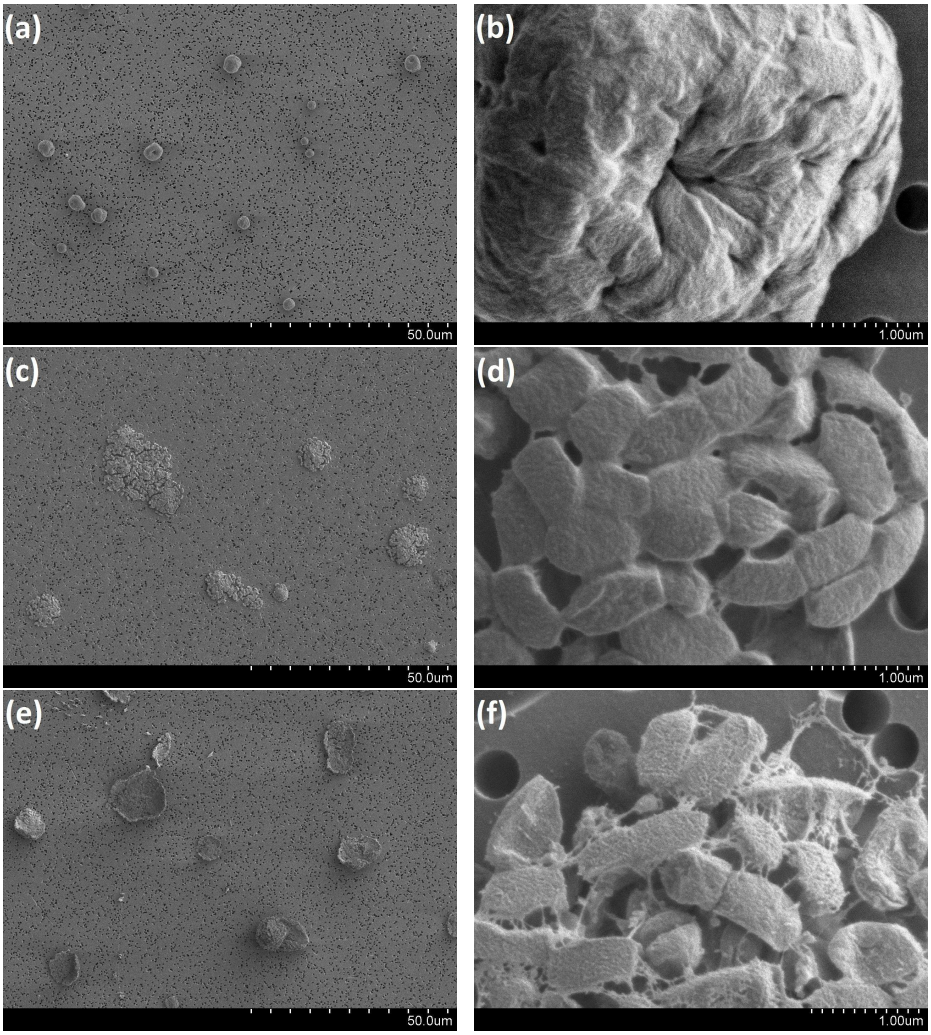

Figure 18: SEM micrographs of large *S. marcescens* bioaerosols sampled on a filter at small and large magnification. The bioaerosols have undergone the following preparation methods: (a) and (b) no fixation, (c) and (d) fixation, no CPD, (e) and (f) fixation and CPD.

A look at the entirety of individual *S. marcescens* bioaerosols, provided by figure 19, helps to establish the large differences between the particles of different preparation methods. While the unfixed *S. marcescens* bioaerosol of figure 19(a) has a close to spherical shape and

consists of what looks like tightly packed, individual bacterial cells, the fixed bioaerosol in figure 19(b) is comparably flat, and the individual bacteria are much more discernible. The critically point dried bioaerosol in figure 19(c) however, although much flatter than the unfixed bioaerosol in figure 19(a), is not as flat as the bioaerosol that is fixed only. The individual bacteria that compose the bioaerosol in figure 19(c) are equally easy to distinguish from another as the ones in figure 19(b).

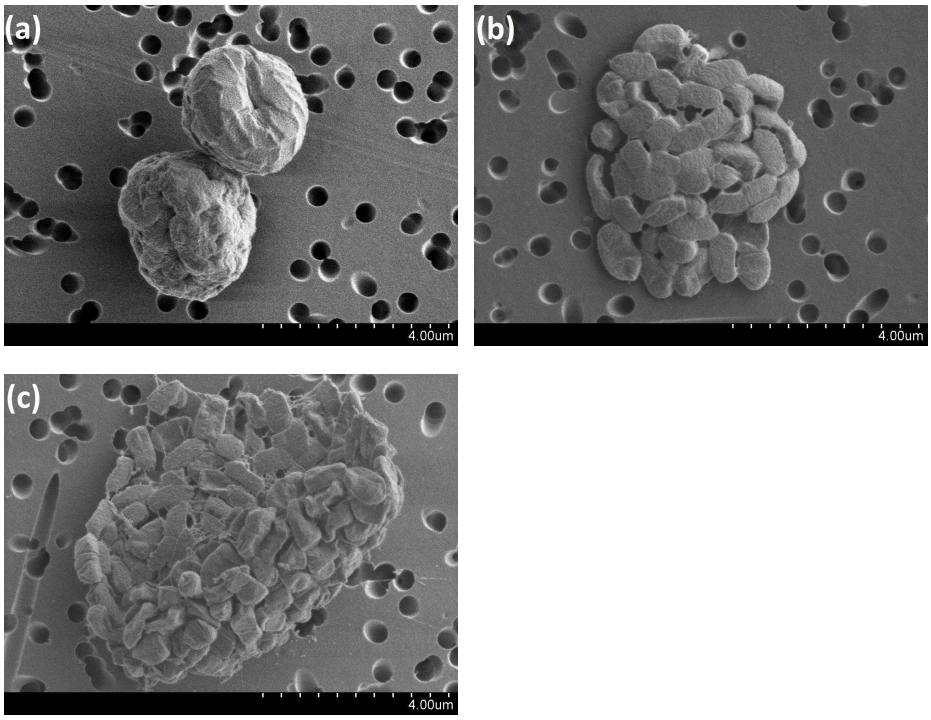

Figure 19: SEM micrographs of large *S. marcescens* bioaerosols sampled on a filter. The bioaerosols have undergone the following preparation methods: (a) no fixation, (b) fixation, no CPD, (c) fixation and CPD.

4.1.2 70% glutaraldehyde vapor fixation

4.1.2.1 Small *S. marcescens* bioaerosols

Figure 20 presents SEM micrographs of small *S. marcescens* bioaerosols sampled on filter and fixed by 70% glutaraldehyde vapor. The bioaerosols in figures 20(c) and (d) have in addition been critically point dried. The bioaerosols in figure 20 are deposited mostly as single bacteria, though some lie next to each other in small groups of two or more bacteria. The density of bioaerosols on the filter is approximately the same for both preparation methods, and the particles on both filters resemble to a great extent the unfixed, small *S. marcescens* bioaerosols imaged in figures 17(a) and (b). The fixed bioaerosols in figure 20(a) do not resemble the equivalent particles fixed by 10% glutaraldehyde vapor in figure 17(c), nor do the critically point dried bioaerosols in figure 20(c) resemble the equivalent particles in figure 17(e), which were fixed by 10% glutaraldehyde vapor and critically point dried.

A closer look at the small, fixed *S. marcescens* bioaerosols, as provided by figures 20(b) and (d), confirms the similarity between these particles, and the equivalent unfixed bioaerosols imaged in figure 17(b). All these particles appear collapsed and far removed from both the shape and size of critically point dried *S. marcescens* bacteria from sources [85], [86] and [87].

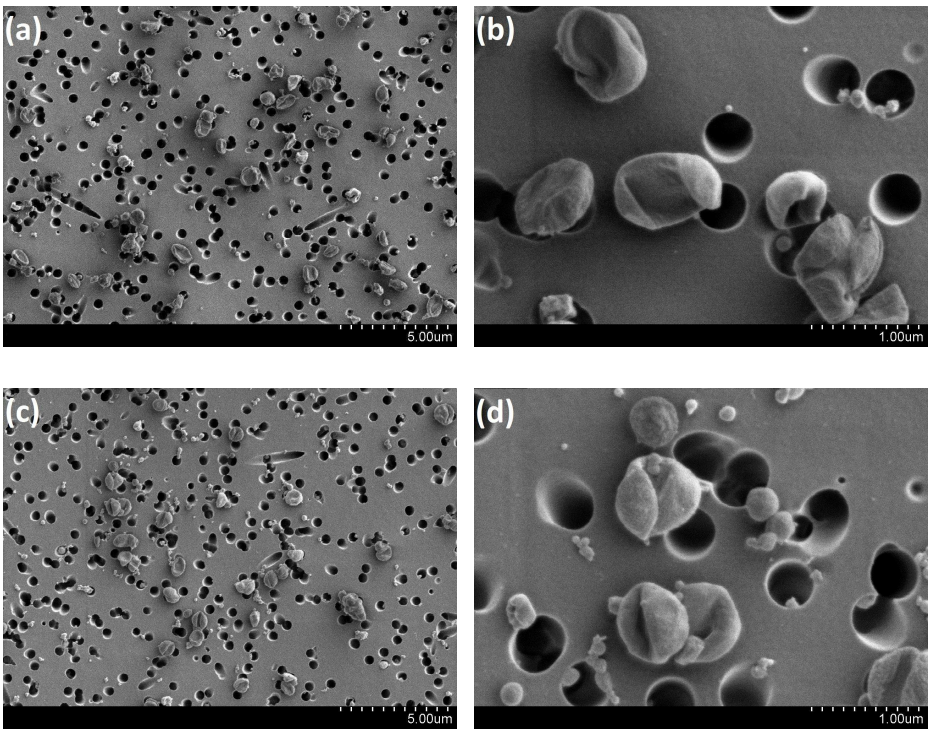

Figure 20: SEM micrographs of small *S. marcescens* bioaerosols sampled on a filter and fixed by 70% glutaraldehyde vapor. Small and large magnification. The bioaerosols have undergone the following preparation methods: (a) and (b) fixation, no CPD, (c) and (d) fixation and CPD.

4.1.2.2 Large *S. marcescens* bioaerosols

Figure 21 presents SEM micrographs of filters on which large bioaerosols containing *S. marcescens* bacteria have been sampled and fixed. While the bioaerosols in figures 21(a) and (b) resemble the equivalent, unfixed bioaerosols in figures 18(a) and (b) and 19(a) both in size, shape and particle density, large bioaerosols are absent from the filter undergone CPD in figures 21(c) and (d). The structures visible on the filter in figure 21(c) are similar to structures which are present on all critically point dried filters seen in this study[27].

Figure 21(d) pictures a rare bioaerosol found on the filter undergone CPD. The filter is mostly lacking particles, except from certain CPD specific structures, and the few bioaerosols present deviate greatly in size and shape from the bioaerosols only fixed by 70% glutaraldehyde vapor. The bioaerosols that do exist on the filter undergone CPD are smaller, and consist apparently of only one, or a few, bacterial cells.

At larger magnification, as provided by figure 21(b), the individual *S. marcescens* bacteria making up the bioaerosol in figure 21(b) are discernible from each other. This bioaerosol appears spherical and very similar to the unfixed bioaerosol in figure 18(b), and equally dissimilar from the bioaerosol fixed by 10% glutaraldehyde vapor in figure 18(d): Bioaerosols fixed by 70% glutaraldehyde vapor (presented in figure 21(b)) do not look dissolved.

[27]See e.g. figure 14(e) and figure B.1 in appendix B.

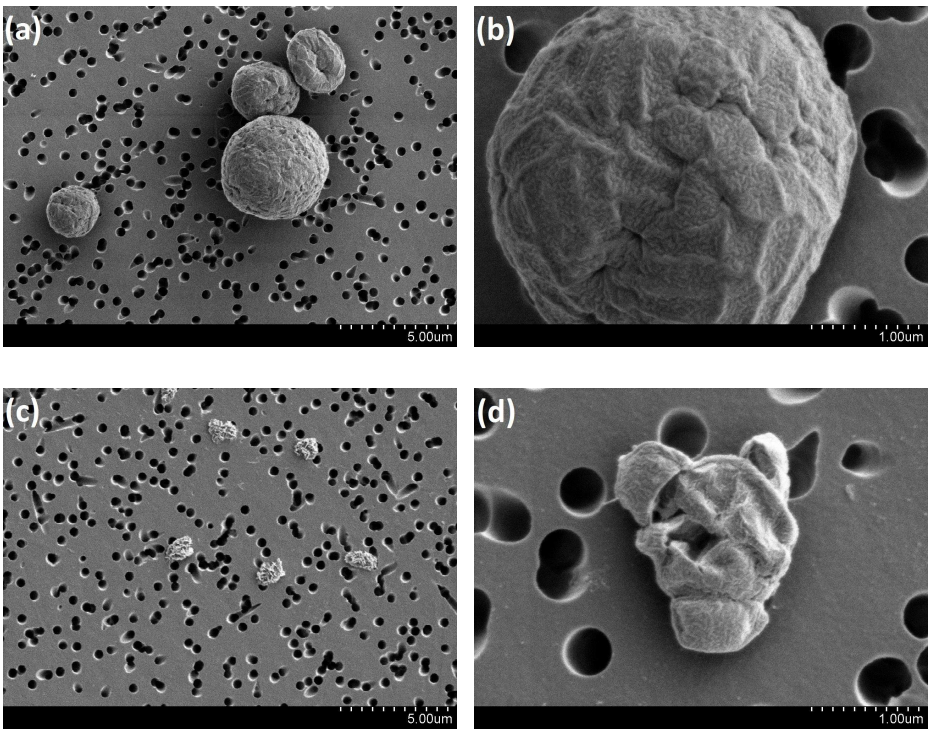

Figure 21: SEM micrographs of large *S. marcescens* bioaerosols sampled on a filter and fixed by 70% glutaraldehyde vapor. Small and large magnification. The bioaerosols have undergone the following preparation methods: (a) and (b) fixation, no CPD, (c) and (d) fixation and CPD. The bioaerosols in (a) and (b) are spherically shaped, and do not look dissolved, as opposed to the bioaerosols fixed by 10% glutaraldehyde vapor in figures 18(c) and (d) and figure 19(b).

4.1.3 Liquid glutaraldehyde fixation

4.1.3.1 *BG* spores

Figure 22 presents SEM micrographs of *BG* spores dispersed on filter from liquid solution. The spores have undergone different preparation methods according to the schematic overview in figure 11[28].

Although of different preparation methods, the spore particles resemble each other regarding both conformation and size. They likewise resemble the air sampled *BG* spores in figure 14, and the critically point dried *Bacillus* spores from source [84]. However, as a general trend, the critically point dried spores in figure 22(f) appear smoother and less "wrinkled" than those not undergone CPD in figures 22(b) and (d).

More critically point dried spores than non-critically point dried spores maintain an intact spore morphology, which is exemplified in figures 22(a), (c) and (e). While several collapsed spores are located across the filters not undergone CPD, collapsed spores appear at a much less frequency at the filter undergone CPD. Even among the critically point dried *BG* spores fixed by 10% glutaraldehyde vapor in figure 14, there are considerably more collapsed spores than among the critically point dried spores in figure 22.

[28] i.e. the spores in figures 22(a) and (b) have neither been fixed nor critically point dried, the spores in figures 22(c) and (d) have been fixed, but not critically point dried, and the spores in figures 22(e) and (f) have been fixed and critically point dried.

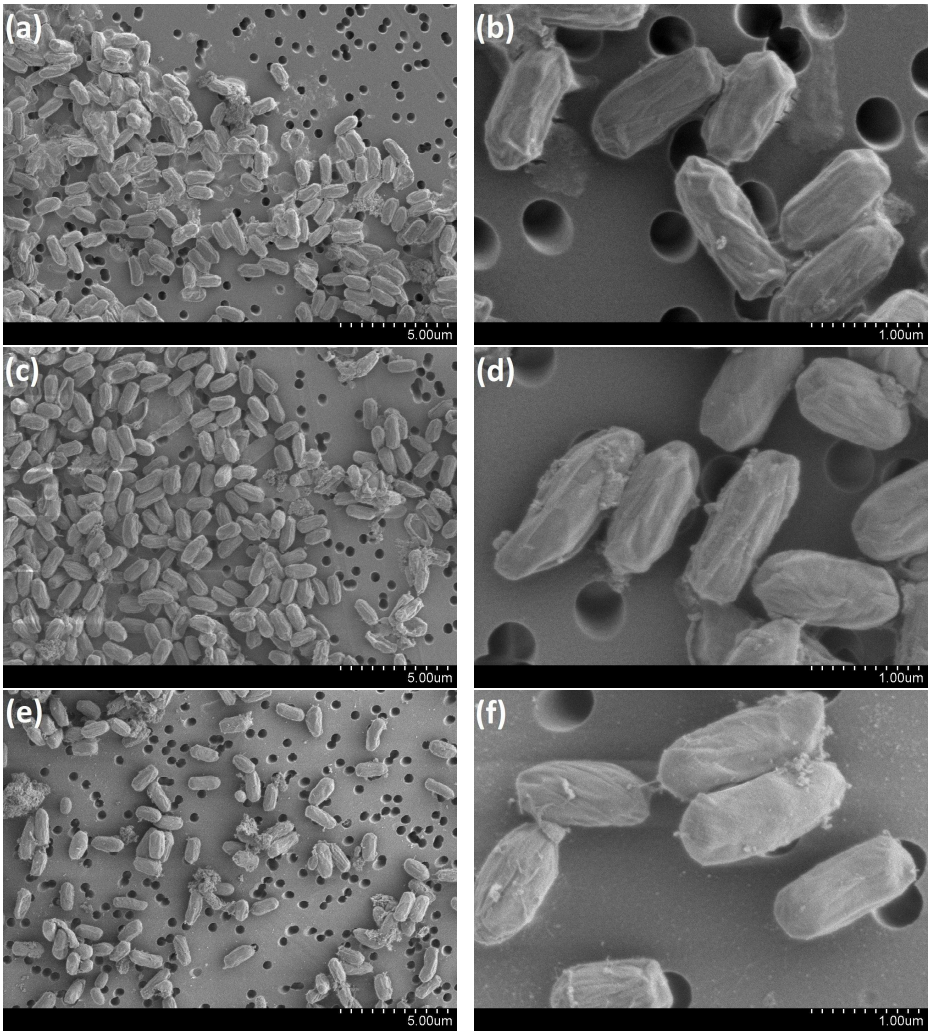

Figure 22: SEM micrographs of *BG* spores from liquid solution dispersed on a filter at small and large magnification. The spores have undergone the following preparation methods: (a) and (b) no fixation, (c) and (d) fixation, no CPD, (e) and (f) fixation and CPD.

4.1.3.2 *S. marcescens* bacteria

Figure 23 presents SEM micrographs of *S. marcescens* bacteria dispersed on filter from liquid solution. The bacteria are prepared differently and according to the schematic overview in figure 11[29].

The *S. marcescens* bacteria in figure 23 differ greatly from each other in terms of morphology. The unfixed particles in figures 23(a) and (b), and the fixed, but not critically point dried particles in figures 23(c) and (d), appear considerably more misshapen and deformed than the critically point dried bacteria in figures 23(e) and (f). The latter bacteria are also far removed in shape from all the air sampled *S. marcescens* bacteria seen earlier in this study in figures 17 and 20. The bacteria in figure 23 appear puffy, and resemble the critically point dried *S. marcescens* bacteria from sources [85], [86] and [87], exhibiting a characteristic rod shape. Very few of the critically point dried *S. marcescens* bacteria dispersed from liquid solution exhibit a collapsed conformation.

Although both far removed from the appearance of that of the critically point dried bacteria, the non-fixed and fixed *S. marcescens* bacteria in figures 23(a)-(d) also differ from each other in shape. While the former particles look severely compressed and seem surrounded by a thin film, the latter particles appear smoother and, to a small extent, fuller. On filter, the particles of both preparation techniques are connected together in clusters and large sheets of bacteria. The critically point dried bacteria do not exhibit this tendency however, and are spread across the filter in a far more individual and discernible manner.

[29] i.e. the bacteria in figures 23(a) and (b) have neither been fixed nor critically point dried, the bacteria in figures 23(c) and (d) have been fixed, but not critically point dried, and the bacteria in figures 23(e) and (f) have been both fixed and critically point dried.

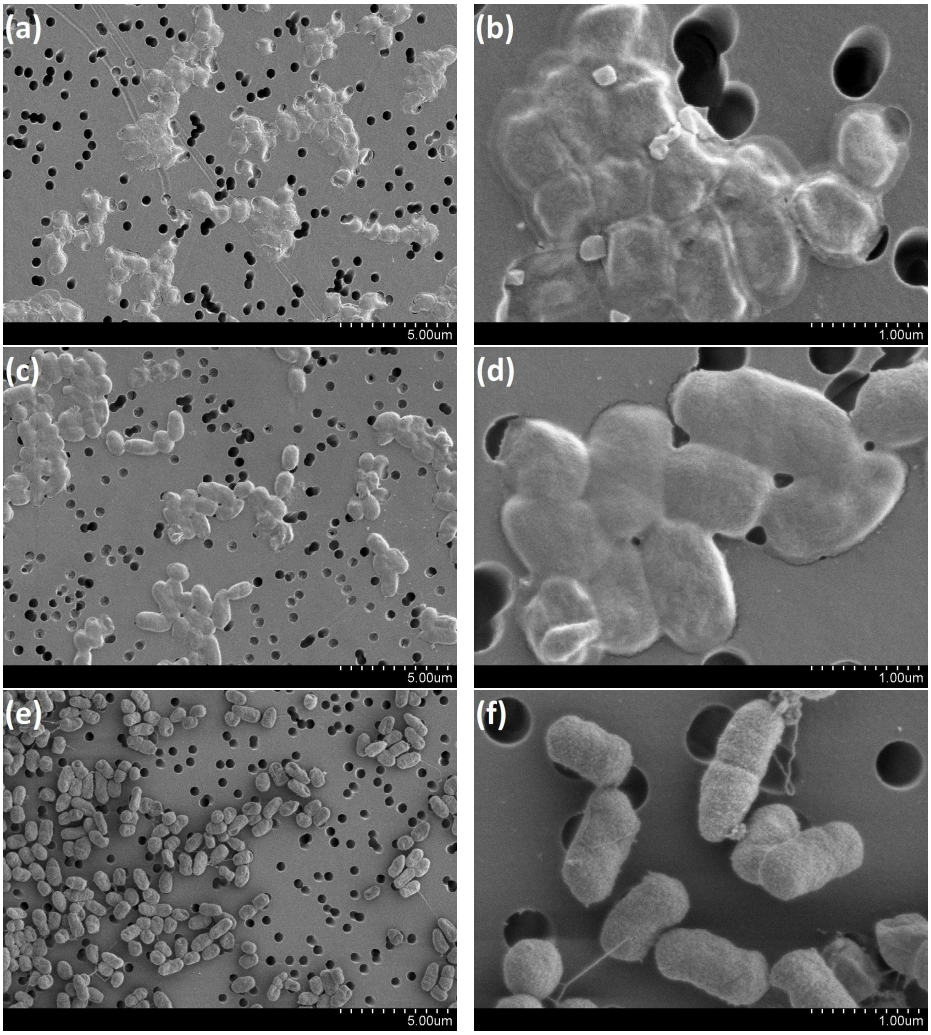

Figure 23: SEM micrographs of *S. marcescens* bacteria from liquid solution dispersed on a filter at small and large magnification. The bacteria have undergone the following preparation methods: (a) and (b) no fixation, (c) and (d) fixation, no CPD, (e) and (f) fixation and CPD.

4.1.4 Sampling on TEM grids for SEM observation

4.1.4.1 Small *BG* spore and S. marcescens bioaerosols

Figure 24 presents overviews of small *BG* spore and *S. marcescens* bioaerosols sampled on TEM grids and imaged by SEM. The bioaerosols have undergone different preparation methods according to the plan in figure 13. The *S. marcescens* bioaerosols have a generally higher particle density on the grids than the *BG* spore bioaerosols.

Comparing the *BG* spores in figures 24(a)-(c), there is no significant difference in neither concentration nor morphology between the different preparation methods. All the *BG* spore morphologies are similar to those found in figure 14, i.e. to small *BG* spore bioaerosols sampled on polycarbonate filters, some fixed by 10% glutaraldehyde vapor and critically point dried.

Greater difference is found upon comparing the *S. marcescens* bioaerosols in figures 24(d)-(f). Although not differing in morphology (they all exhibit a raisin like conformation similar to that seen in figure 20), the bacteria are located differently in figure 24(f) than they are in figures 24(d) and (e). In figure 24(f), bioaerosols are only located on top of the edges of the mesh, not on the support film in the holes between the edges, upon which many of the non-fixed and fixed bacteria in figures 24(d) and (e) are located. A large part of the *BG* spore bioaerosols in figures 24(a)-(c) are also located in the "hole part" of the mesh[30], including the ones undergone CPD.

[30]See figure B.2 in appendix B for explanation to the different TEM grid locations.

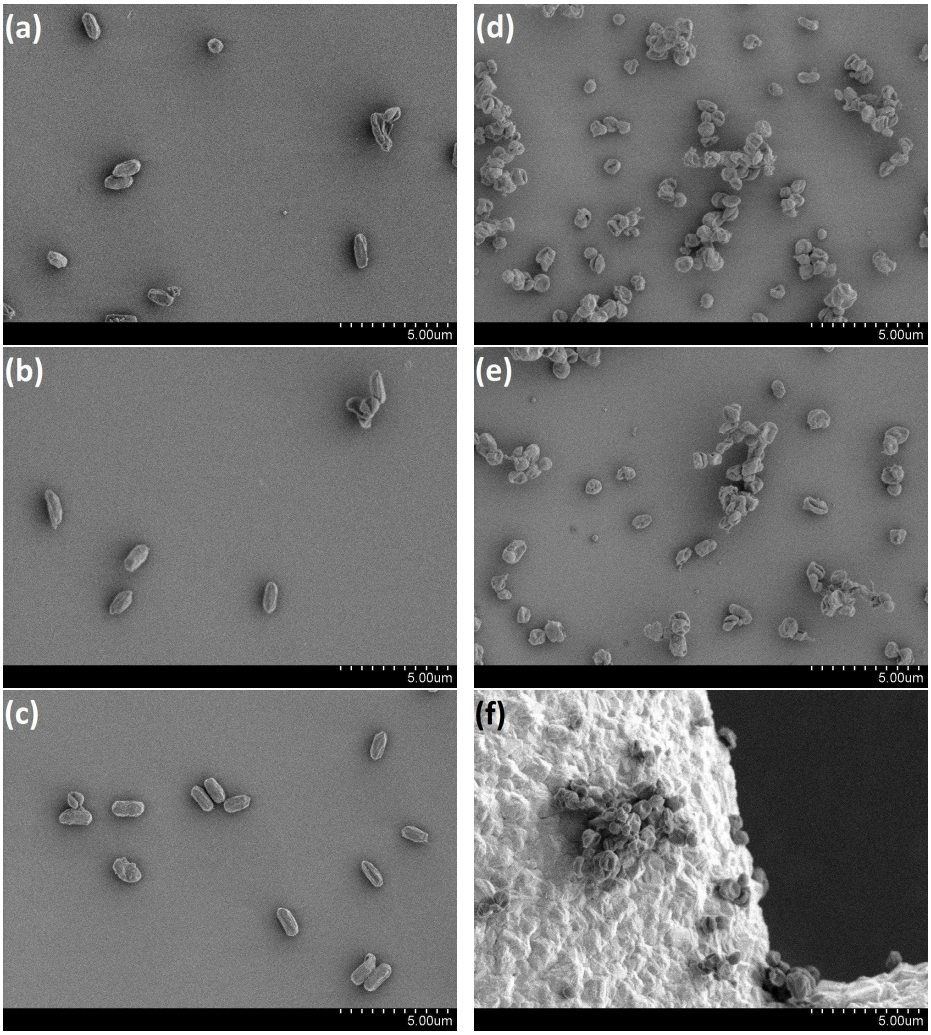

Figure 24: SEM micrographs of small (a)-(c) *BG* spore bioaerosols and (d)-(f) *S. marcescens* bioaerosols sampled on a TEM grid. The bioaerosols have undergone the following preparation methods: (a) and (d) no fixation, (b) and (e) fixation, no CPD, (c) and (f) fixation and CPD. The bioaerosols in (f) are only present on the Cu edge of the TEM grid, and not on the support film in the hole areas of the TEM grid.

4.1.4.2 Large *BG* spore and S. marcescens bioaerosols

In figure 25, selected SEM micrographs of large bioaerosols containing *BG* spores and *S. marcescens* bacteria sampled on TEM grids are presented. The bioaerosols have undergone different preparation methods according to the plan in figure 13.

The concentration of large bioaerosols on the different TEM grids maintains a stable, low number. Most of the bioaerosols are located in close proximity to an edge of the mesh. On the grid that has undergone fixation but not CPD, and should contain large *BG* spore bioaerosols, no bioaerosols were found, hence the missing micrograph.

Large and spherically shaped bioaerosols are observed on the TEM grids undergone CPD in figure 25. This is different from the results obtained when subjecting polycarbonate filters containing large bioaerosols to CPD, see e.g. figures 15, 18 and 21, on which no large, spherically shaped bioaerosols were observed.

Large *BG* spore bioaerosols undergone CPD, as represented by figure 25(b), do not differ significantly in morphology from the equivalent particles not undergone CPD, as represented by figure 25(a). The same is true for *S. marcescens* bioaerosols of different preparation as represented by figures 25(c)-(e).

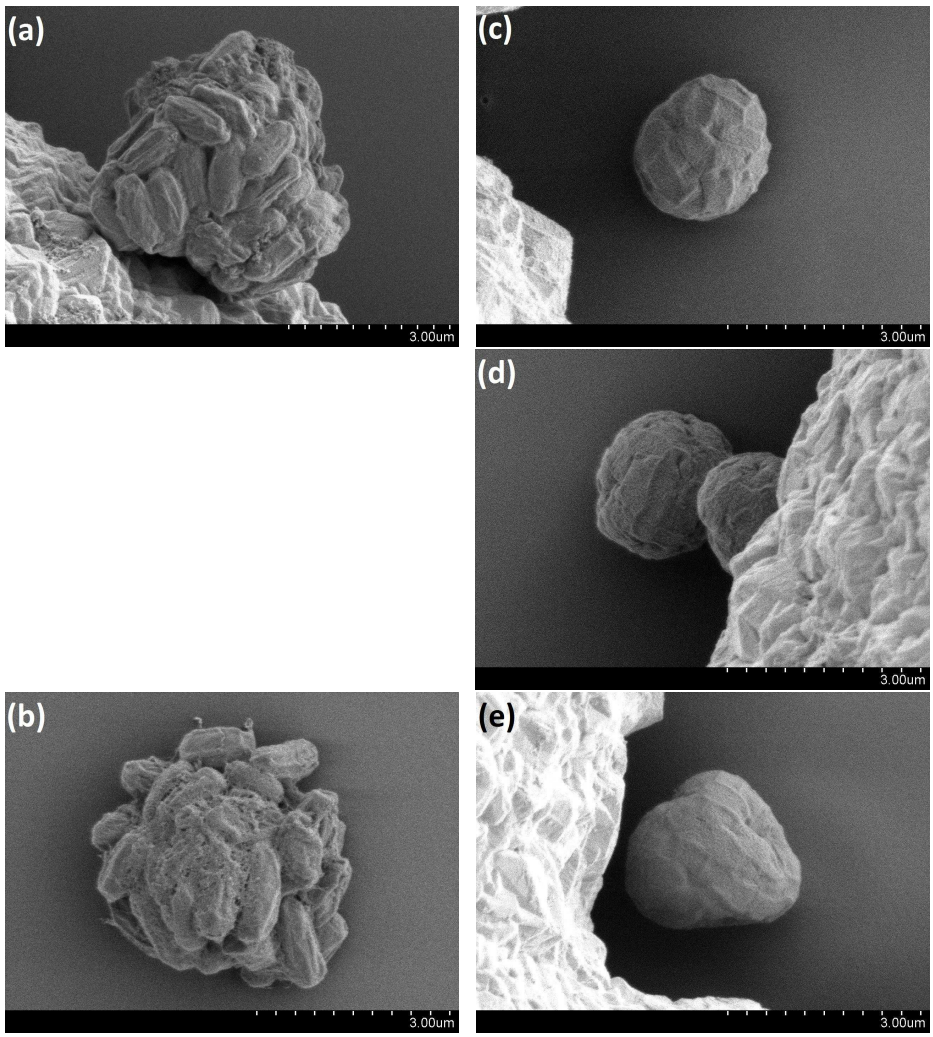

Figure 25: SEM micrographs of large (a)-(c) *BG* spore bioaerosols and (d)-(f) *S. marcescens* bioaerosols sampled on a TEM grid. The bioaerosols have undergone the following preparation methods: (a) and (c) no fixation, (d) fixation, no CPD, (b) and (e) fixation and CPD. No bioaerosols were found on the TEM grid that should have contained fixed *BG* spore bioaerosols.

4.2 TEM

The results of TEM of bioaerosols containing *BG* spores and *S. marcescens* bacteria are presented in this section. The results are divided into sections depending on size of bioaerosols sampled, and what bacterial species they contain.

4.2.1 Small *BG* spore bioaerosols

The particles in figure 26 have been imaged by TEM, and are seemingly dispersed on the TEM grid in singles or in groups of two or more particles. Smaller fragments approximately 0.1-0.2 μm across, are also present on the filters.

Comparing these small *BG* bioaerosols with the corresponding particles imaged by SEM in figures 14(c) and (d), it is clear (given the fact that the particle type dispersed is known) that the two figures depict equivalent *BG* spores: The particles correspond both in shape and size[31]. The TEM imaged spores in figure 26 however, show no color variation, nor any three dimensionality.

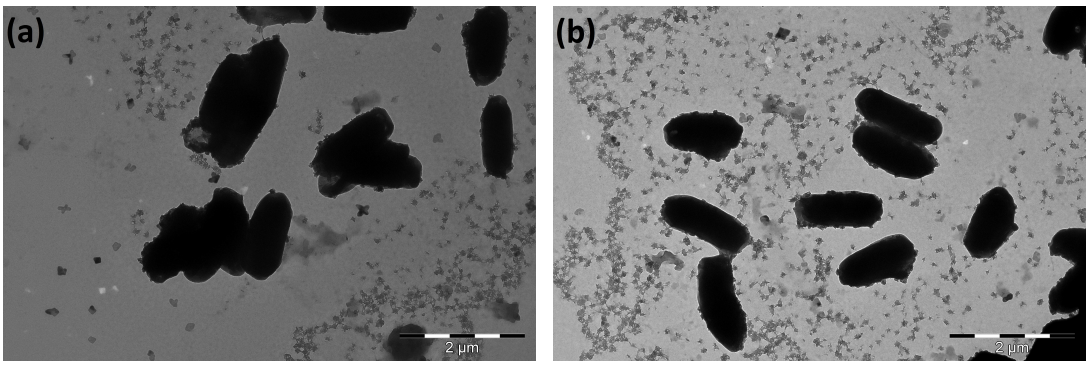

Figure 26: TEM micrographs of small *BG* spore bioaerosols sampled on a TEM grid. (a) and (b) depict different areas of the same TEM grid.

[31]The size of the spores in figure 26 is also within expected size range.

4.2.2 Large *BG* spore bioaerosols

Comparing the particles imaged by TEM in figure 27 with the large *BG* spore bioaerosols imaged by SEM in figures 15(c) and (d), and in figure 16(b), the particles in figure 27 are generally smaller than those imaged by SEM by about half the size. Regarding the outline[32] of the particles, the ones imaged by TEM appear more circular, especially the particle in figure 27(b). The particle in figure 27(a) has a more irregular outline, more indicative of a bioaerosol containing *BG* spores. It is not possible, however, to tell from the TEM micrographs in figure 27 alone whether or not the particles imaged are indeed large *BG* spore bioaerosols.

A few background fragments are present in figure 27(a), while such fragments are absent from figure 27(b).

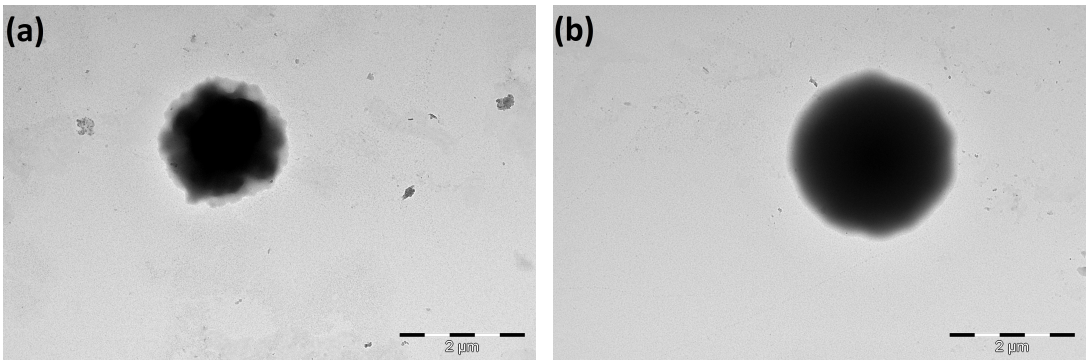

Figure 27: TEM micrographs of large *BG* spore bioaerosols sampled on a TEM grid. (a) and (b) depict different areas of the same TEM grid.

[32]The particles are, except at the very edges, all black, and the shape of the particle is therefore assessed based on outline.

4.2.3 Small *S. marcescens* bioaerosols

Figure 28 presents TEM micrographs a of grid upon which small *S. marsescens* bioaerosols are dispersed. In comparison with the SEM micrographs of the corresponding particles in figures 17(c) and (d), the particles in 28 correspond both in size and general outline.

In addition to the larger, main particles, small, bright fragments approximately 0.1-0.2 μm in diameter are also present on the grids, as well as darker fragments approximately 0.4 μm in diameter (observed in figure 28(b)).

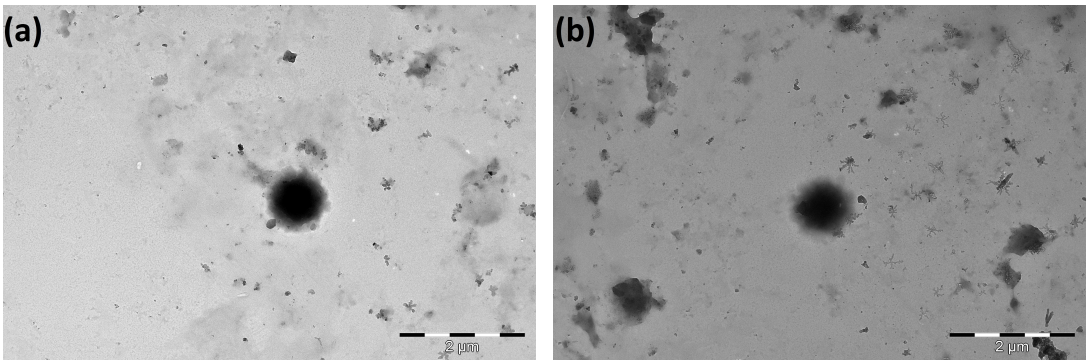

Figure 28: TEM micrographs of small *S. marcescens* bioaerosols sampled on a TEM grid. (a) and (b) depict different areas of the same TEM grid.

4.2.4 Large *S. marcescens* bioaerosols

Large *S. marcescens* bioaerosols have been dispersed on the TEM grid imaged in figure 29. Comparing the particles present in this figure with equivalent particles (fixed by 10% glutaraldehyde vapor) imaged by SEM in figures 18(c) and (d), as well as in figure 19(b), the particles correspond both in size and shape. By the outline of the particles in figure 29 (and also given the fact that the particle type dispersed is known), it is clear that the particles are bioaerosols consisting of *S. marcescens* bacteria. Only the very edges of the bacteria are close to transparent, the rest are homogeneous black.

Very small fragments, approximately 30-50 nm in diameter, are present in the background of figure 29(a), while larger, more translucent particles, approximately 0.2 μm in diameter are present in 29(b).

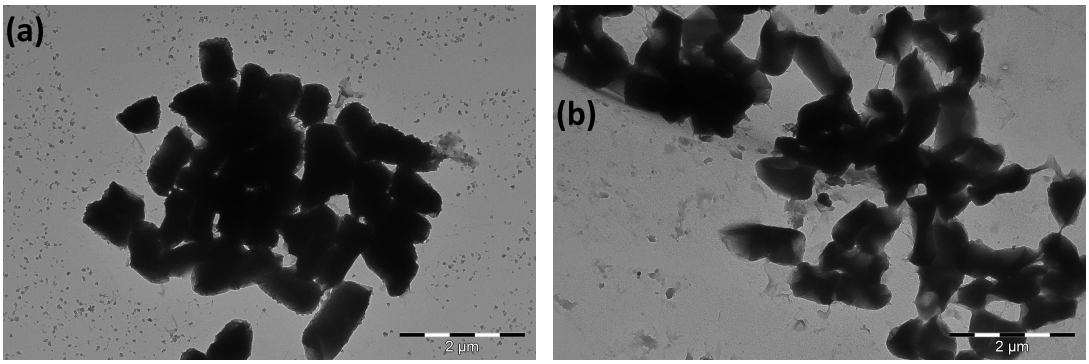

Figure 29: TEM micrographs of large *S. marcescens* bioaerosols sampled on a TEM grid. (a) and (b) depict different areas of the same TEM grid.

4.3 EDX

SEM micrographs, EDX element maps and point spectra of environmental particles sampled at the Nationaltheatret underground subway station are presented in this section. The EDX analysis concentrates on environmental samples as these may contain a variety of material in addition to bioaerosols, hence providing a more realistic environment for bioaerosol detection than samples collected in an aerosol chamber.

Figure 30 presents both SEM micrographs and EDX element maps of aerosols sampled at the Nationaltheatret underground subway station during day- and nighttime, respectively. The most prominent particles in figures 30(a) and (d) have been labeled with which elements they contain according to EDX point spectra and element maps of each particle[33]. Larger SEM micrographs are presented in figure C.3 in appendix C. The spectra and element maps of most of the labeled particles can be found in figures C.5 - C.12 in appendix C.

[33]The coating materials platinum (Pt) and palladium (Pd), as well as carbon (C) (which the filter material is mostly made of) show up on the point spectra of most of the particles, but these elements are omitted from the element labeling of each particle.

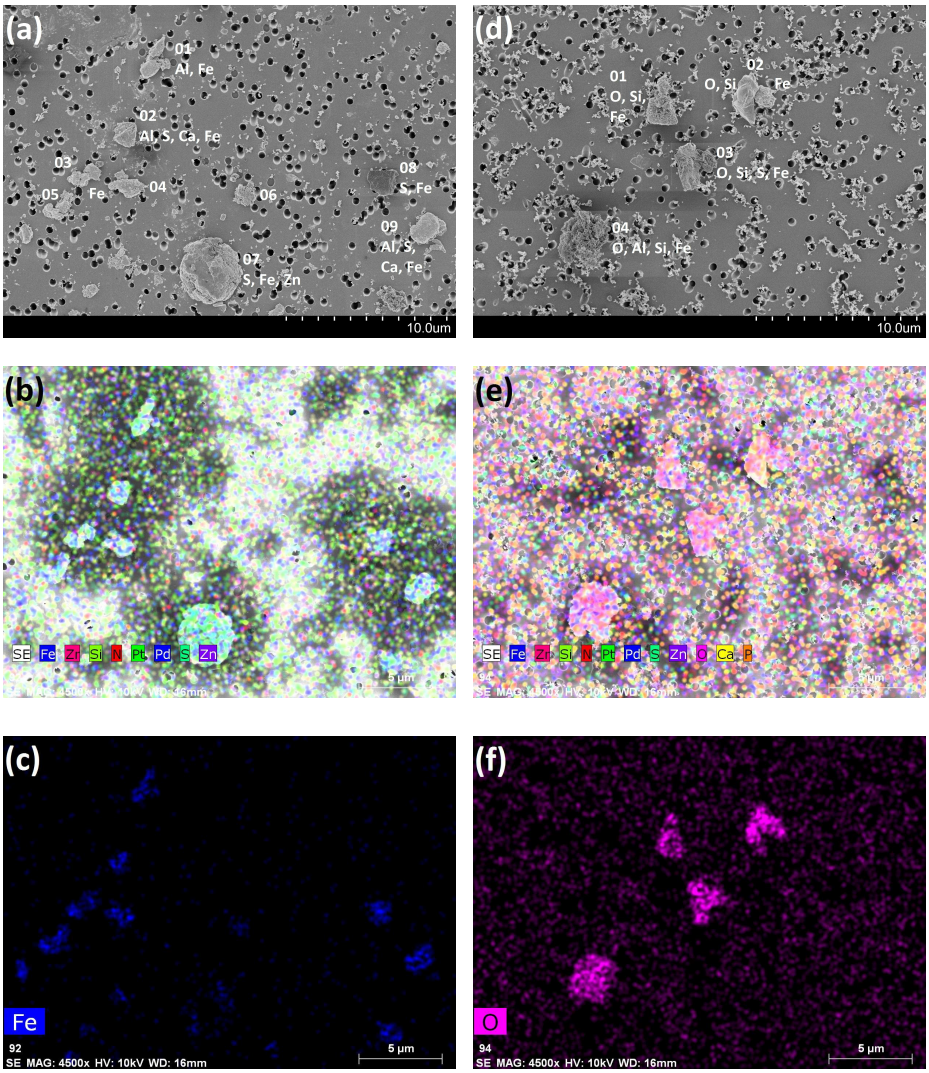

Figure 30: SEM micrographs and element maps of environmental sample. Particles are sampled on polycarbonate filters at the Nationaltheatret underground subway station. (a)-(c) sampled during the day, (d)-(f) sampled during the night. (a) and (d) SE SEM micrographs at small magnification, providing an overview of the sample. Particles are assigned elements according to EDX point spectrum analysis. See larger SEM micrographs in figure C.3 in appendix C. (b) and (e) EDX element maps of all the detected elements in the (a) and (d) overviews, respectively. "SE" label refers to SE (secondary electron) image taken at EDX settings. (c) and (f) EDX element maps showing presence of (c) iron (Fe) and (f) oxygen (O) in the sample.

Based on the limited observations of this study, the particle density and morphology is different between particles sampled during day- and nighttime, as illustrated by figures 30(a) and (d) and figure C.4 in appendix C. Most of the observed particles[34] sampled during daytime are generally smaller (∼1.0 - 2.0 μm in diameter) than the observed particles sampled during nighttime (∼1.5 - 3.0 μm in diameter). The density of the nighttime particles is lower than that of the daytime particles however, and the nighttime filter contains large areas at which only very small particulate material is present. The density of this small particulate material is higher at the nighttime than the daytime filter, as illustrated by figures 30(a) and (d) and figure C.4 in appendix C.

Figures 30(c) and (f) present EDX element maps showing the presence of iron (Fe) and oxygen (O), respectively. These element maps are included because they each illustrate a difference between particle material and background.

EDX point spectra of points at the polycarbonate filter material (between particles) are presented in figure 31. The two spectra in figures 31(a) and (b) represent points at filters used to sample aerosols at the Nationaltheatret underground subway station during day- and nighttime, respectively. The point locations are highlighted by a green cross in figures C.5(a) and C.9(a) in appendix C, respectively. The point spectrum of a point at the daytime filter indicates presence of nitrogen (N), oxygen (O), silicon (Si), palladium (Pd), platinum (Pt) and zirconium (Zr). The equivalent spectrum of the nighttime filter indicates presence of O and Zr. Both filters also exhibit peaks corresponding to carbon (C). The Zr peak corresponds with the Pt peak, for which the presence is known, so it is likely that the software mistakes Pt for Zr, and that the latter is not really present in the sample. Zr presence in spectra and maps is therefore disregarded.

[34]By particles, it is meant larger bulks of material, not the very small particulate material scattered across the filter as aggregates of varying (small) size.

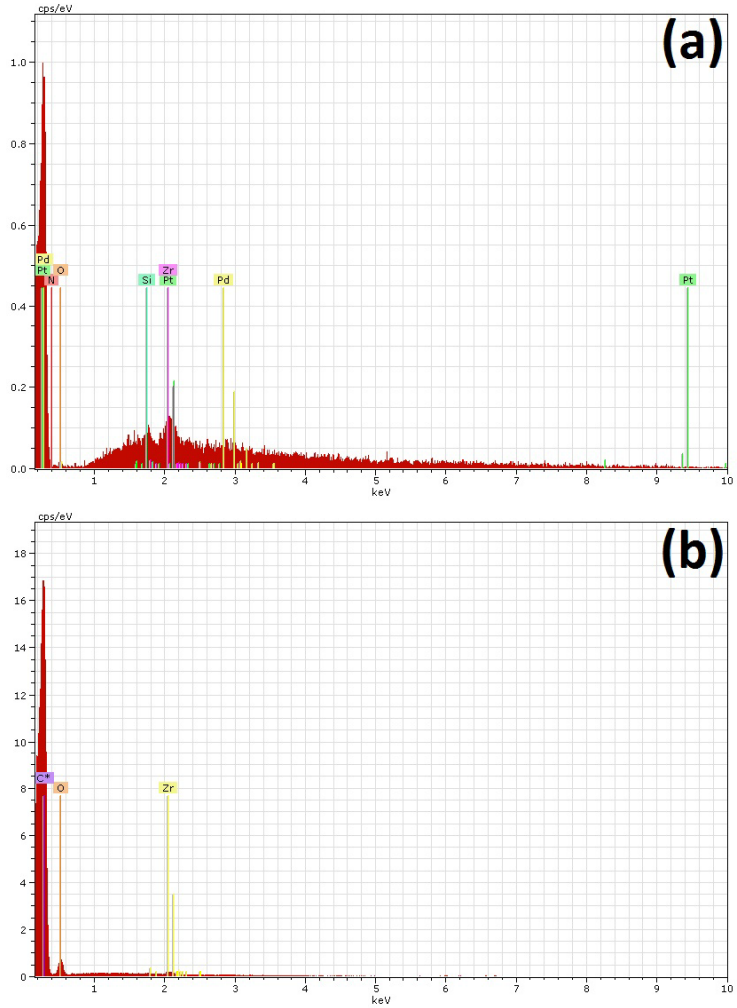

Figure 31: EDX spectra of outside points in environmental sample. The points at which sampling was conducted are highlighted by a green cross in figures C.5(a) and C.9(a) in appendix C, respectively. Particles are sampled on polycarbonate filters at the Nationaltheatret underground subway station. (a) sampled during the day and (b) sampled during the night.

According to the EDX element maps and point spectra of each particle[35], most of the particles labeled in figure 30(a) contain predominantly Fe, while most of the particles in figure 30(d) contain Fe, Si, and O[36]. Particle 06 in figure 30(a) does not contain Fe, however. A large magnification SEM micrograph of this particle is presented in figure 32, along with element maps and point spectrum analysis.

The particle in figure 32 contains Fe, sulfur (S) and zinc (Zn), according to the EDX point spectrum in figure 32(f). The element maps of each of these elements, presented in figures 32(c)-(e) indicate that some areas of the particle, like the right edge area, contain more iron than the rest of the particle. S and Zn is more evenly distributed, but the signal from these elements is stronger from the middle area of the particle.

[35]Some presented in appendix in figure C.5 - C.12 in appendix C.

[36]The results disregard the elements detected in the filter material itself.

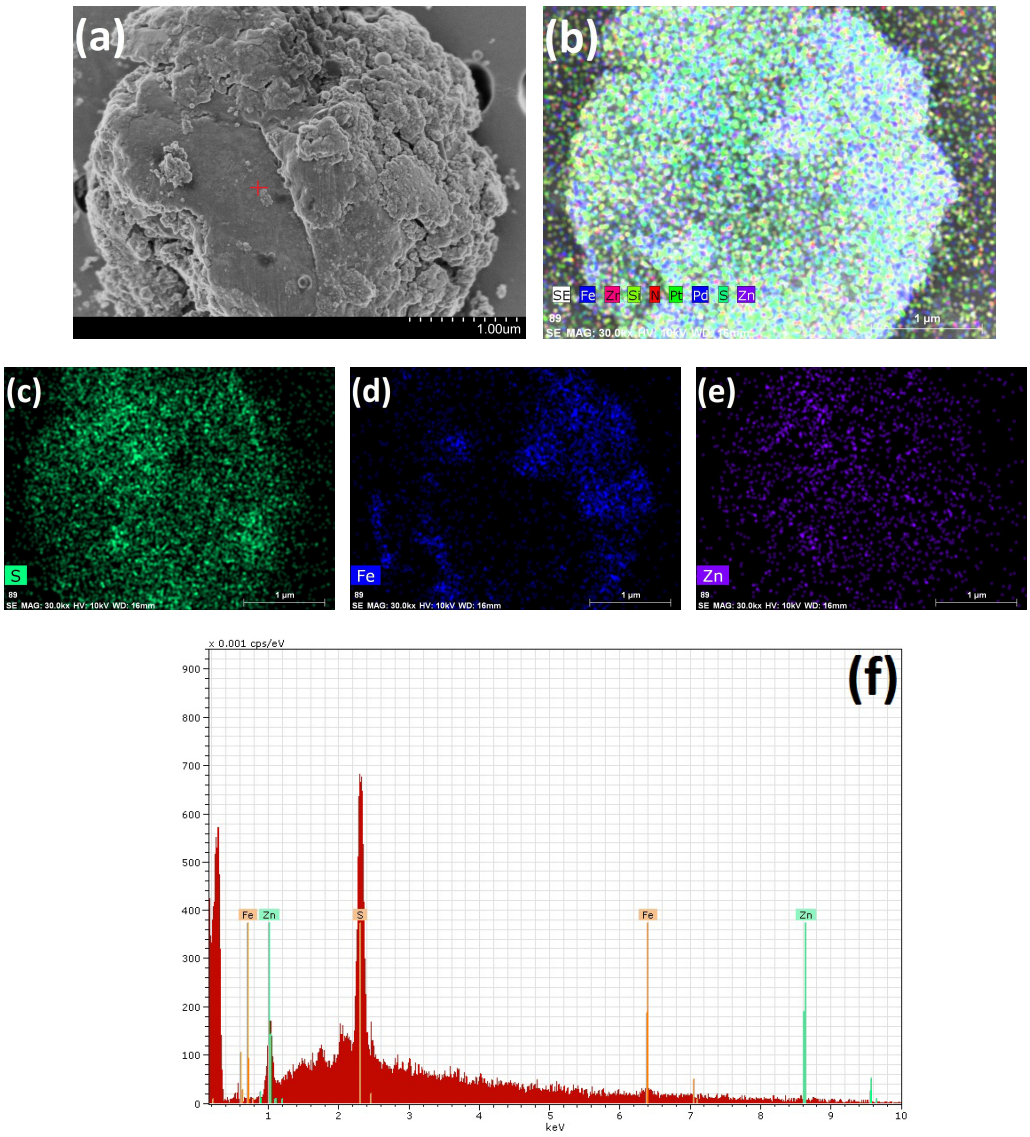

Figure 32: (a) SEM micrograph, (b)-(e) EDX element maps and (f) point spectrum of particle 06 observed in environmental sample presented in figure 30(a). (b) EDX element map of detected elements in the same overview as (a). (c)-(e) EDX element maps showing presence of (c) sulfur (S), (d) iron (Fe) and (e) zinc (Zn) in the sample. The red cross in (a) represents the spot at which the point spectrum analysis in (f) was performed.

On the filter sampled on during nighttime, a particle differing from the particles imaged in figure 30(d) in elemental composition was observed. A small magnification SEM micrograph of this particle is presented in figure 33 and a large magnification SEM micrograph of the same particle is presented in figure 34, along with element maps and point spectrum analysis.

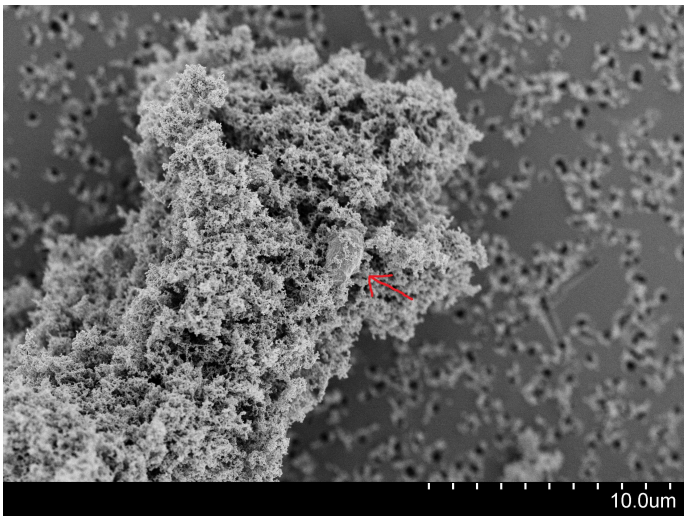

Figure 33: Small magnification SEM micrograph of particle observed in environmental sample sampled during nighttime at the Nationaltheatret underground subway station. The particle is highlighted by the red arrow. The particle is identical to the particle imaged in figure 34(a) at a different magnification.

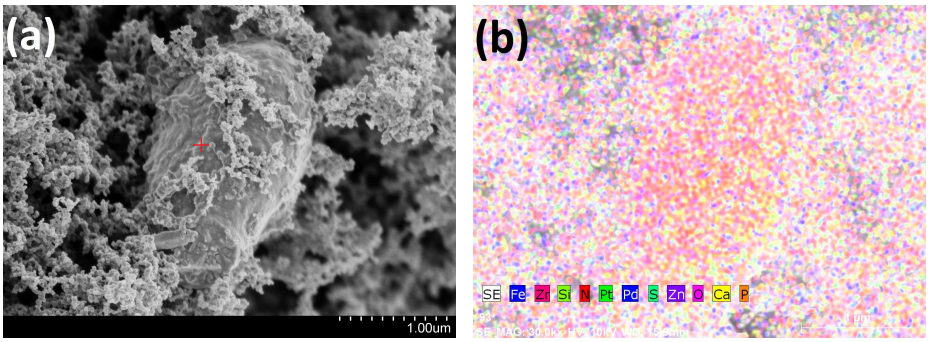

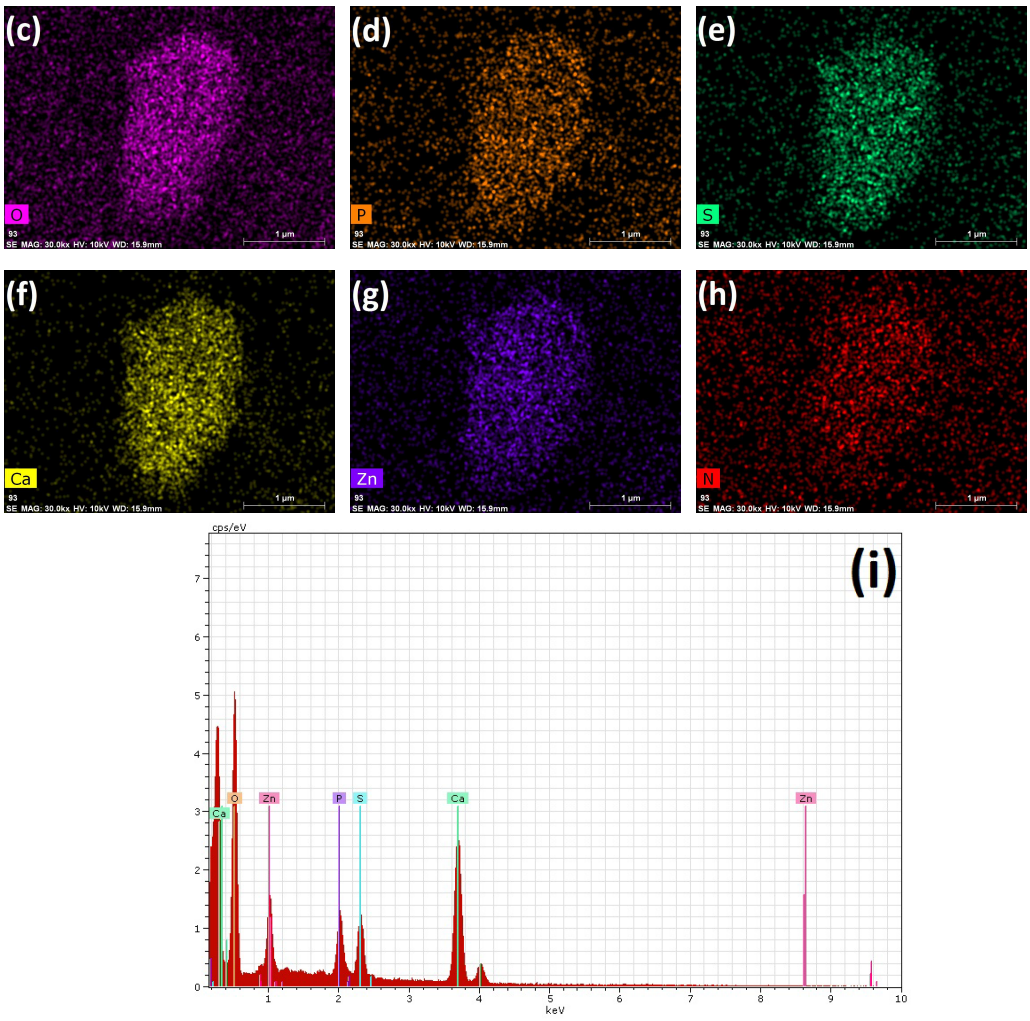

Figure 34: (a) SEM micrograph, (b)-(g) EDX element maps and (f) point spectrum of particle observed in environmental sample sampled during nighttime at the Nationaltheatret underground subway station. (b) EDX element map of detected elements in the same overview as (a). (c)-(g) EDX element maps showing presence of (c) oxygen (O), (d) phosphorus (P), (e) sulfur (S), (f) calcium (Ca), (g) zinc (Zn), and (h) nitrogen (N) in the sample. N was detected during element mapping, but did not show up on the EDX point spectrum in (i). The red cross in (a) represents the spot at which the point spectrum analysis in (i) was performed.

Figure 33 presents a small magnification SEM micrograph of the particle presented in figure 34(a). The particle is highlighted by a red arrow, and is associated with a larger network of other elemental composition, as illustrated by figure 34(b). While the EDX point spectrum in figure 34(h) indicates that the particle contains O, P, S, Ca and Zn, the element map in figure 34(b) also detects presence of N, Si and Fe, not including Pt, Pd and Zr.

The surrounding network also appears morphologically very different than the particle, which looks more similar to a single *BG* spore (as seen in e.g. figures 14 and 22) in overall shape, although the particle in figure 34(a) is bigger (approximately 2.5 μm) than a typical *BG* spore.

5 Discussion

5.1 Bioaerosol morphology

A reason why the fixed and critically point dried small *BG* spore bioaerosols in figure 14 appear marginally smoother and less wrinkled than the unfixed spores, may be due to partial rehydration during fixation in aqueous, 10% glutaraldehyde vapor. A study by Westphal et al. [88] found that *Bacillus* spores swell and shrink in response to changes in humidity. Studies by Plomp et al. [82] suggest that the surface of *BG* spores in dry environments exhibits deformation by way of formation of many thick ridges extending over the spore surface in a wrinkle-like fashion. The same study describes the surface of rehydrated *BG* spores as covered by a continuous layer of very thin (a few nm thick) rodlets, thereby appearing smoother than in dry state. As all the *BG* spores in figure 14 exhibit thick ridges, it can be concluded that they are all at least partly dehydrated, even though states of dehydration seem to vary, however minimal, between fixed and unfixed spores.

The difference in hydration state between spores may also stem from added toughness and ability to withstand dehydration in vacuum imposed on fixed and critically point dried particles during fixation. The differences in surface structure between unfixed, fixed and critically point dried *BG* spores here are however minimal, and hence the results are inconclusive.

Comparing small *BG* spore bioaerosols in figure 14 with *BG* spores from liquid solution in figure 22, the spores from the liquid solution look marginally smoother and puffier than their respective aerosolized counterpart, although also exhibiting thick ridges on the surface. As the critically point dried *BG* spores in figures 22(e) and (f) should represent the state of the spores before aerosolization, and these resemble the aerosolized spores in figure 14, it can be concluded that the spore conformation of these latter particles lie close to the initial conformation, and (de)hydration state, they have upon aerosolization.

The reason why aerosolized *BG* spores appear slightly more dehydrated than the non-aerosolized spores of figure 22, may be attributed to dehydration while in air or at filter, or it can be a result of a difference between properties of the two fixation methods used. The reason

why the spores in figure 14 have not collapsed or dehydrated further, is probably due to the resilience of the spores against desiccation [68] [89]. This resilience is also probably the reason why the morphologies of the aerosolized or non-aerosolized *BG* spores do not differ much from each other regarding preparation method[37].

S. marcescens bacteria, on the other hand, are more sensitive toward physical disruption than *BG* spores. There are hence larger morphological differences between the aerosolized *S. marcescens* bacteria in figures 17 and 20 and the non-aerosolized, critically point dried *S. marcescens* bacteria of figures 23(e) and (f), the latter serving as a reference to the appearance of the particles upon aerosolization. Similar references are found in [85], [86] and [87]. It is reasonable to assume that the physical disruption of the bacteria is a result of dehydration somewhere along the way from aerosolization to observation. For the non-aerosolized *S. marcescens* bacteria in figure 23, the conformation differences between the particles of different preparation method are probably due to differences in toughness provided by the different methods, and subsequent dehydration in vacuum for the unfixed and merely fixed bacteria. This dehydration probably causes larger collapse in unfixed bacteria than in fixed bacteria (as glutaraldehyde fixation provides stabilization of cell cytoplasm), causing the bacterial conformation seen in figure 23(b).

As for the unfixed bacteria in figure 17(b), it may seem likely that dehydration has taken place in vacuum, causing artifacts such as shrinkage due to water loss, as this is known to happen to hydrated specimens [20] [22]. As the *S. marcescens* bacteria in this study have been subjected to vacuum on two occasions, in the sputter coater and SEM vacuum, both of these places are probable points of introduction of vacuum related particle shrinkage. Removing the sputter coating step would probably not improve upon the situation, as the specimens spend more time in the high vacuum of the SEM than the sputter coater, and would thus probably appear the same as had they been sputter coated (or more likely worse, as the particles would have lacked conductive coating[38]). ESEM may be a method to consider regarding imaging of

[37] even though some differences occur, e.g. the fact that there are more collapsed particles among the unfixed than critically point dried *BG* spores in figure 22.

[38] Shown by the author in a previous study [1]: Conventional SEM of uncoated specimens generated drift and poor images.

uncoated bioaerosols, if removal of the sputter coater step is desired.

The theory that dehydration takes place in vacuum, however, does not take into account that, despite some differences, all the *S. marcescens* bacteria of figures 17 and 20 look collapsed and dehydrated, regardless of preparation method. This is true also for large *BG* spore and *S. marcescens* bioaerosols as witnessed in figure 25. As displayed by the critically point dried *S. marcescens* bacteria originating from liquid solution in figures 23(e) and (f), the method of CPD used in this study clearly preserves intact bacterial structure and prohibits collapse inside the SEM. A logical conclusion as to why even the critically point dried, aerosolized small *S. marcescens* bacteria look so dehydrated in the SEM, is then that they dehydrate before CPD.

As it is evident that *S. marcescens* bacteria retain a hydrated morphology in the medium upon aerosolization, the question is at what point between aerosolization and CPD the dehydration of bioaerosol particles occurs. Considering the common dehydrated state of the bacteria of different preparation, also that of unfixed bacteria, fixation may be ruled out as a point of dehydration. The passage through air and the sampling and time spent on the polycarbonate filter/TEM grid therefore remain as possible points of dehydration. Should the first assumption prove correct (that bioaerosols dehydrate through the passage through air), a new question arises, that is whether SEM micrographs of these bioaerosols convey their shape as it is in air, or if the process of imaging deteriorates the particles further.

It is anyway likely that dehydration also occurs during sampling onto substrates. As pointed out by Kenny et al. [90], drawing air over delicate microorganisms[39] reduces particle viability due to dehydration effects. The micrographs presented in this study do possibly therefore misrepresent the morphology of small *S. marcescens* bioaerosols compared to how it is in air regardless of preparation method, because the particles may dehydrate and change already upon sampling. When considering that most bioaerosol detectors need some form of bioaerosol capture, the fact that sampling may dehydrate bioaerosols need not have severe implications for the usability of results obtained by sampling methods used in this study.

[39] as done during sampling on both polycarbonate filters and TEM grids in this study

In light of the theory that most bioaerosol dehydration takes place before preparation, it is hard to explain why the 10% glutaraldehyde vapor fixed and critically point dried *S. marcescens* bacteria in figure 17 look (minimally) more hydrated than the unfixed particles of the same figure. The fact that the 70% glutaraldehyde fixed and critically point dried equivalent bioaerosols in figure 20 exhibit similar, raisin-like conformation as the unfixed bacteria in figure 17, further contributes to discredit the assumption that the fixed and critically point dried bacteria in figure 20 are more hydrated than the unfixed bacteria. A possible explanation for these results, lies in considering the fact that the preparation of the particles, in this case the fixation, has had an altering effect on the particles, rendering them incomparable to the unfixed bacteria and those fixed by 70% glutaraldehyde vapor. The fact that the particles are obscured by a grainy material, supports this theory, and also makes it difficult to assess whether or not the bacterial cells truly are more hydrated.

Comparing the SEM micrographs of large *S. marcescens* bioaerosols of different preparation in figure 18 and 19, the bioaerosols fixed by 10% glutaraldehyde vapor appear dissolved compared to the unfixed particles. The reason is possibly the high water content (90%) in the glutaraldehyde vapor, allowing the water to act as a solvent toward the salt and medium residue binding the bioaerosol together.

The fact that the critically point dried bioaerosols in figure 18 and 19 seem to maintain a three dimensional structure to a larger degree than the unfixed bioaerosols in the same figure, may suggest that at least part of the particle dehydration takes place within the SEM. This lends strength to a second theory explaining why the *S. marcescens* bioaerosols undergone fixation by 10% glutaraldehyde vapor appear so dissolved: The individual bacteria collapse on top of each other. Assuming that CPD dehydrates individual bacteria in a non-destructive way, making them more resilient to vacuum than bacteria that are merely fixed, would then explain why the large, critically point dried *S. marcescens* bioaerosols in figure 18 and 19 look structurally more intact than the particles undergone fixation but not CPD.

To sum up a likely chain of events leading to the bioaerosol conformations seen in figure 18 and 19: Subjected to the water in the glu-

taraldehyde vapor, large bioaerosols dissolve (and spread) partly, but maintain some three dimensional structure. Spreading of the bioaerosols is probably the reason why the large *S. marcescens* bioaerosols do not vanish from the filter surface during CPD, as the large *BG* spore bioaerosols in figure 15 do[40]. When subjected to the vacuum of the SEM, the non-critically point dried, but fixed, bioaerosols, then collapse further due to dehydration of the individual particles, while the critically point dried bioaerosols to a larger degree maintain the structure gained during fixation.

This theory is further supported by the fact that the unfixed bioaerosols in figure 18 and 19 look more like spheres than flakes, even though they are also subjected to dehydrating vacuum. These bioaerosols have not been partly dissolved upon entering the SEM chamber, hence the individual bacteria that constitute the bioaerosols are stacked on top of each other in greater numbers, making particle collapse and conformation change less noticeable than were the particles spread thinner across the substrate.

Small *S. marcescens* bioaerosols fixed by both 10% and 70% glutaraldehyde vapor appear deformed and dehydrated compared to their presumed initial conformation (as presented in figures 23(e) and (f)). Interestingly, individual *S. marcescens* bacteria that are part of larger, fixed and critically point dried bioaerosols seem much more intact than their single equivalents, as witnessed in figures 18 and 19. This is true for bacterial cells and spores fixed by 10% glutaraldehyde vapor.

Working from the theory that bioaerosols also dehydrate before reaching the point of preparation and observation in vacuum, it is interesting to ask whether being part of a larger bioaerosol provides some sort of protection from dehydration in air and on sampling substrate. If assuming that fixation and CPD has a conserving effect, and that fixation in this case simultaneously has an altering, dissolving effect on the bioaerosols, the notion of complex bioaerosols offering protection to the bacterial particles they are composed of, provides a likely explanation as to the results presented in figures 18 and 19.

The unfixed bioaerosols in these figures consist of many individ-

[40]This is probably due to the fixed *S. marcescens* bioaerosols gaining a larger surface contact area in relation to the total volume of the particles.

ual bacteria. Given the bioaerosols' size, some bacteria are probably shielded from the outside by external, visible bacteria, which are hardly discernible as individual particles due to tight packing and dehydration[41]. Assuming that dehydration and morphology change occurs first and foremost to the external particles would provide some protection to the internal particles, allowing these to somewhat retain their shape by fixation and CPD, as they become visible at dissolution of the bioaerosol particle during the former method. This theory of dehydration occuring to external particle may be supported by the fact that some of the *S. marcescens* bacteria in figures 18(d) and (f) and figures 19(b) and (c) appear more collapsed than others.

5.2 Bioaerosol adherence

The results indicated that fewer small, critically point dried *BG* spore bioaerosols were present on polycarbonate filters, than equivalent particles not undergone CPD. This difference in particle density was not observed on filters containing small *S. marcescens* bioaerosols.

Several studies (e.g. Wiencek et al. [91] and Doyle et al. [92]) have concluded that *Bacillus* spores are more hydrophobic than the corresponding vegetative cells[42]. However, in the study by Wiencek et al., 47% of *BG* spores in an aqueous suspension were found to bind to hexadecene. This measure of hydrophobicity is called the BATH test [94].

S. marcescens bacteria are also long known to be hydrophobic [95][43]. Parment et al. [98] found the BATH values of different isolates of *S. marcescens* to be between approximately 7.8% and 27.1%. Although some reservations should be made considering the comparability of these values [99], they suggest that the *BG* spores examined in this study should be more hydrophobic than the *S. marcescens* bacteria.

[41]Donut-like holes in some of the unfixed bioaerosols suggest internal cavities into which external bacteria can collapse.

[42]Mainly due to an abundance of proteins in the spore coats and exosporium, which can act as hydrocarbon adherence sites [92]. *BG* spores lack exosporium, which make them less hydrophobic than spores of other *Bacillus* strains [93].

[43]Probably due to the presence of O-antigen in the bacteria's outer membrane [96] [97].

This difference in hydrophobicity, coupled with the fact that the polycarbonate filters are hydrophilic, and that they are submerged in ethanol before CPD, may explain the loss of *BG* spore bioaerosols in the filter undergone CPD, compared to the filters that have not undergone CPD. This may also explain why the density of *S. marcescens* bioaerosols is apparently more similar from filter to filter, independent of preparation method; *S. marcescens* bacteria are not so prone to leave the polycarbonate filter surface in favor of the ethanol phase as the *BG* spores [100].

The fact that there is no difference in *BG* spore particle density between the hydrophobic TEM grid undergone CPD, and the equivalent TEM grids not undergone CPD in figures 24(a)-(c), supports the theory that it is weak adherence between particle and substrate that causes *BG* spores to detach from polycarbonate filters during CPD. Further support for this theory is found when considering that hydrophilic materials are more resistant to bacterial adhesion than hydrophobic materials [100] [101] [102].

Small *S. marcescens* bioaerosols however, exhibit a different pattern. Their density does not vary between preparation methods when sampled on polycarbonate filters, but when sampled on TEM grids, as in figures 24(d)-(f), the particles seem to disappear from the hole areas of the mesh during CPD, only remaining located on the copper edges of the grid. As *S. marcescens* bacteria are less hydrophobic than *BG* spores, adherence to the hydrophobic, carbon-coated Formvar TEM grid upon exposure to ethanol and CPD is probably weaker than for *BG* spores, and the bacteria are as a consequence more easily washed off[44].

However, the fact that the *S. marcescens* bacterial cells undergone CPD in figure 24(f), have not been washed off the TEM grid altogether, but remained on the edges of the grid, does not fit into this theory, considering that although the edges consist of copper, they too are covered by Formvar and carbon. An explanation of this phenomena may be

[44]For this theory to be correct, it has to be assumed that *S. marcescens* bacteria either adhere more easily to polycarbonate filters than to TEM grids, or that the two sampling methods (Millipore cassette or Andersen sampler) are incomparable in terms of attaching bacteria to substrate.

found in the influence of the surface structure on bacterial adherence. Several studies [103] [104] [105] indicate that rough surfaces promote adherence of bacteria more than smooth surfaces[45]. As the surface of the mesh edges are considerably rougher than that of the mesh holes of the TEM grid (by visual inspection), this may explain why the small *S. marcescens* bioaerosols undergone CPD are only located here.

However, ascribing adherence to only rely on the hydrophobic and hydrophilic properties of bacterial particles and substrates, and the roughness or smoothness of the latter, proves insufficient when observing large bioaerosols. Even though small *BG* spore and *S. marcescens* bioaerosols undergone CPD are present on polycarbonate filters (although in varying degree), the equivalent, spherically shaped, large bioaerosols undergone CPD are missing from polycarbonate filters, as illustrated in figures 15 and 21. As the difference between small and large bioaerosols of respective bacterial species is their shape and size (morphology), it is natural to assume that the difference in adherence properties is related to one or both of these properties. A likely explanation as to why large bioaerosols disappear from polycarbonate filters during CPD, would then be that due to their size and shape, the contact surface between bioaerosol and filter surface is smaller relative to the overall size of the particle, and therefore the large bioaerosols are more easily removed physically from the filter by ethanol than small particles.

Why this physical process has not removed all large, critically point dried bioaerosols sampled on TEM grids (see figures 25(b) and (e)) from the substrate surface, is probably due to the differences in hydrophobicity between polycarbonate filters and TEM grids as previously discussed. It is interesting that small, critically point dried *S. marcescens* bioaerosols are lacking from the mesh hole areas of the TEM grids, while equivalent, large bioaerosols are present at these areas. The former imply that *S. marcescens* bacteria adhere more readily to the polycarbonate filter than the TEM grid, and the latter the opposite. If considering differences in the two sampling methods used, Millipore cassette and Andersen sampler, however, it is only the Andersen sampler that takes advantage of the particles' inertia, as the air

[45]Possibly due to a larger surface area and depressions and sites on the surface that provide favorable adherence sites [100].

stream in the last sampling stage changes direction as it exits[46]. Taking the difference between small and large particles' inertia and velocity[47] into consideration, large particles (that are near spherically shaped and actually reach the final stage) would then be impacted with greater speed onto the TEM substrate than small ones, which could possibly cause large particles to adhere better to the TEM grid surface, and not disappear during CPD.

Inertia also comes into play when considering the difference in density between small and large bioaerosols sampled on TEM grids in figures 24 and 25. The greatest reason why there are more small bioaerosols than large bioaerosols deposited on the TEM grids, is probably due to substantial lower concentrations of large bioaerosols than small bioaerosols in air during sampling[48]. In addition, larger particles are more vulnerable to impaction than small particles due to their inertia [107], hence larger bioaerosols may be retained at early stages during passing through the Andersen sampler, resulting in a lower number of bioaerosols actually depositing on the TEM grid.

Sampling bioaerosols on TEM grids instead of on polycarbonate filters can be advantageous considering the grids' conductive properties (C and Cu conducts electrons)[49], and the fact that large bioaerosols adhere better to TEM grids than polycarbonate filters. Considering the flaws in the method used to sample bioaerosols on TEM grids however (bioaerosols are not guaranteed to hit the grid (in large numbers)), and that not all bioaerosols remain deposited on the smooth surface of the TEM grid hole during CPD, sampling bioaerosols on TEM grids does

[46]See figure 6, the air stream is sucked out of a valve at the base of the sampler

[47]The terminal velocity for a spherical particle traveling through air can be expressed as (based on Stoke's law):

$$v = \frac{\rho \; d^2 \; g \; C}{18 \; \eta} \tag{4}$$

where v equals the terminal velocity $[cm/s]$, ρ particle density $[g/cm^3]$, d particle diameter $[cm]$, g is gravitational acceleration $[cm/s^2]$, η air viscosity $[g/cm\ s^{-1}]$ and C is the Cunningham slip correction [106].

[48]There was also a concentration difference between *BG* spore and *S. marcescens* bioaerosols upon spreading, explaining the difference in density between the two species.

[49]i.e. bioaerosols sampled on TEM grids may not need coating.

not yield more advantages than equivalent sampling on polycarbonate filters, other than when large bioaerosols are to be sampled and undergo CPD prior to SEM.

Regarding the fact that there were no bioaerosols present on the grid which should have contained large, fixed *BG* bioaerosols in figure 25; none of the other results generated when examining TEM grids containing bioaerosols by SEM, suggest that bioaerosols should be lacking from this grid. Both the *BG* spore bioaerosols undergone CPD (after fixation) and the large, fixed *S. marcescens* bioaerosols are present on their respective grids, which indicates that the lack of large, fixed *BG* bioaerosols is not caused by the fixation. As the sampling method does not fully guarantee that particles deposit onto the TEM grid, one possibility is that the TEM grid has been misaligned in relation to the particle-containing air flow. Another likely possibility is that the particle count has been so low that no particles actually passed through the sampler at the location of the TEM grid.

5.3 Presence of non-biological material

The small fragments present on the small bioaerosols and on the filters in e.g. figures 14, 17 and 20, are probably not biological material, but salt and medium residue[50], and probably originate from droplets that have not contained any bacterial cells or spores, and that have dried in air before depositing on the filter. In light of this, the lack of these fragments on filters containing large bioaerosols is expected, considering that in the spreading of these, probably almost all of the drops contained bacterial cells or spores. In the large bioaerosols, this inorganic material is most likely integrated in the particles, functioning as glue to at least partly keep the spores or bacteria in place to form a large bioaerosol particle [108].

The covering of the fixed and critically point dried *S. marcescens* particles in figure 17 in what appears a grainy film, has probably something to do with something that happens during fixation with 10% aqueous glutaraldehyde vapor, e.g. hydration and subsequent dissolving of cellular material and salts to create the grainy texture.

[50]EDX could help confirm this in future studies.

The origin of the unique structures[51] present on all polycarbonate filters undergone CPD (i.e. on all critically point dried filters imaged in figures 14, 15 and 17-21), presents a puzzle. These structures do not directly affect the characterization of the bioaerosols, and their origins are therefore a subordinate matter. A brief theory as to some of the reason for their presence can be attempted however. As these structures only appear on polycarbonate filters undergone CPD, it is natural to assume that the structures' origins are related to the CPD process, either the ethanol administered to the bacterial cells and spores beforehand, or the heat and pressure imposed on the filters during the CPD process. It could also be related to impurities introduced externally during CPD. However, these unique "CPD structures" are not present on TEM grids undergone CPD, hence it is less likely that the structures are externally introduced. It is then most likely that the structures have originated during the CPD process because of some reaction involving the polycarbonate filter. The exact nature of this reaction however, will not be explored further in this context.

[51] as highlighted in figure 14(e) and figure B.1 in appendix B

5.4 TEM

Because electrons in TEM convey information by transmission through samples, and the bioaerosols imaged by TEM in figures 26-29 are too thick for the electrons to escape through, the particles appear homogeneous black. This makes it impossible to establish the three dimensional morphology of any of the bioaerosols imaged, and very difficult to ascertain the identity of the particles, unless this is known beforehand. Thus, TEM does not yield further information about the morphology of bioaerosols when used to image unsectioned, large and small *BG* spore and *S. marcescens* bioaerosols.

The identity of the particles on the TEM grids that should contain large *BG* spore bioaerosols in figure 27 is especially difficult to assess, as these are smaller than the equivalent large *BG* spore bioaerosols imaged by SEM. This could be related to miscalibration of the TEM scale bar, but as all the other bioaerosols match with the equivalent SEM images regarding size, this is less probable. It is more probable that the particles imaged in figure 27 are not large *BG* spore bioaerosols, but unknown particles stemming from contamination of the TEM grid. The reason for the absence of large *BG* spore bioaerosols from the grid may be due to an error in the sampling method, which does not guarantee the sampling of particles unless the grid is placed exactly beneath a hole in the Andersen sampler.

Because SEM and TEM both take place in vacuum, and the bioaerosols imaged by these two methods have not been prepared differently after sampling, their conformation should not diverge largely. However, as the acceleration voltage of the electron beam used in TEM is different (larger) than that used in SEM, this could induce differences in the shape of the bioaerosols imaged by the two methods [57] [41] [22]. Any potential difference, damage or dehydration is difficult to assess, however, as the bioaerosols in the TEM micrographs lack three dimensionality and color variation, and are hence reduced to mere black spots.

Present on the TEM micrographs are, besides the larger, assumed bioaerosols, also smaller fragments, which are most likely salt and

medium residue as seen in some of the SEM micrographs[52]. The reason for their absence in the micrographs in figure 27 depicting large *BG* spore bioaerosols, is probably the same as for the SEM micrographs, i.e. that most droplets contain spore particles, so that most particulates are contained within a larger bioaerosol, if this is at all present on the filter[53].

[52]Even though the fragments observed on the polycarbonate filter appear minimally bigger, which could be attributed to difficulties associated with assessing fragment size accurately and representatively, as well as to differences in sampling methods.

[53]It is likely that the small fragments on the TEM grids containing large *S. marcescens* bioaerosols, stem from the transformation of the bioaerosols and their contents during fixation with 10% glutaraldehyde vapor, a transformation apparent upon study of equivalent bioaerosols in figures 18(d) and (e).

5.5 EDX

The main objective of the EDX analysis in this work, is to assess whether or not EDX can be used to distinguish biological material from inorganic material, with the aim of automatic detection of interesting particles. However, regarding detector research, naturally occurring background is also of interest, and differences in particle density, morphology and composition between specimens sampled during day- and nighttime will also be dicussed here.

EDX analysis and SEM of environmental samples sampled at the Nationaltheatret underground subway station, indicate a difference in both density, morphology and composition between particles sampled during day- and nighttime.

Most of the particles sampled during daytime are smaller than the particles sampled during nighttime. As there was less traffic through the sampling location during the nighttime than the daytime, it is natural to assume that the difference in density is due to less generation of particles during nighttime, along with a reduction of airflow through the station. The fact that large particles generally resuspend[54] more easily than small particles [106] [109], is probably the reason why particles sampled during nighttime as a trend appear to be larger than daytime sampled aerosols. When less aerosols are generated by activity, resuspension becomes more important as an aerosolizing factor.

Based on the elemental composition of the day- and nighttime particles, adjusted for the composition of the surrounding areas, it appears that most of the observed particles sampled during daytime consist of predominantly Fe, while most of the observed particles sampled during nighttime consist of Fe, Si and O. If considering that activity on train tracks consisting of Fe, generates aerosols during daytime, but not during nighttime, these results are as expected. From the elements present in the nighttime particles, it is natural to assume that these are glass particles, mixed with some Fe.

Fe is most likely the major element of the grainy material covering some of the particles in figure 30(d), presented more clearly in figures

[54]Here, resuspension describes the process in which deposited material becomes airborne [106].

C.9(a), C.11(a) and C.12(a) in appendix C, because when comparing these particles' EDX point spectra to that of the smooth looking particle in figure C.12 in appendix C, this particle does not contain Fe. Particles sampled during daytime also exhibit this grainy surface structure. Looking at particle 06 in figure 32 (both SEM micrograph and EDX element map for Fe), Fe is detected mostly at the grainy, not the smooth, areas of the particle, which supports the theory that Fe has a grainy appearance.

As the particle presented in figure 32 only contains S and Zn in addition to Fe[55], it is probably not of biological origin, considering that neither O, N or P is detected. O, N and P constitute, together with C, H and S, the majority of elements in all biological cells [110] [111] [112]. According to EDX element maps and point spectrum analysis, the particle in figure 34 however, contains five of these six major elements (C, N, O, P and S), along with Zn and Ca, which can be present in cellular material in lesser quantities [110]. H has a low atomic number, and is thereby difficult to detect by EDX, which means that the particle in figure 34 contains all the major elements that cellular material contains.

Matthias-Maser and Jaenicke [10] and Matthias-Maser et al. [55] classified bioaerosols as having small peaks of (Si, Cl), P, S, K and Ca. The EDX analysis did not detect Si, Cl or K in the particle in figure 34, but it does have a rod-shaped morphology, which means that the particle can almost be classified as a bioaerosol according to the criteria set in the study by Matthias-Maser and Jaenicke. A study by Genga et al. [113] classifies bioaerosols as having regular and symmetrical shapes, e.g. elliptical, and having high contents of C and O, and sometimes containing Na, Mg, P, K and Ca. The particle in figure 34 could thus be a biological particle according to Genga et al. All the results, the morphology and elemental composition of the environmental particle in figure 34, strongly indicate that the particle is of biological origin. The network surrounding the particle however, is probably not biological, as both the element map in figure 34(b) and morphology of the network indicate that it, for a major part, consists of Fe. The biological particle is hence part of an inorganic network, and is not a free bioaerosol.

[55]and carbon (C), which is disregarded as it is present in most point spectra and element maps, and has such a low atomic number that its presence is difficult to establish accurately by CPD.

The samples are not flat, and are hence not ideal for EDX analysis, as the EDX detector count rate is affected by the direction the sample is facing, along with its thickness. This can affect the results, generating more signal from the particle than the background, and hence provide misleading element maps. Comparing point spectra of particle and outside filter points however, should provide sufficient information to qualitatively assess element composition of particles imaged.

The fact that EDX analysis easily distinguishes Fe and other inorganic material from organic material in environmental samples, indicates that bioaerosols in theory could be distinguished from inorganic aerosols by detecting the latter using EDX in an automated process[56]. This strategy, however, requires bioaerosols to be free of any inorganic material or network, in order for the system to detect the bioaerosols, and not dismiss them as inorganic material. Considering that the one probable biological particle observed among the environmental particles investigated in this study, was associated with an inorganic network, indicates that masking of biological material by inorganic material occurs, and will possibly lead to this material not being detected by automated EDX sample analysis.

[56]E.g. the Esprit Feature software by Bruker is designed to, in combination with an X-ray detector, conduct automatic particle recognition and element analysis over a large area, provided sufficient contrast between particles and background [114].

6 Conclusions

- After passage through air, bioaerosols probably dehydrate both upon sampling on polycarbonate filters and TEM grids, and, if not undergone any preparation, in the vacuum of the electron microscope.
- Bioaerosols of *BG* spores (from Gram positive microorganisms) withstand dehydration and morphology changes better than bioaerosols of *S. marcescens* bacteria (Gram negative), regardless of bioaerosol size. The former bioaerosols undergo only minimal conformational changes from aerosolization to imaging.
- CPD preserves the morphology of small bioaerosols, but as this changes upon sampling, the bioaerosol morphology observed by SEM is probably misrepresented relative to that in air. Large, spherically shaped bioaerosols are removed from polycarbonate filters during CPD.
- 70% glutaraldehyde vapor fixation does not alter bioaerosol morphology, as opposed to 10% glutaraldehyde vapor fixation, which dissolves large bioaerosols. Fixation is necessary to preserve the morphology of individual bacterial cells, but may also destroy the overall conformation of large, complex bioaerosols.
- Being part of a larger, complex bioaerosol seems to provide some protection from dehydration for individual *S. marcescens* bacteria.
- SEM only provides information about the external part of the bioaerosols, the contents of large, complex bioaerosols remain obscured.
- Large bioaerosols adhere better to hydrophobic TEM grids than hydrophilic polycarbonate filters, but sampling bioaerosols on TEM grids is more challenging.
- TEM as is, does not yield further (or bulk) information about the morphology of bioaerosols when used to image unsectioned, large and small *BG* spore and *S. marcescens* bioaerosols.
- EDX analysis may be a powerful technique to distinguish particles of inorganic origin from other particles in environmental samples.

7 Further work

CPD exhibits promise to preserve the structure of even large and complex bioaerosols, but further studies need to be made to e.g. assess whether or not this method interferes with the overall structure of large bioaerosols. As the results in this study indicate that large bioaerosols may be removed from polycarbonate filters during CPD, and that dehydration also occurs during sampling, further efforts should be made in exploring the optimum bioaerosol sampling substrate, preventing bioaerosol dehydration and keeping bioaerosols adhered to the substrate also during CPD.

Assessment of bioaerosol adherence to substrates with different properties can be further explored, based on sampling on TEM grids as presented in this thesis.

Different methods of preparation and imaging should be explored regarding preservation of especially large and complex bioaerosols, with the aim of developing an optimal preparation protocol for bioaerosol preservation. After a thorough literature study, particularly cryopreparation and cryo-SEM emerge as promising alternatives, as these methods have the potential to fix and subsequently image specimens without using chemicals which could interfere with both bioaerosol adherence and structure. These methods may prove especially advantageous regarding imaging of large bioaerosols.

Investigations regarding automated element analysis using EDX and specialized software (e.g. using the Esprit Feature software by Bruker available at FFI), could be conducted in order to further address the issue of detecting bioaerosols in environmental samples. EDX analysis could also be conducted for the non-environmental samples in this study, in order to assess elemental composition of the known biological material, and of the unknown small fragments which are presumed to be salts and medium residue.

Future work could include investigations into the nature of the CPD structures seen in e.g. figure B.1 in appendix B. EDX analysis could be involved in order to assess their elemental composition. Filters of different material, along with unsampled filters, could undergo CPD to decide whether the reaction is polycarbonate filter specific or not, and whether the formation of the structures is related to bioaerosol

sampling, respectively.

Because TEM of unsectioned bioaerosols does not yield any inside information of the particles, e.g. ultramicrotomy prior to TEM or STEM could be a method of interest in further work to reveal the inner composition of bioaerosols. Ultramicrotomy of bioaerosols may be challenging to conduct however, due to difficulties which could arise regarding precise, structure preserving microtomy of biological material. Locating sampled bioaerosols for microtomy will probably also prove difficult.

References

[1] H. Grydeland. Characterization of Bioaerosols using Electron Microscopy with Special Emphasis on Bacteria. Project Thesis, Norwegian Institute of Science and Technology (NTNU), 2013.

[2] P. A. Ariya, J. Sun, N. A. Eltouny, E. D. Hudson, C. T. Hayes, and G. Kos. Physical and chemical characterization of bioaerosols: Implications for nucleation processes. *International Reviews in Physical Chemistry*, 28(1):1–32, 2009.

[3] K. Wittmaack, H. Wehnes, U. Heinzmann, and R. Agerer. An overview on bioaerosols viewed by scanning electron microscopy. *Science of the Total Environment*, 346(1):244–255, 2005.

[4] S. Matthias-Maser, V. Obolkin, T. Khodzer, and R. Jaenicke. Seasonal variation of primary biological aerosol particles in the remote continental region of Lake Baikal/Siberia. *Atmospheric Environment*, 34(22):3805–3811, 2000.

[5] Y. S. Kim, K. Y. Yoon, J. H. Park, and J. Hwang. Application of air ions for bacterial de-colonization in air filters contaminated by aerosolized bacteria. *Science of the Total Environment*, 409(4):748–755, 2011.

[6] C. E. Main. Aerobiological, ecological, and health linkages. *Environment International*, 29(2):347–349, 2003.

[7] C. E. Morris, D. C. Sands, M. Bardin, R. Jaenicke, B. Vogel, C. Leyronas, P. A. Ariya, and R. Psenner. Microbiology and atmospheric processes: research challenges concerning the impact of airborne micro-organisms on the atmosphere and climate. *Biogeosciences*, 8(1):17–25, 2011.

[8] M. Dybwad, P. E. Granum, P. Bruheim, and J. M. Blatny. Characterization of Airborne Bacteria at an Underground Subway Station. *Applied and Environmental Microbiology*, 78(6):1917–1929, 2011.

[9] M. J. Heard and R. D. Wiffen. Electron Microscopy of Natural Aerosols and the Identification of Particulate Ammonium Sulphate. *Atmospheric Environment*, 3(3):337–340, 1969.

[10] S. Matthias-Maser and R. Jaenicke. Examination of Atmospheric Bioaerosol Particles with radii >0.2 µm. *Journal of Aerosol Science*, 25(8):1605–1613, 1994.

[11] M. Glikson, S. Rutherford, R. W. Simpson, C. A. Mitchell, and A. Yago. Microscopic and Submicron Components of Atmospheric Particulate Matter During High Asthma Periods in Brisbane, Queensland, Australia. *Atmospheric Environment*, 29(4):549–562, 1995.

[12] M. Mastalerz, M. Glikson, and R. W. Simpson. Analysis of atmospheric particulate matter; application of optical and selected geochemical techniques. *International Journal of Coal Geology*, 37(1):143–153, 1998.

[13] E. Ganor, Z. Levin, and R. van Grieken. Composition of Individual Aerosol Particles Above the Israelian Mediterranean Coast During the Summer Time. *Atmospheric Environment*, 32(9):1631–1642, 1998.

[14] M. Ebert, S. Weinbruch, P. Hoffmann, and H. M. Ortner. Chemical Characterization of North Sea Aerosol Particles. *Journal of Aerosol Science*, 31(5):613–632, 2000.

[15] E. K. Bigg. Brochosomes - a tracer for near-surface air. Letter to the editor, 2003.

[16] M. Pósfai, J. Li, J. R. Anderson, and P. R. Buseck. Aerosol bacteria over the Southern Ocean during ACE-1. *Atmospheric Research*, 66(4):231–240, 2003.

[17] E. J. L. Torres, W. de Souza, and K. Miranda. Comparative analysis of Trichuris muris surface using conventional, low vacuum, environmental and field emission scanning electron microscopy. *Veterinary Parasitology*, 196(3):409–416, 2013.

[18] S. H. Coetzee, A. Jordaan, and S. F. Mpuchanee. Low Pressure Mode Combined With OsO4 Vapor Fixation and Sputter-Coating for the Preservation of Delicate Aerial Hyphae and Conidia in the ESEM. *Microscopy Research and Technique*, 67(5):265–270, 2005.

[19] S. Reese and B. Guggenheim. A Novel TEM Contrasting Technique for Extracellular Polysaccharides in In Vitro Biofilms. *Microscopy Research and Technique*, 70(9):816–822, 2007.

[20] A. T. Vestlund. *Characterisation and Dispersal of Bioaerosols Emitted from Composting Facilities*. PhD thesis, Cranfield University, 2008-2009.

[21] V. H. Heywood. Scanning electron microscopy in the study of plant materials. *Micron*, 1(1):1–14, 1969.

[22] P. Gwaze, H. J. Annegarn, J. Huth, and G. Helas. Comparison of particle sizes determined with impactor, AFM and SEM. *Atmospheric Research*, 86(2):93–104, 2007.

[23] A. C. Dohnalkova, M. J. Marshall, B. W. Arey, K. H. Williams, E. C. Buck, and J. K. Fredrickson. Imaging Hydrated Microbial Extracellular Polymers: Comparative Analysis by Electron Microscopy. *Applied and Environmental Microbiology*, 77(4):1254–1262, 2011.

[24] E. W. Henningson and M. S. Ahlberg. Evaluation of Microbiological Aerosol Samplers: A Review. *Journal of Aerosol Science*, 25(8):1459–1492, 1994.

[25] R. Maier, I. L. Pepper, and C. G. Gerba, editors. *Environmental Microbiology*, pages 83–92, 149–153. Academic Press, 2009.

[26] K. F. Martinez, C. Y. Rao, and N. C. Burton. Exposure assessment and analysis for biological agents. *Grana*, 43(4):193–208, 2004.

[27] L. D. Stetzenbach, M. P. Buttner, and P. Cruz. Detection and enumeration of airborne biocontaminants. *Current Opinion in Biotechnology*, 15(3):170–174, 2004.

[28] K. R. Spurny. On the Chemical Detection of Bioaerosols. *Journal of Aerosol Science*, 25(8):1533–1547, 1994.

[29] W. D. Griffiths and G. A. L. DeCosemo. The Assessment of Bioaerosols: A Critical Review. *Journal of Aerosol Science*, 25(8):1425–1458, 1994.

[30] A. Nevalainen, J. Pastuszka, F. Liebhaber, and K. Willeke. Performance of Bioaerosol Samplers: Collection Characteristics and Sampler Design Considerations. *Atmospheric Environment*, 26A(4):531–540, 1992.

[31] M. P. M. Taha, G. H. Drew, A. Tamer, G. Hewings, G. M. Jordinson, P. J. Longhurst, and S. J. T. Pollard. Improving bioaerosol exposure assessments of composting facilities: Comparative modelling of emissions from different compost ages and processing activities. *Atmospheric Environment*, 41(21):4504–4519, 2007.

[32] M. A. Hayat, editor. *Principles and Techniques of Electron Microscopy: Biological Applications*, pages 1–137, 174–180. Macmillan Press, 1989.

[33] M. Hoppert and A. Holzenburg, editors. *Electron Microscopy in Microbiology*, pages 5–10, 42–43, 80. Bios Scientific Publishers, 1998.

[34] W. Li and L. Shao. Transmission electron microscopy study of aerosol particles from the brown hazes in northern China. *Journal of Geophysical Research*, 114:1–10, 2009.

[35] PIXE International Corporation. The Streaker Air-Particulate Sampler Instruction Manual. https://pixeintl.com/S2Pmanual.pdf, 2007. Online; last accessed: 06.02.14.

[36] I. Hurbain and M. Sachse. The future is cold: cryo-preparation methods for transmission electron microscopy of cells. *Biology of the Cell*, 103(9):405–420, 2011.

[37] J. R. McIntosh, editor. *Cellular Electron Microscopy*, pages 1–5. Academic Press, 2007.

[38] J. Dubochet. The Physics of Rapid Cooling and Its Implications for Cryoimmobilization of Cells. In J. R. McIntosh, editor, *Cellular Electron Microscopy*, pages 7–21. Academic Press, 2007.

[39] K. McDonald. Cryopreparation Methods for Electron Microscopy of Selected Model Systems. In J. R. McIntosh, editor, *Cellular Electron Microscopy*, pages 23–56. Academic Press, 2007.

[40] A. M. Glauert and P. R. Lewis, editors. *Biological Specimen Preparation for Transmission Electron Microscopy*, pages 21–75, 77–85, 129–146. Portland Press, 1998.

[41] J. J. Bozzola and L. D. Russell, editors. *Electron microscopy: principles and techniques for biologists*, pages 4–11, 16–37, 42–61, 136–182, 186–212, 332–348. Jones and Bartlett, 1992.

[42] E.-M. Füchtbauer, A. M. Rowlerson, K. Götz, G. Friedrich, K. Mabuchi, J. Gergely, and H. Jockusch. Direct Correlation of Parvalbumin Levels with Myosin Isoforms and Succinate Dehydrogenase Activity on Frozen Sections of Rodent Muscle. *The Journal of Histochemistry and Cytochemistry*, 39(3):355–361, 1991.

[43] I. A. Staff, P. E. Taylor, P. Smith, M. B. Singh, and R. B. Knox. Cellular localization of water soluble, allergenic proteins in rye-grass (Lolium perenne) pollen using monoclonal and specific IgE antibodies with immunogold probes. *Histochemical Journal*, 22(5):276–290, 1990.

[44] University of Georgia Center for Ultrastructural Research. Protocols and Recipes. http://caur.uga.edu/recipes.pdf. Online; last accessed: 20.01.14.

[45] Q. Jiang, N. Reddy, S. Zhang, N. Roscioli, and Y. Yang. Water-stable electrospun collagen fibers from a non-toxic solvent and crosslinking system. *Journal of Biomedical Materials Research A*, 101A(5):1237–1247, 2012.

[46] M. C. McManus, E. D. Boland, H. P. Koo, C. P. Barnes, K. J. Pawlowski, G. E. Wnek, D. G. Simpson, and G. L. Bowlin. Mechanical properties of electrospun fibrinogen structures. *Acta Biomaterialia*, 2(1):19–28, 2006.

[47] J. Liang, S. Zheng, and S. Ye. Inactivation of Penicillium aerosols by atmospheric positive corona discharge processing. *Journal of Aerosol Science*, 54:103–112, 2012.

[48] K. Ratnayake, D. C. Joyce, and R. I. Webb. A convenient sample preparation protocol for scanning electron microscope examination of xylem-occluding bacterial biofilm on cut flowers and foliage. *Scientia Horticulturae*, 140:12–18, 2012.

[49] Y.-C. Chung, Y.-Y. Lin, and C.-P. Tseng. Operational Characteristics of Effective Removal of H_2S and NH_3 Waste Gases by Activated Carbon Biofilter. *Journal of the Air & Waste Management Association*, 54(4):450–458, 2004.

[50] J. C. Gilkey and L. A. Staehelin. Advances in Ultrarapid Freezing for the Preservation of Cellular Ultrastructure. *Journal of Electron Microscopy Technique*, 3(2):177–210, 1986.

[51] N. L. Burstein and D. M. Maurice. Cryofixation of Tissue Surfaces by a Propane Jet for Electron Microscopy. *Micron*, 9(4):191–198, 1978.

[52] N. Roos and A. J. Morgan, editors. *Cryopreparation of Thin Biological Specimens for Electron Microscopy: Methods and Applications*, pages 9–18. Oxford University Press, 1990.

[53] R.M Glaeser. Cryo Electron Microscopy of Biological Nanostructures. *Physics Today*, 61(1):48–54, 2008.

[54] Cressington Scientific Instruments Ltd. Cressington 208HR High Resolution Sputter Coater for FE-SEM. Operating manual, 2003.

[55] S. Matthias-Maser, B. Bogs, and R. Jaenicke. The size distribution of primary biological aerosol particles in cloud water on the mountain Kleiner Feldberg/Taunus (FRG). *Atmospheric Research*, 54(1):1–13, 2000.

[56] D. B. Williams and C. B. Carter, editors. *Transmission Electron Microscopy: A Textbook for Materials Science*, pages 3–71, 91–114, 581–662. Springer, 2009.

[57] J. Goldstein, D. Newbury, D. Joy, C. Lyman, P. Echlin, E. Lifshin, L. Sawyer, and J. Michael, editors. *Scanning Electron Microscopy and X-ray Microanalysis*, pages 1–390. Springer, 2003.

[58] P. C. Tiemeijer, M. Bischoff, B. Freitag, and C. Kisielowski. Using a monochromator to improve the resolution in TEM to below 0.5 Å. Part I: Creating highly coherent monochromated illumination. *Ultramicroscopy*, 114:72–81, 2012.

[59] L. Muscariello, F. Rosso, G. Marino, A. Giordano, M. Barbarisi, G. Cafiero, and A. Barbarisi. A Critical Overview of ESEM Applications in the Biological Field. *Journal of Cellular Physiology*, 205(3):328–334, 2005.

[60] S. J. Pennycook, A. R. Lupini, M. Varela, A. Y. Borisevich, Y. Peng, M. P. Oxley, and M. F. Chisholm. Scanning transmission electron microscopy for nanostructure characterization. In W. Zhou and Z. L. Wang, editors, *Scanning Microscopy for Nanotechnology: Techniques and Applications*, pages 152–188. Springer, 2006.

[61] J. S. Wall and J. F. Hainfeld. Mass Mapping with the Scanning Transmission Electron Microscope. *Annual Review of Biophysical Chemistry*, 15(1):355–376, 1986.

[62] C. Colliex and C. Mory. Scanning transmission electron microscopy of biological structures. *Biology of the Cell*, 80(2-3):175–180, 1994.

[63] NanoProbe Network. Scanning Transmission Electron Microscope (STEM). http://nanoprobenetwork.org/probepedia/index.php/Scanning_Transmission_Electron_Microscope_(STEM). Online; last accessed: 16.12.13.

[64] M. Bárcena, G. T. Oostergetel, W. Bartelink, F. G. A. Faas, A. Verkleij, P. J. M. Rottier, A. J. Koster, and B. J. Bosch. Cryo-electron tomography of mouse hepatitis virus: Insights into the structure of the coronavirion. *PNAS*, 106(2):582–587, 2009.

[65] M. Bárcena, R. I. Koning, and A. J. Koster. Attachment of Staphylococci to Various Synthetic Polymers. In G. Van Tendeloo, D. Van Dyck, and S. J. Pennycook, editors, *Handbook of Nanoscopy*, pages 1303–1333. Wiley, 2012.

[66] D. Mavrocordatos, W. Pronk, and M. Boller. Analysis of environmental particles by atomic force microscopy, scanning and transmission electron microscopy. *Water Science and Technology*, 50(12):9–18, 2004.

[67] R. F. Egerton, editor. *Electron Energy-Loss spectroscopy in the Electron Microscope*, pages 1–28. Springer, 2011.

[68] M. T. Madigan, J. M. Martinko, D. A. Stahl, and D. P. Clark, editors. *Brock Biology of Microorganisms*, pages 97, 524. Pearson, 2012.

[69] M. Carrera, R. O. Zandomeni, J. Fitzgibbon, and J.-L. Sagripanti. Difference between the spore sizes of *Bacillus anthracis* and other *Bacillus* species. *Journal of Applied Microbiology*, 102(2):303–312, 2007.

[70] The Center for Research Information Inc. for National Academics. Health Effects of Project SHAD Biological Agent: Bacillus Globigii. http://www.iom.edu/ /media/Files/Report%20Files/2007/Long-Term-Health-Effects-of-Participation-in-Project-SHAD-Shipboard-Hazard-and-Defense/BACILLUSGLOBIGII.pdf, 2004. Online; last accessed 16.12.13.

[71] M. Fricker, J. Ågren, B. Segerman, R. Knutsson, and M. Ehling-Schulz. Evaluation of Bacillus strains as model systems for the work on Bacillus anthracis spores. *Biology of the Cell*, 145:S129–S136, 1994.

[72] L. Jeffrey, D. DeCesaro, S. Le, and C. Miller. Growth Characteristics and Membrane Retention Profile of *S. marcescens* as a Model for Aqueous Solution Filtration. http://www.americanpharmaceuticalreview.com/Featured-Articles/118497-Growth-Characteristics-and-Membrane-Retention-Profile-of-S-marcescens-as-a-Model-for-Aqueous-Solution-Filtration/, 2012. Online; last accessed: 03.03.14.

[73] C. L. Kurz, S. Chauvet, E. Andrès, M. Aurouze, I. Vallet, G. P. F. Michel, M. Uh, J. Celli, A. Filloux, S. de Bentzmann, I. Steinmetz, J. A. Hoffmann, B. B. Finlay, J.-P. Gorvel, D. Ferrandon, and J. J. Ewbank. Virulence factors of the human opportunistic pathogen *Serratia marcescens* identified by *in vivo* screening. *The EMBO Journal*, 22(7):1451–1460, 2003.

[74] S. Srivastava and P. S. Srivastava, editors. *Understanding Bacteria*, page 30. Kluwer Academic Publishers, 2003.

[75] Inc. Ted Pella. Substrates, Support Films for Transmission Electron Microscopy Grids. http://www.tedpella.com/Support_Films_html/Support_Films_and_Substrates_Overview.htm. Online; last accessed: 12.05.14.

[76] Inc. Ted Pella. Support Film Product Note, How the Material is Layered on the Grid. http://www.tedpella.com/Support_Films_html/support-film-tech.htm. Online; last accessed: 12.05.14.

[77] M. Kaláb, A.-F. Yang, and D. Chabot. Conventional Scanning Electron Microscopy of Bacteria. *infocus Magazine*, 10:42–61, 2008.

[78] H.-J. Eom, D. Gupta, X. Li, H.-J. Jung, H. Kim, and C.-U. Ro. Influence of Collecting Substrates on the Characterization of Hygroscopic Properties of Inorganic Aerosol Particles. *Analytical Chemistry*, 86(5):2648–2656, 2005.

[79] S. Maskey, M. Choël, S. Kang, H. Hwang, H. Kim, and C.-U. Ro. The influence of collecting substrates on the single-particle

characterization of real atmospheric aerosols. *Analytica chimica acta*, 658(2):120–127, 2010.

[80] M. E. Wise, G. Biskos, S. T. Martin, L. M. Russell, and P. R. Buseck. Phase Transitions of Single Salt Particles Studied Using a Transmission Electron Microscope with an Environmental Cell. *Aerosol Science and Technology*, 39(9):849–856, 2005.

[81] M. Dybwad, G. Skogan, and J. M. Blatny. Temporal Variability of the Bioaerosol Background at a Subway Station: Concentration Level, Size Distribution, and Diversity of Airborne Bacteria. *Applied and Environmental Microbiology*, 80(1):257–270, 2014.

[82] M. Plomp, T. J. Leighton, K. E. Wheeler, and A. J. Malkin. The High-Resolution Architecture and Structural Dynamics of *Bacillus* Spores. *Biophysical Journal*, 88(1):603–608, 2005.

[83] S. A. Burke, J. D. Wright, M. K. Robinson, B. V. Bronk, and R. L. Warren. Detection of Molecular Diversity in *Bacillus atrophaeus* by Amplified Fragment Length Polymorphism Analysis. *Applied and Environmental Microbiology*, 70(5):2786–2790, 2004.

[84] W. Zhou, S. K. Watt, D.-H. Tsai, V. T. Lee, and M. R. Zachariah. Quantitative Attachment and Detachment of Bacterial Spores from Fine Wires through Continuous and Pulsed DC Electrophoretic Deposition. *Journal of Physical Chemistry*, 117(6):1738–1745, 2013.

[85] R. Lamed, J. Naimark, E. Morgenstern, and E. A. Bayer. Scanning electron microscopic delineation of bacterial surface topology using cationized ferritin. *Journal of Microbiological Methods*, 7(4):233–240, 1987.

[86] G. Strobel, J.-Y. Li, F. Sugawara, H. Koshino, J. Harper, and W. M. Hess. Oocydin A, a chlorinated macrocyclic lactone with potent anti-oomycete activity from *Serratia marcescens*. *Microbiology*, 145(12):3557–3564, 1999.

[87] M. A. Mondaca, V. Campos, R. Moraga, and C. A. Zaror. Chromate Reduction in Serratia marcescens Isolated from Tannery Effluent and Potential Application for Bioremediation of Chromate Pollution. *TheScientificWorldJOURNAL*, 2:972–977, 2002.

[88] A. J. Westphal, P. B. Price, T. J. Leighton, and K. E. Wheeler. Kinetics of size changes of individual *Bacillus thuringiensis* spores in response to changes in relative humidity. *PNAS*, 100(6):42–61, 2003.

[89] G. O. Rubel. A non-intrusive method for the measurement of water vapour sorption by bacterial spores. *Journal of Applied Microbiology*, 83(2):243–247, 1997.

[90] L. C. Kenny, J. D. Stancliffe, B. Crook, S. Stagg, W. D. Griffiths, I. W. Stewart, and S. J. Futter. The Adaptation of Existing Personal Inhalable Aerosol Samplers for Bioaerosol Sampling. *American Industrial Hygiene Association*, 59(12):831–841, 1998.

[91] K. M. Wiencek, N. A. Klapes, and P. M. Foegeding. Hydrophobicity of *Bacillus* and *Clostridium* Spores. *Applied and Environmental Microbiology*, 56(9):2600–2605, 1990.

[92] R. J. Doyle, F. Nedjat-Haiem, and J. S. Singh. Hydrophobic Characteristics of *Bacillus* Spores. *Current Microbiology*, 10(6):329–332, 1984.

[93] T. Koshikawa, M. Yamazaki, M. Yoshimi, S. Ogawa, A. Yamada, K. Watabe, and M. Tori. Surface Hydrophobicity of Spores of *Bacillus* spp. *Journal of General Microbiology*, 135(10):2717–2722, 1989.

[94] J. Škvarla, D. Kupka, and L. Turcániová. A complementary study of hydrophobicity and surface charge of *Thiobacillus ferrooxidans*. The effect of ionic surfactants. *Acta Montanistica Slovaca*, 7(2):85–88, 2002.

[95] S. Mudd and E. B. H. Mudd. The Penetration of Bacteria Through Capillary Spaces. IV. A kinetic mechanism in interfaces. *Journal of Experimental Medicine*, 40(5):633–645, 1924.

[96] A. Hejazi and F. R. Falkiner. *Serratia marcescens*. *Journal of Medical Microbiology*, 46(11):903–912, 1997.

[97] L. Wang, Q. Wang, and P. R. Reeves. The Variation of O Antigens in Gram-Negative Bacteria. In X. Wang and P. J. Quinn, editors, *Endotoxins: Structure, Function and Recognition*, pages 123–152. Springer, 2010.

[98] P. A. Parment, C. Svanborg-Ede'n, M. J. Chaknis, A. D. Sawant, L. Hagberg, L. A. Wilson, and D. G. Ahearn. Hemagglutination (Fimbriae) and Hydrophobicity in Adherence of *Serratia marcescens* to Urinary Tract Epithelium and Contact Lenses. *Current Microbiology*, 25(2):113–118, 1992.

[99] M. C. M van Loosdrecht, J. Lyklema, W. Norde, G. Schraa, and A. J. Zehnder. The role of bacterial cell wall hydrophobicity in adhesion. *Applied and Environmental Microbiology*, 53(8):1893–1897, 1987.

[100] Y. H. An and R. J. Friedman. Concise Review of Mechanisms of Bacterial Adhesion to Biomaterial Surfaces. *Journal of biomedical materials research*, 43(3):338–348, 1998.

[101] A. H. Hogt, J. Dankert, J.A. De Vries, and J. Feijen. Adhesion of Coagulase-negative Staphylococci to Biomaterials. *Journal of General Microbiology*, 129(9):2959–2968, 1983.

[102] A. Ludwicka, B. Jansen, T. Wadström, L. M. Switalski, G. Peters, and G. Pulverer. Attachment of Staphylococci to Various Synthetic Polymers. In S. W. Shalaby, A. S. Hoffman, B. D. Ratner, and T. A. Horbett, editors, *Polymers as Biomaterials*, pages 241–255. Springer, 1984.

[103] E. W. McAllister, L. C. Carey, P. G. Brady, R. Heller, and S. G. Kovacs. The role of polymeric surface smoothness of biliary stents in bacterial adherence, biofilm deposition, and stent occlusion. *Gastrointestinal Endoscopy*, 39(3):422–425, 1993.

[104] A. S. Baker and L. W. Greenham. Release of gentamicin from acrylic bone cement. Elution and diffusion studies. *The Journal of Bone & Joint Surgery*, 70(10):1551–1557, 1988.

[105] M. Quirynen, H. C. Van Der Mei, C. M. L. Bollen, A. Schotte, M. Marechal, G. I. Doornbusch, I. Naert, H. J. Busscher, and D. Van Steenberghe. An *in vivo* Study of the Influence of the Surface Roughness of Implants on the Microbiology of Supra- and Subgingival Plaque. *Journal of Dental Research*, 72(9):1304–1309, 1993.

[106] C. S. Cox and C. M. Wathes, editors. *Bioaerosols Handbook*, pages 16, 46. Lewis Publishers, 1995.

[107] Y. Zhao, A. J. A. Aarnink, P. Hofschreuder, and P. W. G. Groot Koerkamp. Evaluation of an impaction and a cyclone pre-separator for sampling high PM_{10} and $PM_{2.5}$ concentrations in livestock houses. *Journal of Aerosol Science*, 40(10):868–878, 2009.

[108] Committee on Materials and National Research Council Manufacturing Processes for Advanced Sensors, editors. *Sensor Systems for Biological Agent Attacks: Protecting Buildings and Military Bases*, page 23. The National Academies Press, 2005.

[109] K. W. Nicholson. Wind tunnel experiments on the resuspension of particulate material. *Atmospheric Environment*, 27A(2):181–188, 1993.

[110] J. Koolman and K.-H. Roehm, editors. *Color atlas of biochemistry* , page 2. Thieme Medical Publishers, Inc., 2013.

[111] Committee on Research Priorities for Earth Science and National Research Council Public Health, editors. *Earth Materials and Health: Research Priorities for Earth Science and Public Health*, page 29. The National Academies Press, 2007.

[112] F. Wolfe-Simon, J. S. Blum, T. R. Kulp, G. W. Gordon, S. E. Hoeft, J. Pett-Ridge, J. F. Stolz, S. M. Webb, P. K. Weber, P. C. W. Davies, A. D. Anbar, and R. S. Oremland. A Bacterium That Can Grow by Using Arsenic Instead of Phosphorus. *Science*, 332(6034):1163–1166, 2011.

[113] A. Genga, F. Baglivi, M. Siciliano, T. Siciliano, M. Tepore, G. Micocci, C. Tortorella, and A. Domenico. SEM-EDS investigation on PM10 data collected in Central Italy: Principal Component Analysis and Hierarchical Cluster Analysis. *Chemistry Central Journal*, 6(2):1–15, 2012.

[114] Bruker Nano. Esprit Feature brochure. http://www.bruker.com/fileadmin/user_upload/8-PDF-Docs/X-rayDiffraction_ElementalAnalysis/Microanalysis_EBSD/Brochures/Bro_esprit_feature_8p_en_rev2_low_res.pdf. Online; last accessed: 23.05.14.

Appendices

A Protocols

A.1 2.5% glutaraldehyde-PIPES buffer

1 3.05 g. of PIPES is dissolved in 50 ml distilled water in a glass beaker.

2 8.1 ml of a solution containing 1 M NaOH[57] is added to the beaker.

3 ∼3.5 ml of 70% aqueous glutaraldehyde solution is added to the beaker by a disposable Pasteur pipette.

4 The beaker is filled with distilled water until the volume reaches 100 ml, and the solution is stirred by a magnetic stirrer for 30 minutes.

5 To adjust the pH, 1 M NaOH is added until the pH is in the range 7.2 - 7.4.

The work should be conducted inside a fume hood.

The protocol is a modified version of a protocol presented in Glauert and Lewis [40].

[57] 4 g. NaOH dissolved in 100 ml distilled water.

A.2 CPD

1 The filter pieces are quickly transferred from 70% ethanol solution to individual compartments of a CPD holder and subjected to dehydration through a 80% - 90% - 96% - 100% ethanol series.

2 The chamber of a Bal-Tec CPD 030 instrument is filled with 100% ethanol and the CPD holder containing the filters is placed inside. The chamber is sealed and the instrument switched on.

3 After the CPD instrument has cooled the chamber to 10 °C, the chamber is filled with liquid CO_2, which is subsequently pumped out. This is repeated six times, until all the ethanol has been replaced by liquid CO_2.

4 The chamber is then heated to 40 °C and brought to 100 bar pressure, to reach conditions above the critical point[58].

5 After the pressure is reduced to atmospheric conditions, the dry filter pieces can be removed from the CPD holder.

The protocol is a standard protocol from the instruction folder of the Bal-Tec CPD 030 instrument.

[58] 31 °C and 73.8 bar.

A.3 Sputter coating

1 Double-sided carbon tape is attached onto 25 mm x 6 mm SEM aluminum stubs. The filters containing specimens are carefully removed from their sampling cassettes and deposited onto the filters with the particle side up.

2 A Pt/Pd alloy target is mounted in a Cressington 208 HR High-Resolution Sputter Coater for FE-SEM.

3 One stub is put into one of four stub holders (sample tables) in the sputter coater. The system is sealed by closing the chamber top-plate. The high chamber configuration is utilized.

4 The sputter coater is turned on and the following settings inputted: 40 mA current; density: 19.52; tooling factor: 1; thickness: 2 nm. The vacuum system pumps the chamber down to 0.15 mbar during the process.

5 The coating process is turned on at automatic program, and turns itself off after achieving desired thickness.

6 After coating, each stub is removed and placed in a box awaiting observation in SEM.

The protocol is a standard protocol from the instruction folder of the Cressington 208 HR sputter coater.

B Additional SEM micrographs

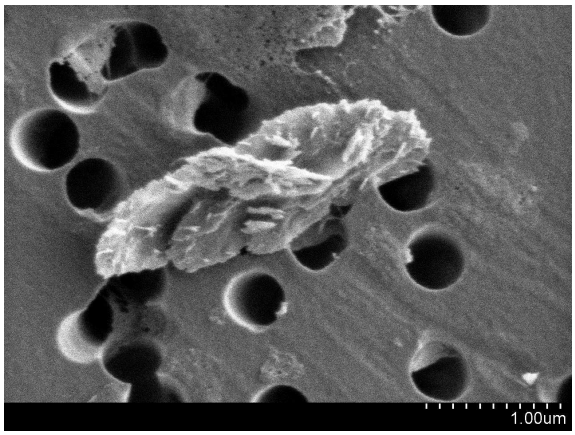

Figure B.1: SEM micrograph of unique structure found on critically point dried filter containing small *S. marcescens* bioaerosols fixed by 10% glutaraldehyde vapor.

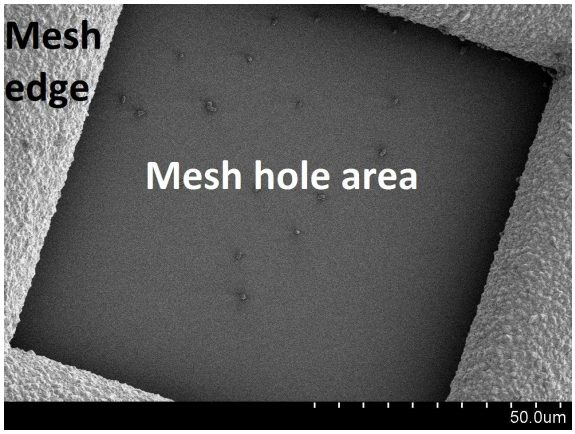

Figure B.2: SEM micrograph of TEM grid (containing fixed small *BG* spore bioaerosols) with assignments for mesh edge and hole area.

C Additional SEM micrographs, EDX point spectra and element maps of environmental samples

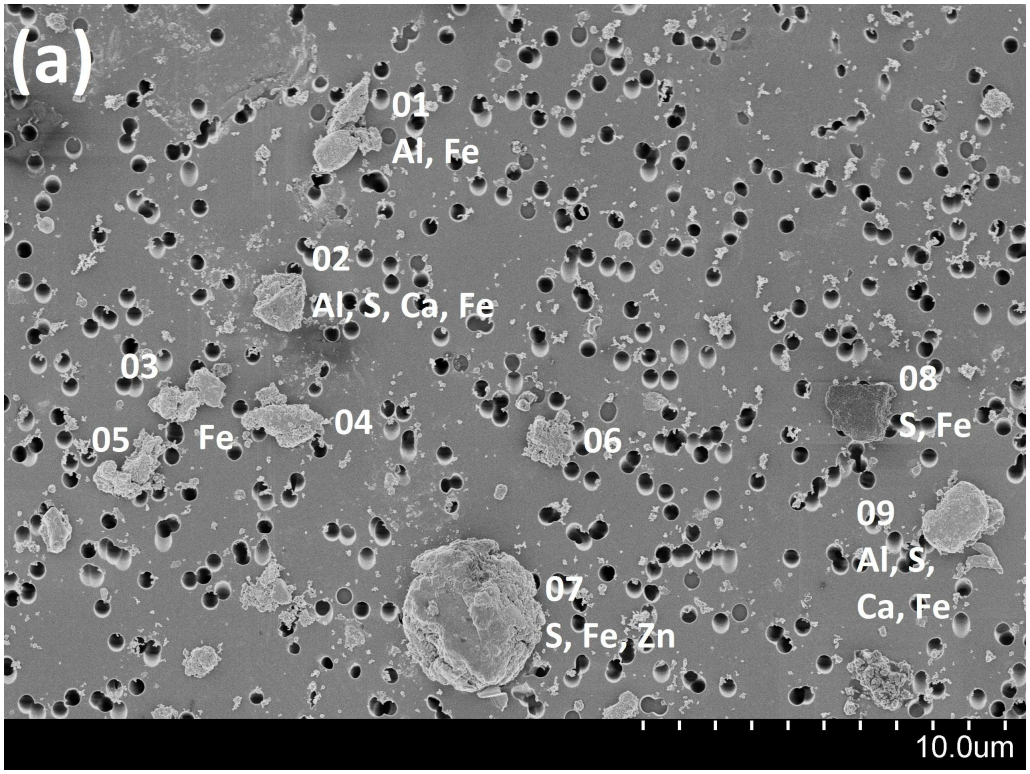

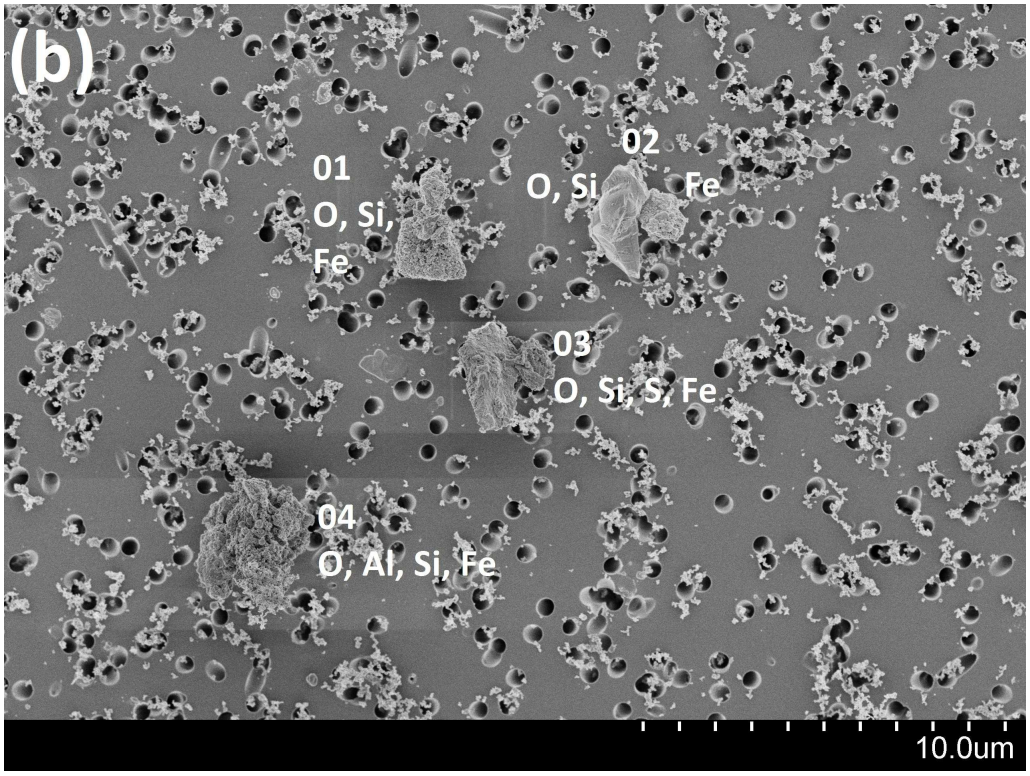

Figure C.3: Larger SEM micrographs identical to those found in figures 30(a) and (d). The micrographs provide an overview of environmental particles sampled during (a) daytime and (b) nighttime at the Nationaltheatret underground subway station. Particles are assigned elements according to EDX point spectrum analysis.

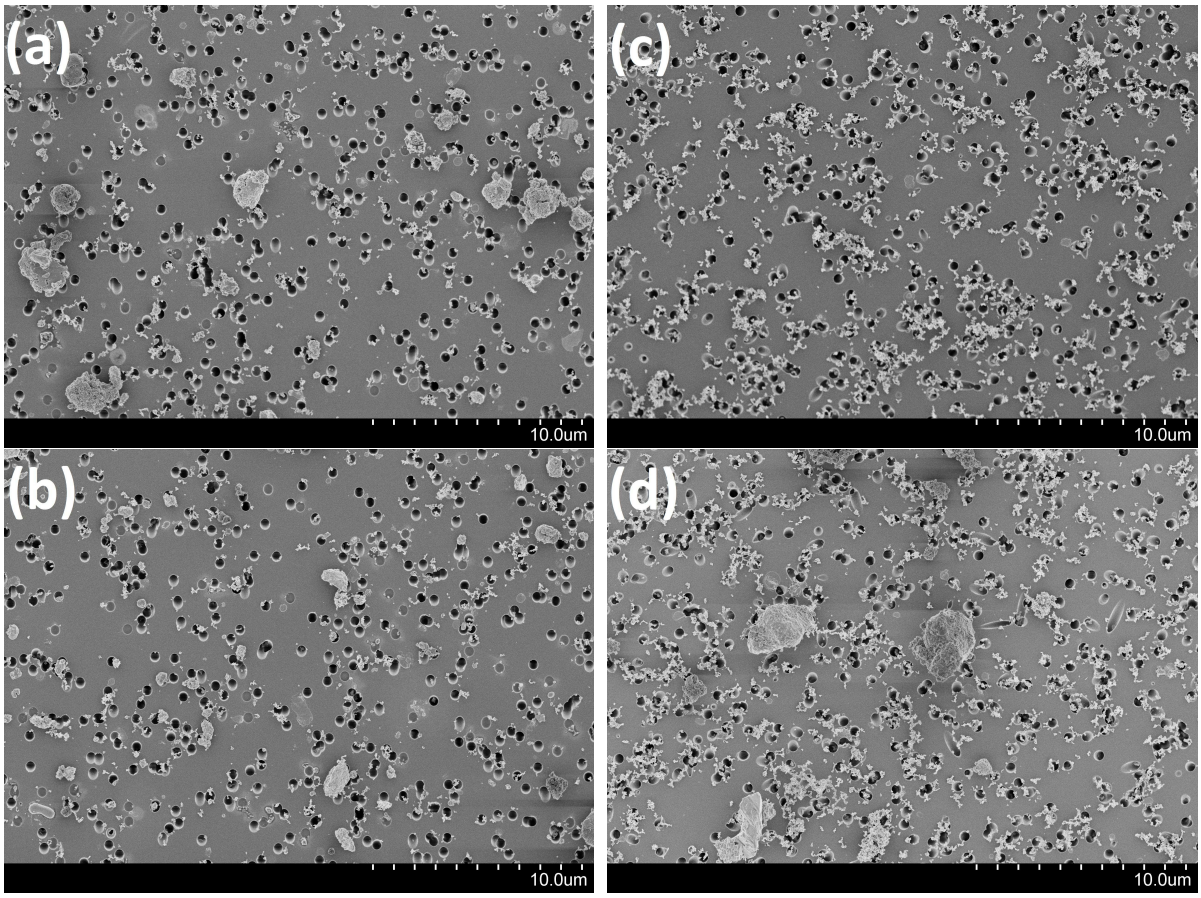

Figure C.4: SEM micrographs providing overviews of environmental particles sampled during (a) and (b) daytime and (c) and (d) nighttime at the Nationaltheatret underground subway station.

C.1 Aerosols sampled during the day

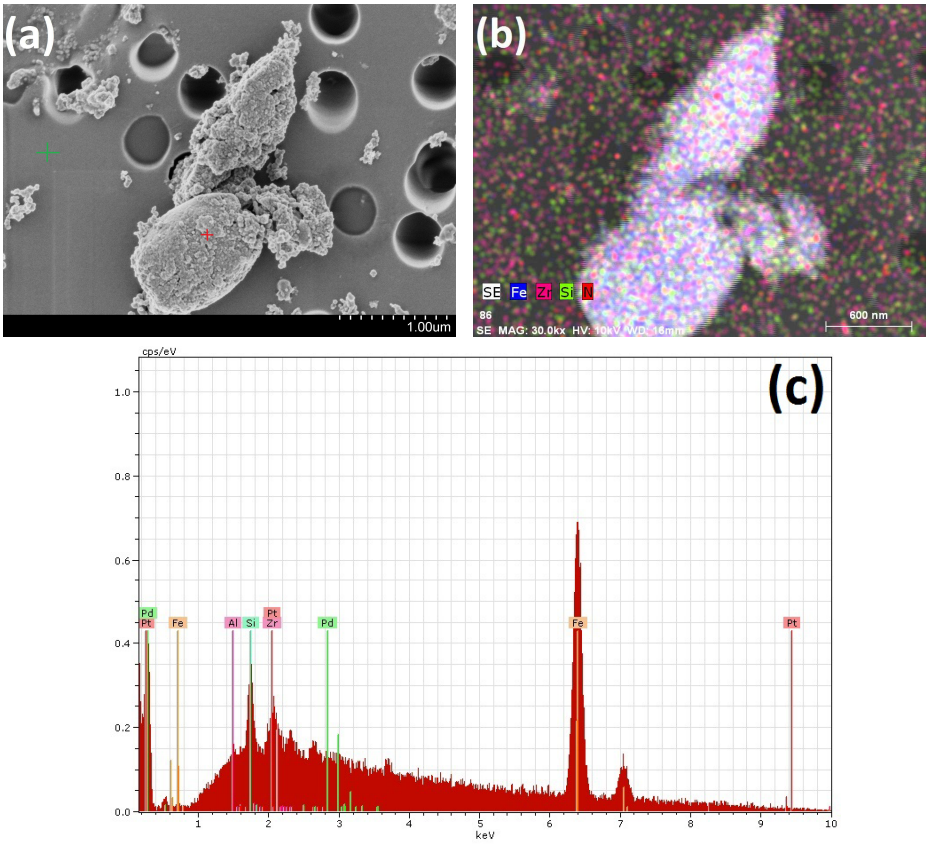

Figure C.5: (a) SEM micrograph, (b) EDX element map and (c) point spectrum of particle 01 observed in environmental sample presented in figure 30(a). The red cross in (a) represents the spot at which the point spectrum analysis in (c) was performed. The green cross in (a) represents the spot at which the outside point spectrum analysis in figure 31(b) was performed.

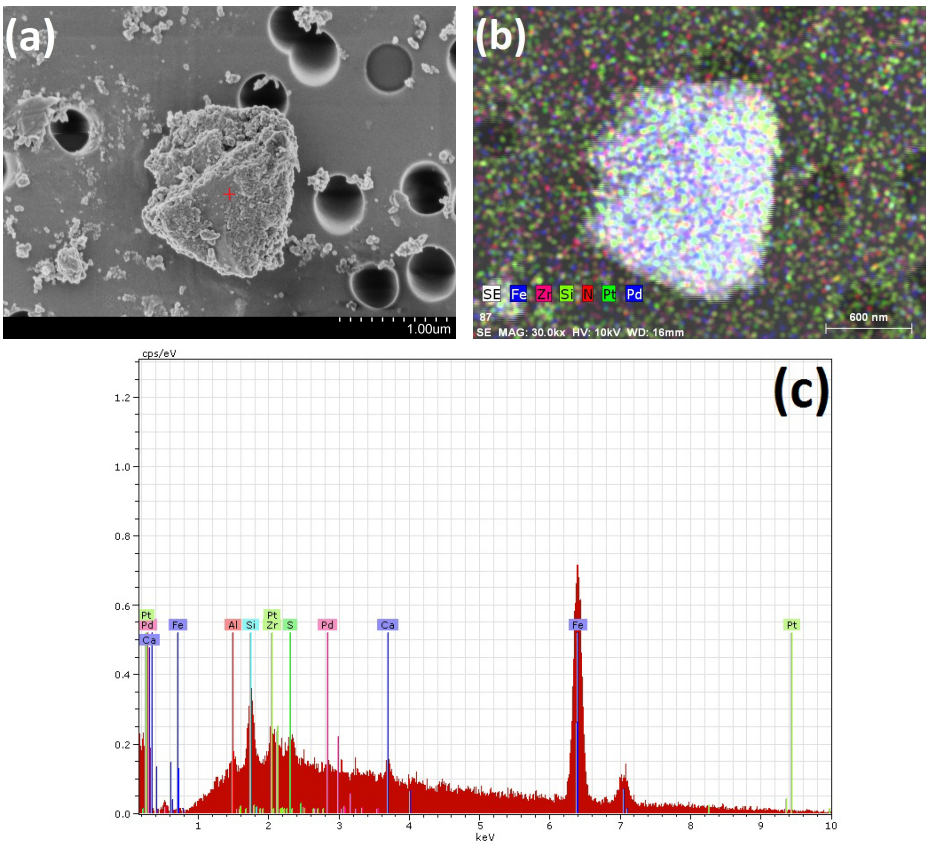

Figure C.6: (a) SEM micrograph, (b) EDX element map and (c) point spectrum of particle 02 observed in environmental sample presented in figure 30(a). The red cross in (a) represents the spot at which the point spectrum analysis in (c) was performed.

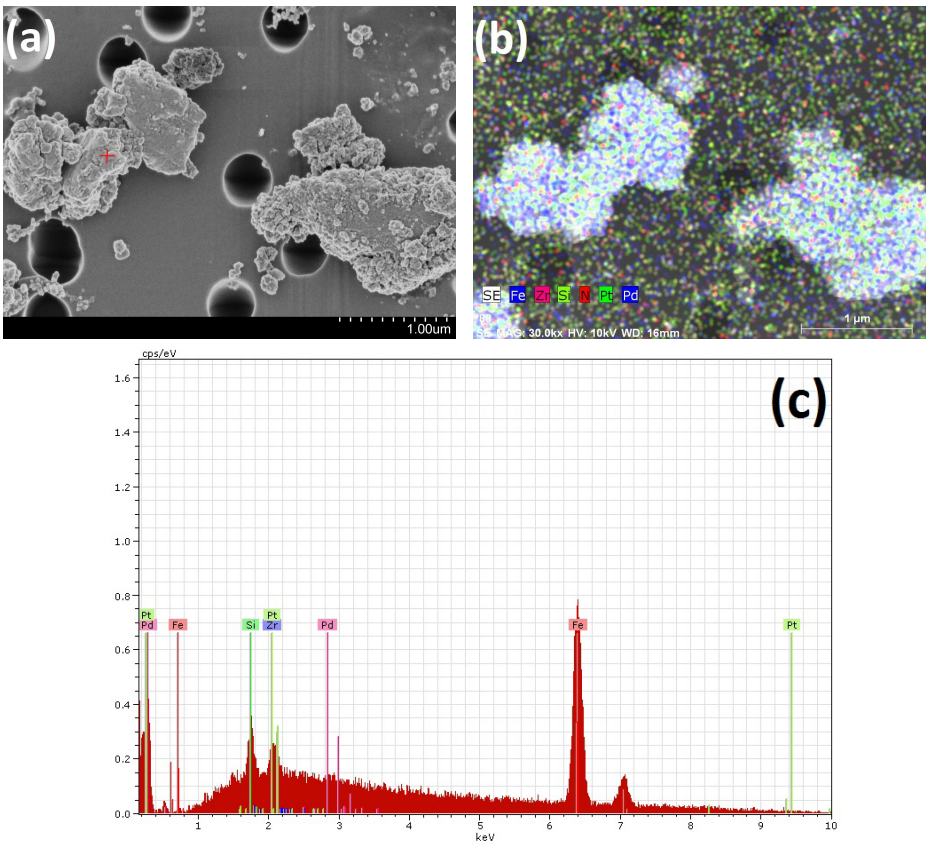

Figure C.7: (a) SEM micrograph, (b) EDX element map and (c) point spectrum of particle 03 and 04 observed in environmental sample presented in figure 30(a). The red cross in (a) represents the spot at which the point spectrum analysis in (c) was performed.

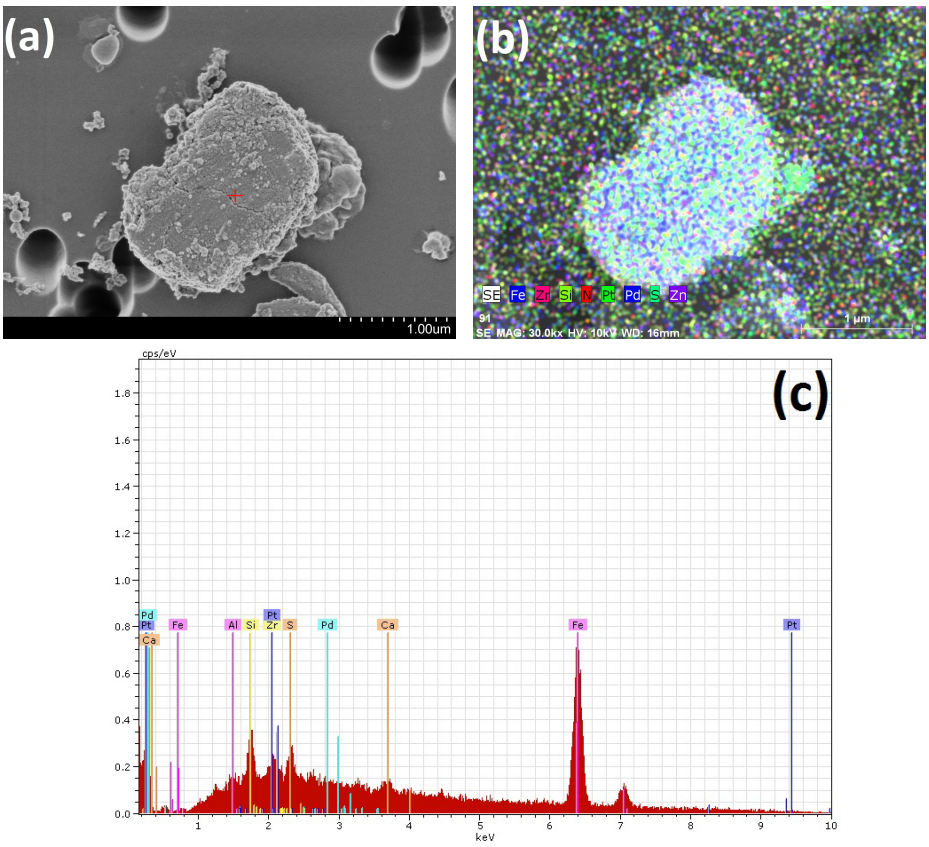

Figure C.8: (a) SEM micrograph, (b) EDX element map and (c) point spectrum of particle 09 observed in environmental sample presented in figure 30(a). The red cross in (a) represents the spot at which the point spectrum analysis in (c) was performed.

C.2 Aerosols sampled during the night

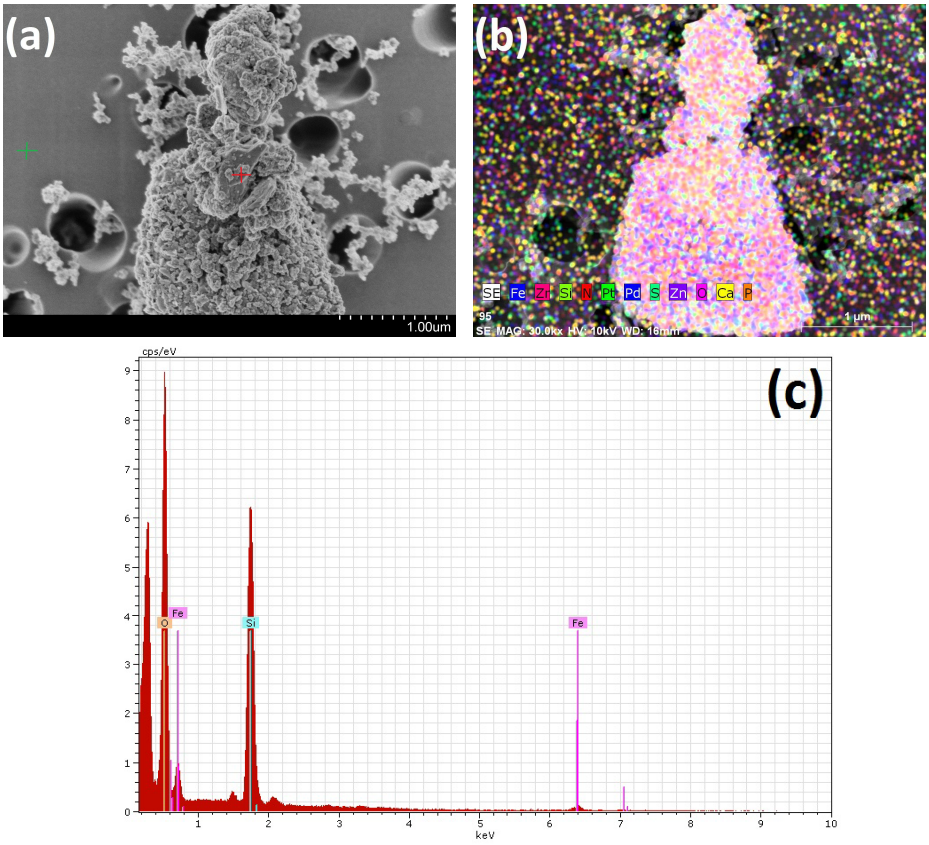

Figure C.9: (a) SEM micrograph, (b) EDX element map and (c) point spectrum of particle 01 observed in environmental sample presented in figure 30(d). The red cross in (a) represents the spot at which the point spectrum analysis in (c) was performed. The green cross in (a) represents the spot at which the outside point spectrum analysis in figure 31(b) was performed.

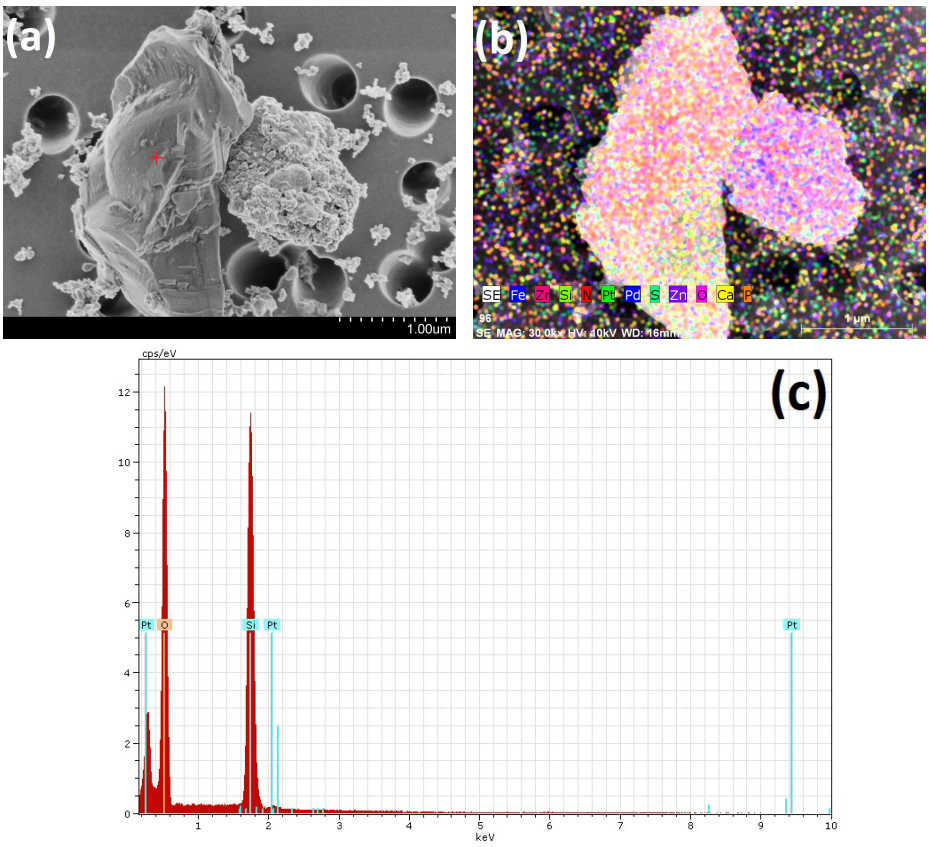

Figure C.10: (a) SEM micrograph, (b) EDX element map and (c) point spectrum of particle 02 observed in environmental sample presented in figure 30(d). The red cross in (a) represents the spot at which the point spectrum analysis in (c) was performed.

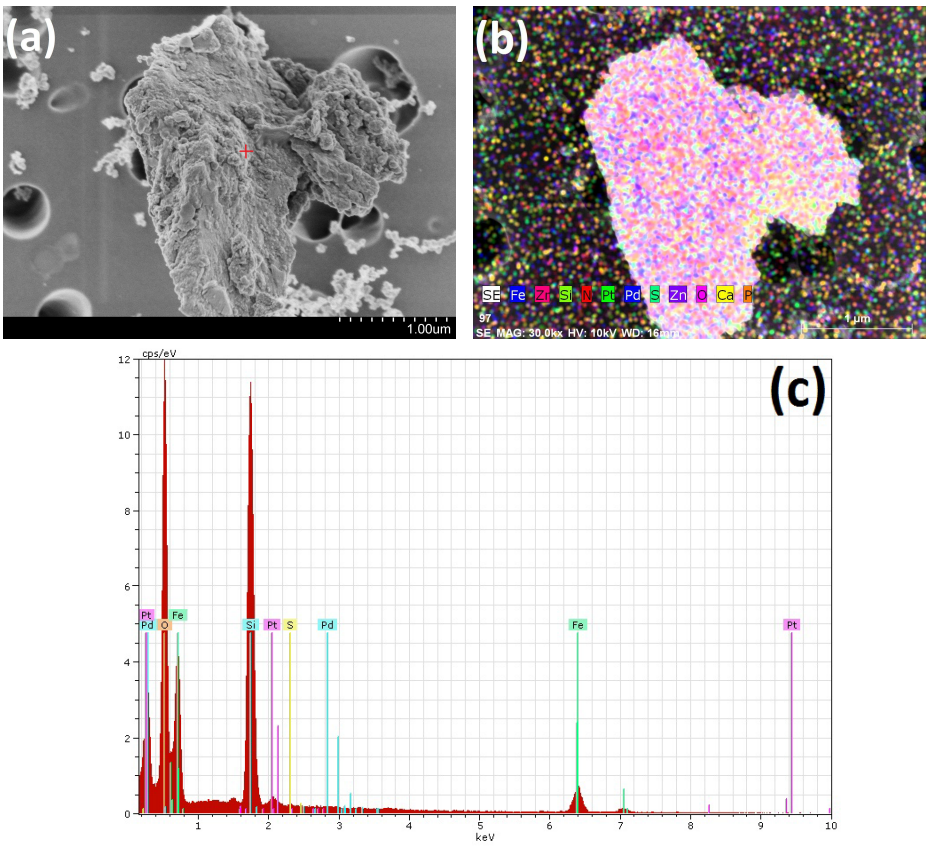

Figure C.11: (a) SEM micrograph, (b) EDX element map and (c) point spectrum of particle 03 observed in environmental sample presented in figure 30(d). The red cross in (a) represents the spot at which the point spectrum analysis in (c) was performed.

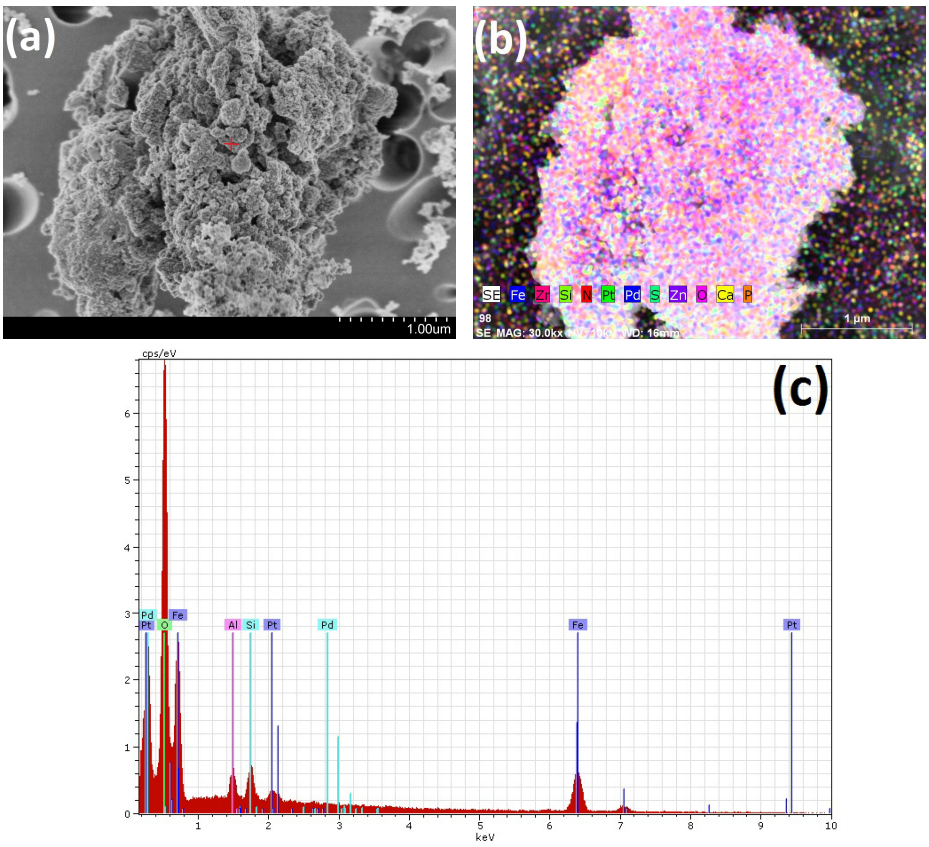

Figure C.12: (a) SEM micrograph, (b) EDX element map and (c) point spectrum of particle 04 observed in environmental sample presented in figure 30(d). The red cross in (a) represents the spot at which the point spectrum analysis in (c) was performed.